Direct Chill Casting of Aluminum Alloys: Experimental Methods and Design

by

Harry Ng

A thesis
presented to the University of Waterloo
in fulfillment of the
thesis requirement for the degree of
Master of Applied Science
in
Mechanical Engineering

Waterloo, Ontario, Canada, 2011

Author's Declaration

I hereby declare that I am the sole author of this thesis. This is a true copy of the thesis, including any required final revisions, as accepted by my examiners.

I understand that my thesis may be made electronically available to the public.

Abstract

Novelis Global Technology Centre (NGTC) in Kingston, Ontario have been developing a relatively new technology known as Novelis Fusion™ Technology, which is a new variant of the traditional direct chill (DC) casting process that allows co-casting of multi-layered composite aluminum alloy ingots. One of the first steps in this development program is to create a mathematical model of conventional DC casting and validate it through experimentation before proceeding to the next step of modeling, designing, testing, and experimenting with the co-casting process. The focus of this document is on the design of the experiments, measurement technique, and analysis of the experimental results to be used to validate the models for conventional DC casting. A series of experiments was conducted using a lab scale caster using a 95 mm × 227 mm rectangular mould available at the Novelis Global Technology Centre in Kingston, Ontario. AA3003, AA6111, and AA4045 aluminum alloys were chosen for this study since these aluminum alloys are commonly used in clad products.

Two series of experiments were performed to investigate the effect of casting parameters on the solidification and cooling of the ingots such as casting speed, water flow rate, and the superheat of the molten aluminum. A set of seven thermocouples were embedded in the ingot during the cast to capture the thermal history of the ingot. Melt poisoning with a zinc rich alloy was also performed as an independent method of determining the sump depth and shape.

Experienced gained from the first series of experiments allowed improvements to be made to the experiment design for the second series of experiments. Thermocouples must be supported so they are not pushed out of position by the jet of molten aluminum entering the mould. Grounded thermocouples of at least 1.5 mm in diameter were recommended to survive the high temperatures of the molten aluminum. Knowledge gained from the experiments of the conventional DC caster allowed design and development of an experimental co-caster mould that will be useful for future research at NGTC.

Melt poisoning and thermocouples were complementary measurement methods that should be used together. In all three alloys, the liquidus sump profile generated by the thermocouple implants correlated well with the etched sumps of the melt poisoned ingots. Primary and secondary water flow rates beyond 1.79 L/s and increasing the superheat by 30°C did not have significant effect of the cooling rate with solidified ingots, but all casting experiments showed that the thermal histories and sump profiles were very sensitive to the casting speed. The sump depth increased with increasing casting speed in all casting experiments. The sump depth increased directly proportionally to the Péclet number and the sump depth could be predicted using a linear regression model by calculating the Péclet

number. The formation of remelting bands were seen in the surface of the AA3003 and AA4045 ingots, but were not apparent in the AA6111 ingots. A fast Fourier transform performed on the data obtained from the thermocouples that were inserted in the mould wall showed that remelting occurred at regular intervals and that the frequency increased with casting speed. The thermocouples in the mould also indicated that AA6111 had a higher rate of heat transfer than AA3003 or AA4045. The AA6111 ingots had a higher rate of heat transfer in the mould than for the other alloys. This was evidence that there was a smaller air gap formation between the ingot and the mould in AA6111.

This research on the effects of casting parameters on DC cast ingots made using the three alloys, AA3003, AA6111, and AA4045, is beneficial in the development of a design of an experimental lab-scale co-caster for validation of a computational fluid dynamics (CFD) model of the Fusion™ Technology process.

Acknowledgements

I would like to thank my supervisors, Dr. M. Wells, and Dr. D.C. Weckman for their invaluable guidance and time they spent helping me in my studies as well as proofreading my thesis. I thank Dr. A. Baserinia for sharing his knowledge of casting with me. I want to thank Dr. S. Barker, Rick Lees, Dr. M. Gallerneault, Dr. D. Doutre, Peter Rice, Peter Wales, and Ed Luce, for their help with running my casting experiments at Novelis. I also thank Rosa Pelayo for providing me with diagrams. I thank Billy Tam for his work welding my thermocouples during the preparation of my experiment as well as Richard Gu for assisting me with setting up the experiment. I thank Professor C. Hansson and Professor R. Culham for reviewing my thesis.

I thank Novelis Global Technology Centre in Kingston, Ontario, Ontario Centre of Excellence (OCE-EMK), and Natural Sciences and Engineering Research Council of Canada (NSERC) for supporting this work.

Finally, I want to thank my mother and father for supporting me and making my achievements possible.

Dedication

I dedicate this thesis to my father, mother, brother, and sister.

Table of Contents

List of Figures

List of Tables

Nomenclature

Acronyms and Abbreviations:

ASTM	American Society for Testing and Materials
AWG	American Wire Gauge
CFD	Computational Fluid Dynamics
DAQ	Data Acquisition
DC	Direct Chill
FFT	Fast Fourier Transform
Nd: YAG	Neodymium-Doped Yttrium Aluminum Garnet
NGTC	Novelis Global Technology Centre
NI	National Instruments
RRS	Root Square Sum
SCXI	Signal Conditioning Extension for Instrumentation
TC	Thermocouple
WSF	Water Soluble Flux
wt. %	Weight Percent

Symbols:

α	Thermal Diffusivity [m^2/s]
C_p	Specific Heat Capacity [J/kg°C]
Δh_f	Specific Latent Heat of Fusion [J/kg]
ΔT	Temperature Change [°C]
dT	Temperature Change [°C]
dz	Change in Vertical Distance [m]
h	Heat Transfer Coefficient [W/m^2K]

k_L	Thermal Conductivity in the Liquid [W/m°C]
k_S	Thermal Conductivity in the Solid [W/m°C]
ρ	Density [kg/m³]
Pe	Péclet Number
q_L	Heat Flux in the Liquid [W/m²]
q_S	Heat Flux in the Solid [W/m²]
T	Temperature [°C]
T_{Boil}	Boiling Temperature of the Coolant [°C]
T_C	Temperature Deviation Caused by Thermocouple Connector [°C]
T_{EC}	Temperature Deviation Caused by Extension Cable [°C]
T_L	Liquidus Temperature [°C]
T_M	Temperature Deviation Caused by Voltage Input Module [°C]
T_{RJ}	Temperature Deviation Caused by Reference Junction [°C]
T_S	Solidus Temperature [°C]
T_{TC}	Thermocouple Temperature [°C]
T_{VT}	Temperature Deviation Caused by Voltage to Temperature Conversion [°C]
T_{Wall}	Temperature of the Material Surface [°C]
r	Linear Correlation Coefficient
r^2	Coefficient of Determination
v	Casting Speed [m/s]
W	Ingot Width [m]
W_C	Uncertainty in the Thermocouple Connector Temperature [°C]
W_{EC}	Uncertainty in the Extension Cable Temperature [°C]
W_M	Uncertainty in the Voltage Input Module Temperature [°C]
W_n	Uncertainty in the Independent Variable

W_{RJ}	Uncertainty in the Reference Junction Temperature [°C]
W_T	Uncertainty in the Temperature [°C]
W_{TC}	Uncertainty in the Thermocouple Temperature [°C]
W_{VT}	Uncertainty in the Voltage to Temperature Conversion Temperature [°C]
x_n	Independent Variable

Chapter 1
Introduction

1.1 Direct Chill Casting of Aluminum Alloys

Direct Chill (DC) casting has been used for more than 70 years and continues to be the dominant manufacturing process for producing non-ferrous metal billets and ingots for further processing, especially in the aluminum industry. It is used to produce billets to be extruded and ingots to be made into slabs for rolling from a wide range of aluminum alloys [1]-[4]. Approximately 10 million tonnes of aluminum are produced by 200 DC casting machines in the world every year [3].

1.2 Direct Chill Casting Process Description

The direct chill continuous casting process developed in the early 1930s for casting of aluminum alloys is very similar to the process that is used today. A schematic diagram of the process is shown in Figure 1-1 and Figure 1-2. To start the process, a starting block is positioned inside the open mould from the bottom such that it is slightly above the lower lip of the mould to seal off the bottom of the mould. Liquid metal is then poured into the water cooled mould until the desired melt level is reached. Mould cooling water circulates in the water manifold and cools the mould so that the melt inside the mould will begin to solidify and form a solid shell. This is called primary cooling [1][5][6].

The starting block is then lowered by a hydraulic cylinder into a pit at the desired casting speed drawing the solidifying ingot down as more melt is introduced into the mould to maintain a constant metal level. During the startup phase, the starter block is lowered slowly to ensure the initial shell has solidified a sufficient amount to prevent liquid metal breakout. When the partially solidified shell of the ingot emerges below the mould, cooling water is jetted from the bottom of the mould directly onto the emerging ingot surface and further cools the casting. After the direct spray of water impinges on the surface, it runs down the perimeter of the ingot and into the pit. This direct water quench by the free-falling film of water is called secondary cooling. The casting speed is gradually increased and when the desired speed is reached, the ingot is lowered at a constant rate. Steady state is reached when the physical sump profile stops changing shape with the passage of time. The casting continues until the desired or maximum length of the ingot has been reached [1][5][6].

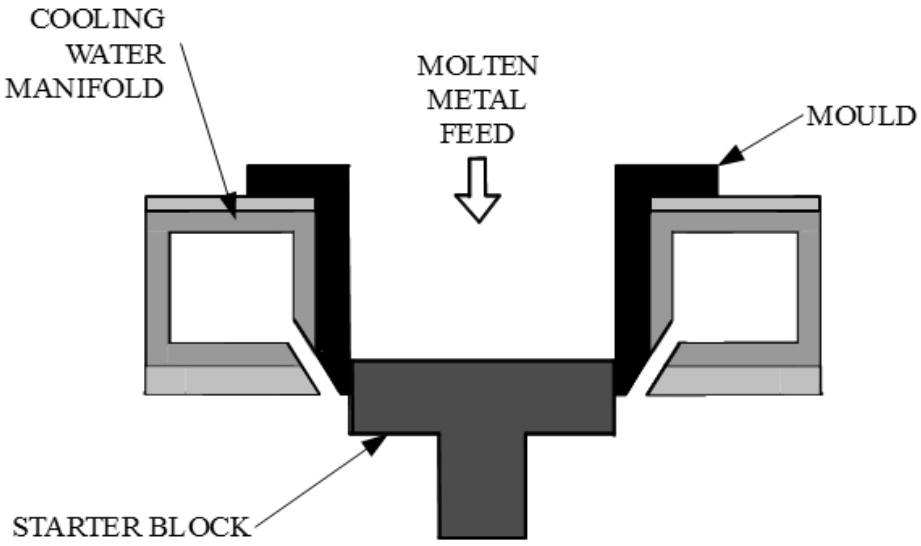

Figure 1-1: Schematic diagram of the DC casting process at the start.

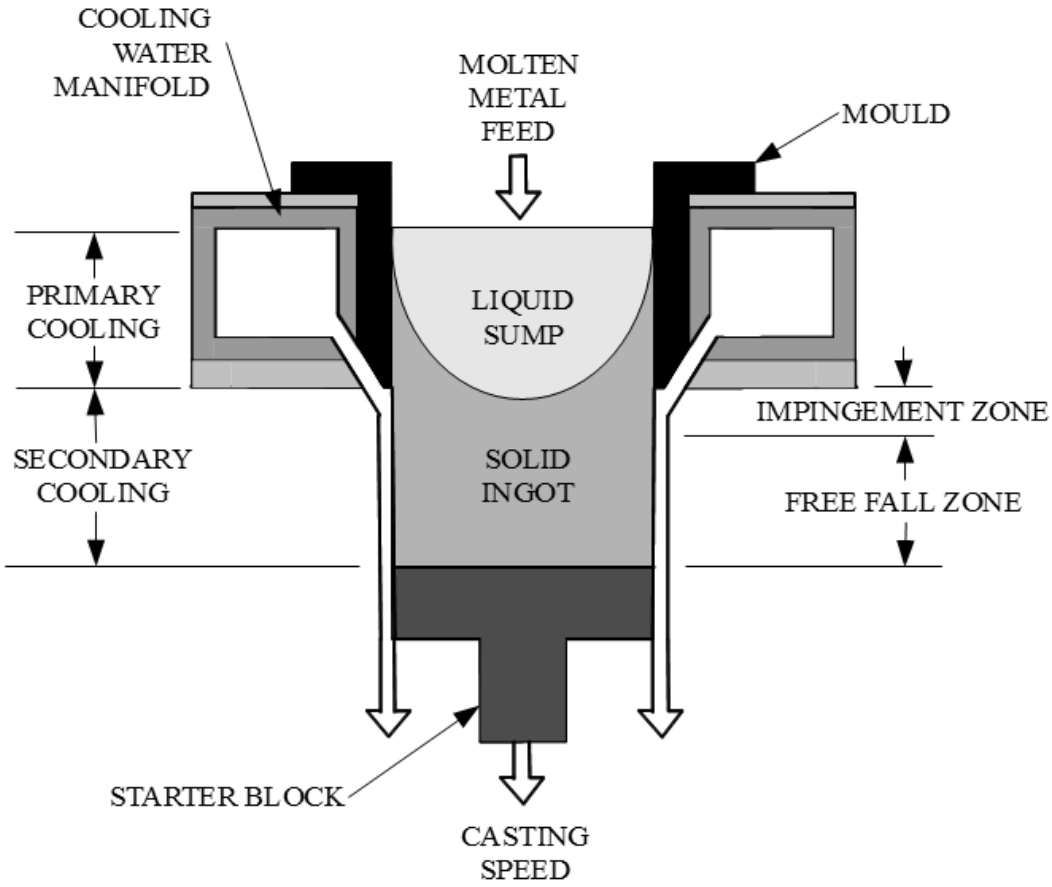

Figure 1-2: The primary and secondary cooling regions during steady state DC casting.

Although DC casting has been used for many decades, there is still room for improvement. The aluminum industry has always been striving to improve the productivity and product quality of DC casting, consequently, much research has been done to continue to develop this technology [3]. Over the last 30 years, industries have been focusing on creating computer models and simulations to advance our understanding of the DC casting process in order to develop better technologies [1].

Developing new casting procedures for new alloys and mould dimensions is very expensive and time consuming since a lot of experimentation and large volumes of molten metal are required. One solution is to develop mathematical models to simulate the casting process on computers so new casting procedures may be refined prior to final validation experiments. Determining the casting parameters required for a successful cast using simulations is more economical than making an expensive series of experiments that require some trial and error [7][8]. Computer models must be validated by experiments, but fortunately, a relatively small number of experiments are required to verify the accuracy of the model [8]. Where measurements are not possible such as measuring flow patterns in the sump, simulations are very valuable in helping researchers understand the behaviour of the process during a cast and the effects of various process parameters on the casting process [1].

Although DC casting is a dominant manufacturing process used for producing billets and ingots with no rival technology capable of replacing it anytime in the foreseeable future [1], technologies such as twin-roll casting of thin alloys for rolling into sheet product to produce aluminum sheet compete with its share of production. Improvements to the productivity, cast quality, and developing new products for DC casting have been the focus of the aluminum casting industry as they strive to remain competitive [9].

1.3 Co-casting Technology

Novelis Global Technologies Inc., a major producer of aluminum rolled products, has recently developed a new technology known as Novelis Fusion™ Technology which is a variant of the traditional DC casting process. A schematic of a Fusion™ Casting is shown in Figure 1-3. This process permits co-casting of two or more different alloys simultaneously. This composite ingot can then be rolled down into sheet with a clad layer that has different physical and mechanical properties than the core material. Further development of this technology and application to co-casting of different alloy combinations requires both computer simulations as well as experiments to test the accuracy of the computer models. The first step is to develop and validate the simulations for conventional DC casting

and the second step is to develop and validate models for co-casting. The focus of this document is on the experimental results and analysis to be used to validate the CFD model for conventional DC casting.

A large market exists for composite ingots that can be rolled down to produce composite clad sheet aluminum product to be used in the aerospace industry such as Alclad used in the aircraft industry where the surface properties of a material need to be different from those of the core [10]. Co-casting is advantageous because it creates a metallurgically defect free interface with almost any combination of core and clad alloys [11][12].

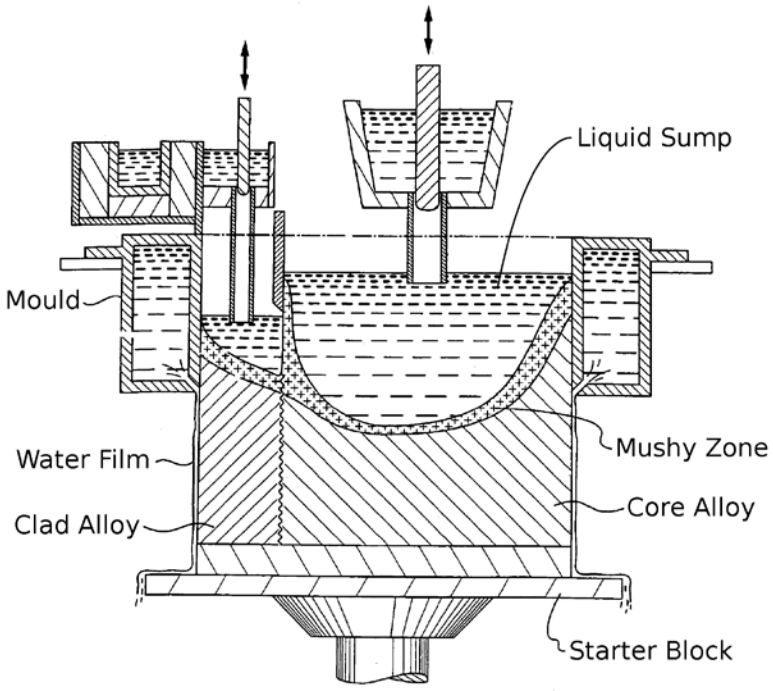

Figure 1-3: Novelis Fusion™ caster **[10]**.

Cladding materials allow two or more desirable physical and mechanical properties to be combined in a product that a single material does not possess. Often a general purpose alloy, for example a 3XXX series Al-Mn alloy such as AA3003 or an Al-Mg-Si-Cu AA6111 alloy is used as the core and a 4XXX series Al-Si alloy such as AA4045 is used for the cladding. AA3003 is one of the most commonly used aluminum alloys due to its high corrosion resistance [13]. AA6111 is used in the automotive industry for the outer body panels due to its high strength and excellent corrosion resistance [14]. The cladding material, AA4045, is a brazing alloy and is often used in the fabrication of furnace brazed aluminum radiators in the automotive industry [12][15].

Prior to the invention of the Fusion™ Technology, commercially produced clad products were generally roll bonded at elevated temperatures by pressing the layered sheets of core and clad material together through a rolling mill [11]. Producing clad alloys for aluminum requires multiple steps and requires high loads and temperatures during rolling for the two materials to bond. In roll bonding, the clad layers are made from ingots produced by conventional DC casting. The core material needs to be homogenized for around 20 hours at temperatures up to 600°C. Afterwards, the material must be cooled before scalping the surface, a process to prevent defects from being rolled into the surface. The clad material must be heated, rolled and trimmed after scalping. After cleaning the surfaces of the core and clad materials, they are assembled, welded together at the edges, and reheated before hot roll bonding may take place [12]. One of the difficulties of roll bonding is when large differences between the yield strengths of the core and clad alloys occur, core materials which are only clad on one side do not roll bond well [12]. Many alloy combinations cannot be roll bonded because the oxide films or defective interfaces on the surface of aluminum products cause the bonds between the core and clad materials to be weak [11]. Ingots produced by co-casting are advantageous because fewer processing steps are required and more core and clad alloy combinations are possible [12].

Co-casting differs from conventional DC casting in that the mould is divided into two or three sections by one or two chill bars, or divider walls, which run parallel to the length of the mould. The divider wall is water cooled and separates the two different streams of alloys [12].

In casting of a composite ingot with a rectangular cross section, two separate feeding systems are used. The core alloy is introduced first to one side of the mould and cast forming a self supporting partially solidified surface. The second alloy is added and solidified between the solidified surface of the first alloy and the mould wall. The interface temperature of the two alloys is between the liquidus and solidus temperatures when the second clad alloy first contacts the solidified surface. The two streams of different alloys fill each section and are cast simultaneously. As the ingot cools, the alloys will form two distinct layers fused at the interface. The metal levels and cooling rate must be carefully controlled to create and maintain the solid shell interface between the core and clad materials [10][12].

In a co-casting process where only a single side cladding is required, only one chill bar is required to divide the mould. Melt for the core alloy is introduced to the mould first where it begins to solidify and forms a shell against the mould and the chill bar. The starter block is then lowered and the melt for the clad alloy enters next. The clad shell is formed by solidifying against the mould wall and the solidified interface of the core alloy. As the casting continues and reaches steady state, the metal level is maintained for the duration of the cast [12].

Novelis Fusion™ casting technology is a unique and economical manufacturing process with a large potential for commercial use. Once the model of conventional DC casting is complete and validated, a model for Fusion™ casting will be developed. Since Fusion™ casting is significantly more complex than conventional casting, simulations are essential for testing new alloys, casting parameters, and mould shapes to increase the likelihood of a successful cast and reducing expensive trial and error experiments during the development of new products.

1.4 Problem Statement and Objective

To validate the results of the computer simulations of the DC casting process, experimental measurements of the industrial process must be taken and compared with model predictions. The focus of this document is on the design of experiments used to obtain accurate temperature measurements and sump profiles from the direct chill casting process. One of the challenges in taking measurements is that measurement devices can perturb the local environment of what is being measured. Proper experiment design is essential to obtain results which are reliable and repeatable.

Two sets of experiments were performed to generate the validation data required. The first set of experiments uncovered unforeseen weaknesses in the design of the experiments that affected the final results. These deficiencies were corrected in the second set of experiments. Improvements were made to the experiment design to minimize the effect the experiment equipment had on the measurements.

The outline of this work is on the measurements taken using the DC laboratory scale caster at the Novelis Global Technology Centre (NGTC) in Kingston, Ontario. These measurements included the thermal history in both the ingot and mould as well as sump profiles identified using a melt poisoning technique where a 50% zinc and 50% aluminum mixture was added the liquid metal during casting. Data were collected from a set of experimental casts using a conventional direct chill casting machine. These data were then used to validate a computational fluid dynamics (CFD) model of the process being developed by Dr. Amir Baserinia at the University of Waterloo. The main objective of the experiments was to measure the thermal histories in the ingot, the temperature change in the ingot over time, through the use of thermocouples and obtain the liquid sump shape using the melt poisoning technique and the thermocouple data. The effects on the process of parameters such as the casting speed, water inlet temperature, water outlet temperature, tundish temperature, mould temperatures, and the alloy chemistry were also measured and analyzed to provide additional information for model validation.

The experiments were performed on a lab-scale DC caster, since it is more economical than using full scale production DC casters. Lab-scale casters operate on the same principle as a full-scale production caster. Future research on co-casting will also take place on a lab-scale caster. The limitations of experimenting with smaller ingots is that the flow fields within the mould are more sensitive to objects such as thermocouples being placed in the melt during casting, while there would be less effect in large moulds. Another limitation is that very fine measurements used to detect events such as air gap formation are required, may be done in large moulds, but is practically impossible with lab-scale casters. Commonly used aluminum alloys in clad products, such as AA3003, AA6111, and AA4045 were used in the experiments so the behavior of the alloys will be known when developing a lab scale co-caster.

In this thesis, the results of the etched sump and thermocouple cooling curves from the ingots were plotted and compared. The effects of casting parameters such as superheat, cooling water flow rate, and the casting speed on the sump shape and measured temperatures within the ingots were analyzed and observations such as surface texture of the ingots, defects, microstructure, and sump shapes were discussed. Good experiment design is essential to obtain meaningful data. Knowledge and experience gained from the first series of experiments that improved the quality and reliability of the measurements from the second series of experiments are also presented.

Research of literature on DC casting experiments performed by researchers in the past was reviewed to aid in the design of the experiments. Descriptions of the heat transfer that occurs during the DC casting process and measurement techniques commonly used in DC casting experiments are provided in the following chapter.

Chapter 2
Literature Review

In this chapter, the literature related to the direct chill casting process, the heat transfer involved in cooling the ingot, the effect of casting parameters on the ingot, as well as the work and experimental techniques that have been done on DC casting by other researchers is reviewed. Background is also given on co-casting to produce laminate ingots, since research presented in this thesis will be used to help develop and test DC co-casting technology.

2.1 Heat Transfer in DC Casting

Having an understanding of the heat transfer and the solidification process that occurs in the ingot during casting is essential for analyzing and interpreting experimental results. Four main regions defined by the solid fraction exist during solidification. The liquid region has a solid fraction of 0.0, the slurry region has solid fractions between 0.0 and 0.3, the mushy region ranges from 0.3 to 1.0 and the solid region has a solid fraction of 1.0 meaning the ingot in this region is fully solidified [1].

Figure 1-2 from the previous chapter illustrates the cooling regions in the steady-state DC casting process. During DC casting, the sensible heat, the heat released to the surrounding environment, of the superheated molten metal, latent heat from the liquid-solid phase change, and sensible heat from the solidified ingot is conducted away from the ingot by the primary and secondary cooling water [7]. Cooling water which flows through the mould water manifold removes heat from the melt by convection and conduction from the molten metal to the mushy zone and solid shell, and then by conduction through the shell to the mould walls. The heat is then transferred from the water cooled mould to the water in a process known as primary cooling [1][16][17]. After the water flows down the mould, further heat is removed by the direct impingement of the water around the perimeter of the ingot in a process known as secondary cooling. The impingement zone is the area water first hits the ingot surface as it emerges from the mould. Very high heat transfer rates exist in this direct impingement zone. Below this, the free-fall zone is where a free-falling film of water runs down the side of the ingot [6][18]. Forced convection due to direct water contact with the ingot below the mould is the primary means of removing heat from the ingot during casting. Primary cooling in the mould is responsible for extracting about 20 percent of the heat while the remaining 80 percent is extracted by secondary cooling during steady-state operation [1][5].

The heat transfer to the water during secondary cooling is complicated as boiling water heat transfer occurs due to the high surface temperature of the ingot. Hence, the heat extraction varies as the water transitions from film boiling, to transition boiling, nucleate boiling, and finally to forced convective cooling [18].

The boiling curve showing heat flux versus temperature change is illustrated in Figure 2-1. This boiling curve was produced by electrically heating a wire surrounded by water, but it may also be used to describe the heat transfer on the ingot surface in DC casting. The temperature change, ΔT, is equal to $T_{Wall} - T_{Boil}$ where T_{Wall} is the temperature of the hot surface and T_{Boil} is the boiling temperature of the coolant which for water is about 100°C. The transition from nucleate to film boiling may occur as the solidifying ingot first emerges from the mould and the impinging jet of water first comes in contact with the very high temperature ingot surface. During film boiling, the surface temperature is so high that a continuous layer of vapor will be created between the water and the ingot surface. This drastically reduces the rate of heat extraction, with the heat flux reaching a local minimum at the Leidenfrost point shown in Figure 2-1. As the ingot surface cools down, the water on the ingot surface goes through transition boiling where the rate of heat transfer gradually increases until nucleate boiling occurs and the maximum heat transfer rate is obtained at the critical heat flux. During nucleate boiling, vapour bubbles nucleate on the heated surface, move off the surface and are quickly cooled and collapse in the liquid close to the heated surface. The number of nucleation sites increase with temperature [19].

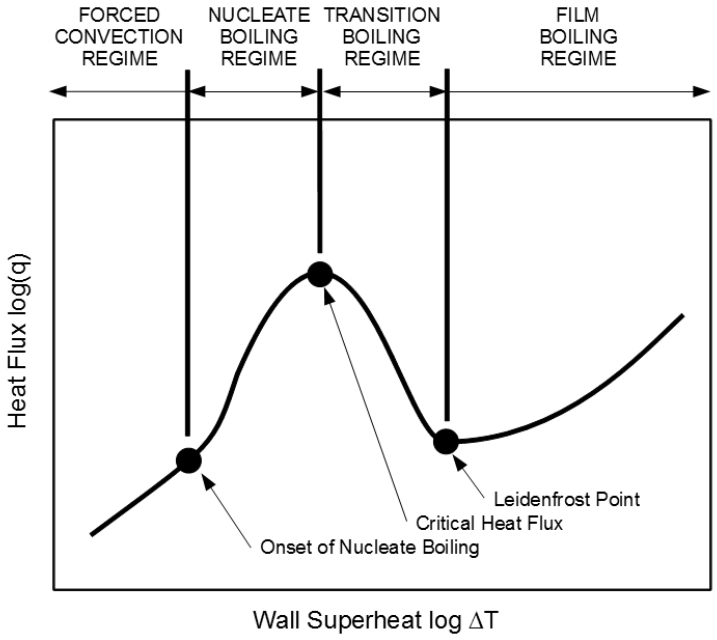

Figure 2-1: Wall superheat, ΔT, versus heat flux, q, boiling curve of water **[20]**.

As the ingot surface cools below the boiling point of water, the heat is extracted by forced convection to the film of water [16][17]. During forced convection, the rate of heat transfer increases with the velocity of the flowing water down the ingot surface [19]. Heat transfer is limited by the conductivity of the alloy in the nucleate boiling region and limited by the rate of heat transfer to the water in the transition region [18]. Although low heat transfer rates from film boiling are desirable during startup to reduce butt curl, high heat transfer rates from nucleate boiling are ideal for steady-state casting conditions as it allows higher casting speeds to be used, and therefore increased productivity [21].

Although it is often assumed in many models of DC casting that the ingot's surface experiences uniform cooling, Weckman and Niessen [4] were the first to show that there are actually different cooling zones with different heat transfer rates [1]. In the primary cooling zone within the mould, the melt close to the mould walls solidify first to form a solid shell. As the shell experiences thermal contractions, it pulls away from the mould easily since the centre of the ingot, which is still liquid, can offer little resistance to the solid shell contracting towards the centre. This thermal contraction forms an air gap between the ingot and the mould, which behaves as an insulating layer, causing the heat transfer coefficient to decrease from about 2.0 to 0.5 kW/m²K [1]. This reduced heat extraction rate can result in the shell reheating and remelting within the mould. The cycle of remelting continues throughout the cast and in extreme cases where the cooling rate is too low, bleed out of the melt or liquid metal exudation through the 2-phase remelted shell may occur [1]. In the extreme, a complete remelt and very dangerous liquid metal breakout can occur. Such liquid aluminum breakouts into water-filled casting pits have been known to cause catastrophic steam and hydrogen explosions [22].

In the primary region, heat transfer coefficients of the order of 3,500 W/m²K occur when the metal is in contact with the mould and drops to about 300 W/m²K when an air gap forms. Heat transfer coefficients of around 10,000 – 12,000 W/m²K are typical in the secondary cooling region [4][5]. The rate of heat transfer from the ingot is most efficient with nucleate boiling during direct chill of water on the ingot below the mould. The coefficient of heat transfer and heat fluxes is approximately 40 kW/m²K and 6,000 kW/m^2 respectively [1][23].

2.2 Effect of Casting Parameters

The isotherm profiles within the DC cast ingot are influenced by the pouring temperature, alloying elements, melt temperature, metal level, casting speed, ingot dimensions, the feeding system used to introduce melt into the mould, the water flow rate and its heat transfer coefficient, h. The way the billet or ingot solidifies, the temperature distribution in the ingot, and the casting defects produced are

dependent on these parameters. Casting speed has a major impact on the sump depth and the solidification rate [1][8]. The heat input from the melt being introduced to the mould increases linearly with the casting speed [19] and the depth of the sump is directly proportional to the casting speed [1].

2.2.1 Effect of Water Temperature and Flow Rate

Water flow rate is an important aspect of DC casting and can affect the sump geometry and the cast quality. More importantly, a sufficiently high water flow rate is essential for safety reasons. Molten aluminum can break out of the ingot as it emerges from the mould if the water flow rate is too low, since the solid shell might only be in the slurry or mushy region and not form properly in the mould, leading to a potentially dangerous situation as water contacting the molten aluminum would flash boil, thereby, spattering molten aluminum in the work place [1][4].

Wiskel and Cockcroft [16] and Wiskel [17] studied the thermal behaviour of a 1680 × 800 mm rectangular ingot during DC casting of AA5182 aluminum. They confirmed that changing the casting speed and flow rate affects the shape of the solidus isotherm, since the rate of heat extraction also changes. The city water used in the water manifold for mould coolant was warmer during the summer and cooler in the winter. It was found that the water temperature in the winter was 7°C and cracking on the ingot surface occurred while summer water temperatures were above 16°C and the severity of these surface defects were reduced, however, the correlation between water temperature and the magnitude of the butt curl was poor [17]. Higher water flow rates produced shallower sumps and higher water temperature reduced cracking on the ingot surface.

Grandfield *et al*. [19] performed spray tests on heated materials containing embedded thermocouples to study the heat transfer rates. Heat was applied on one side of the material and a water spray was applied on the opposite side. The heat transfer for water temperatures ranging from 15°C to 35°C did not show significant difference, but with temperatures above 43°C, during the transition from nucleate to film boiling, film boiling occurred at lower surface temperatures. According to Grandfield *et al.* [19] and Langlais *et al*. [24], using cooling water with temperatures up to 30°C has little effect on the ingot cooling rate. The cooling water temperature needed to be above 70°C to have any noticeable effect on the depth and the thickness of the mushy region [19][25]. The experiments also showed that the heat transfer in the nucleate boiling region was not significantly affected by the cooling water flow rate [19]. The amount of heat extraction possible is limited by the thermal properties of the alloy and the heat capacity of the cooling fluid, i.e., it is conduction limited, so using water flow rates beyond a certain value does not contribute to higher cooling rates [1].

Wells and Cockcroft [18] and Grandfield *et al*. [19] observed that increasing the water flow rates from 0.33 to 0.66 L/s did not have a significant impact on the heat flux in the nucleate boiling region when they experimented with stationary test samples 127 × 305 × 50 mm that have been heated in a furnace. In the experiment, flow rates of 0.25, 0.32, 0.38, 0.43, and 0.47 L/s were used on the alloys AA1050, AA3004, and A5182. Results from their experiments showed that the heat flux is greatly affected by the thermal conductivity of the aluminum alloy. Heat flux increases with higher water flow rates, ingots with rougher surfaces, and lower water temperature [18]. It was found that heat transfer increased with flow rate, but since these tests were performed on stationary test samples rather than during a DC casting, it does not capture the effects of advance cooling, which is the heat transfer above the water impingement zone due to secondary cooling [18].

Hao *et al*. [5] performed experiments with DC casting of AZ31 billets 455 mm in diameter at 0.847 mm/s, but found that changes in water flow rate ranging from 3.15 L/s to 6.75 L/s and water temperature ranging from 32.8°C to 37.8°C had little effect. The findings of Hao *et al*. [5] were consistent with Prasso *et al*. [26] who demonstrated that decreasing the water flow rate by 20% only deepened the sump by 4%. It was found that water flow rates had greater effect on the sump depth at low casting speeds [1].

2.2.2 Effect of Metal Level

The metal level is the distance between the meniscus and the bottom of the mould and affects the thermal gradient within the mould. As the metal level decreases, the thermal gradient increases since the heat source and heat sink, i.e., the direct secondary water quench, are closer together. However, Larouche *et al*. [6] suggested that metal level changes do not affect the thermal contours as much as changing the casting speed. As the cross sections of billets and ingots were increased, a low melt level became more important to maintain during the cast. High melt levels caused larger thermal stresses, wider transition regions, and a larger air gap region between the partially solidified ingot and the mould. Other problems included the shell pulling away from the mould walls creating a larger air gap during thermal contraction. The shell remelts as a result of the low heat transfer due to the air gap and the periodic cycle continues throughout the cast which caused remelting bands on the surface of the ingots with liquid metal exudations and inverse segregation. The larger the metallostatic head, the more the remelted metal was able to squeeze through the shell and leave larger bands on the ingot surface [1].

2.2.3 Effect of Pouring Temperature

Larouche and Brochu [6] found that the heat input from higher pouring temperatures only had a minor impact on the thermal contours of the ingot. Higher pouring temperatures created deeper sumps and moved the solidification front downward and closer to the water impingement region leading to higher heat transfer rates. Reese [27] investigated the effects ingot size, casting speed, and pouring temperature on the flow of aluminum in the molten metal sump during DC casting using an analytical model. He found that increasing the superheat from 30°C to 70°C increased the sump depth [27]. Higher superheats shifted the liquidus and solidus isotherm downward, but it affected the solidus isotherm to a lesser extent [1].

2.2.4 Effect of Casting Speed

It is well known that as casting speed is increased, the depth of the sump is increased. Hao *et al*. [5] concluded that casting speed has a large impact on the sump depth, as it increased with speed. This has been confirmed by many other researchers. The sump depth increases proportionally to higher casting speed, even for various alloy compositions [1]. Casting speed affects the centre of a billet or ingot the most, with its effects decreasing towards the edge.

The upper limit of casting speed is limited by the ability of the cooling water to remove sufficient heat from the emerging ingot. The surface temperature of the emerging ingot increases with casting speed and will lead to a sudden transition to film boiling. The subsequent dramatic drop in heat extraction rate will result in remelting of the emerging ingot shell followed by a catastrophic liquid metal breakout of molten aluminum into the water filled casting pit and a high risk of a hydrogen and steam explosion [4][21].

2.3 Measurement Techniques

The measurement techniques researchers have used in DC casting experiments are summarized in this section along with some of their relevant findings. Although the alloys, mould dimensions, casting parameters and goals of the experiments may vary from one researcher to another, some techniques and procedures used in their experiments are helpful to consider when designing an experiment for a unique caster.

2.3.1 Thermocouple Measurement Techniques

The temperatures and cooling rates in an ingot or billet during direct chill casting are typically measured by inserting an array of thermocouples into the liquid sump and allowing them to be cast into the solidifying ingot. A similar method may be used with rectangular moulds that produce ingots. The thermocouples are lowered into the mould at the casting speed and the thermocouple beads will travel through the liquid, slurry, mushy, and solid regions of the billet or ingot providing time temperature measurements. The location of the liquidus and solidus along vertical lines at specific horizontal positions in the ingot at a specific lateral location within the ingot can be determined from the temperature readings of the thermocouples. The cooling rate can be calculated by finding the time required for the junctions of the thermocouples to pass through certain temperature ranges [1]. The solid phase is formed rapidly in many aluminum alloys, often within only a few degrees below the liquidus temperature [1].

Drezet *et al*. [28] performed experiments to investigate the thermomechanical effects during direct chill casting and compared the results with electromagnetic casting. 1XXX series alloy ingot with a cross section of 1860 mm × 510 mm was cast at 80 mm/min to a length of approximately 4 metres using conventional direct chill casting. The sump depths and cooling curves were measured using a set of five thermocouples attached to stainless steel rods. The thermocouples were positioned along the width of the mould using guide rails, from the centre to the lateral side due to symmetry at 255, 173, 118, 68, and 28 mm from the ingot surface, 850 mm from the short side of the mould [28]. The stainless steel rods entered the mould once steady-state casting conditions were reached and were lowered by guiding rods moving along rails to keep the assembly straight. The sump was measured using type K thermocouples and readings were taken every 0.1 seconds. The thermocouple measurement technique was effective in finding the sump depth of 580 mm. The liquidus and solidus temperature profiles were determined using the vertical positions of the thermocouples at given temperatures [28]. Since the ingot was relatively large, it was assumed that the presence of thermocouples did not have significant effect on the sump shape and the symmetry of the sump.

Wiskel and Cockcroft [16] and Wiskel [17] investigated crack formation during the start-up of direct chill casting using AA5182 aluminum 1680 × 800 mm ingots cast at 0.899 mm/s with a cooling water flow rate of 3.33 L/s. Type K thermocouples that were 0.5 mm in diameter with exposed beads were connected to a data acquisition system which recorded temperatures at a rate of one reading every three seconds. Lower sampling rates that were used by Drezet *et al*. [28] were possible due to the slow casting speed. Pairs of thermocouple were positioned on a frame so that it was held centered along the

broad face of the mould and cast into the ingot. One of the thermocouples was placed 8 mm from the ingot surface and its thermal response was used quantitatively in an inverse heat transfer analysis. The second thermocouple was 25 mm from the ingot surface and used for qualitative verification [16][17]. Although, some of the data from the thermocouples had to be omitted from analysis due to faulty readings from failed thermocouples for unspecified reasons, good agreement was found between the thermocouples and the model.

Zuo *et al.* [2] compared the sump shapes of low frequency electromagnetic casting (LFEC) and conventional direct chill casting [2]. In their experiments, a 200 mm diameter billet of Al-Zn-Mg-Cu alloy was cast at 75 mm/min. The casting temperature was 730ºC, the cooling water temperature was 16ºC, and the water flow rate was 70 L/min. Seven K-type thermocouples oriented about the centre were positioned along the diameter at 10, 60, 80, 100, 120, 140, and 190 mm from the edge in order to obtain cooling curves at different locations away from the surface. The data acquisition system took 10 measurements per second from the thermocouples. Stainless steel rods attached to the starter block were used to anchor the thermocouples in position so that during the cast, the starter block would pull the thermocouples down into the melt at the same casting speed and fixed positions within the ingot. X-rays were used to confirm the thermocouple location after the cast. The sump depth was determined by measuring the distance between the melt top and the end of the solidification in the measured thermocouple temperature profiles [2]. The experiment was successful in determining the liquidus temperature, 632ºC, and solidus temperature, 470ºC, of the alloy [2]. It was found that using the low frequency electromagnetic casting process produced a shallower sump of 65 mm while DC casting had a sump depth of 110 mm [2].

Embedding an array of thermocouples into an ingot during casting has been shown to be an effective method in determining the sump shape. Slight movements of the thermocouple position may be neglected in larger ingots since the distance moved is relatively small in comparison to the mould size. Thermocouple position is more sensitive in smaller ingots so it is important to confirm the location of the thermocouples using x-rays of the ingots.

2.3.2 Melt Poisoning Measurement Technique

A technique known as melt poisoning is a common method used to determine the solid-liquid interface during direct chill casting of aluminum alloys. Melt poisoning involves adding a molten tracer, such as an Al-Zn mixture, directly into the melt so that the turbulence caused by the pouring of the tracer into the mould will allow the mixture to be distributed rapidly throughout the melt. After the cast, the ingot is sectioned and etched to reveal the sump shape [4].

Melt poisoning results, provided by Neil Bryson at the Alcan Kingston Labs, with an Al-Zn mixture were utilized by Weckman and Niessen [4] to validate a numerical simulation for studying nucleate boiling during direct chill casting. AA6063 Al-Mg-Si billets with a diameter of 152.4 mm were cast at 1.69 mm/s, 2.54 mm/s, and 2.81 mm/s using a cooling water temperature of 10°C with a flow rate of 1.89×10^{-3} m³/s and a pouring temperature of 690°C. To capture the thermal history of the cast, five type K thermocouples were placed along the radius of the billet and held in position by a wire frame while being solidified in place during the cast. Alloys such as AA6063 have a short freezing range and a small mushy zone resulting in excellent correlations between the thermocouple measurements and the etched sump.

In a series of casting experiments performed by Zuo *et al*. [2], an Al-30%Cu molten tracer was used. The mixture was poured into the mould after steady state had been reached, and seven thermocouples were also embedded into the billet to obtain a thermal history. After the billet was sectioned and etched, the results of the sump depth was compared with the calculated results from the thermocouple curves. There was close agreement between the two methods [2].

Melt poisoning is a reliable method to determine the sump shape at the moment the molten tracer mixture is introduced to the mould. The advantage of this technique is that any ingot or billet dimensions may be melt poisoned. In addition, the technique shows the entire sump shape at a particular moment including the small primary shell in the mould. The weakness of this method is that it only provides the sump shape, but does not provide thermal histories or the temperature the profile represents. Furthermore, in situations where the sump is large and deep with a large mushy zone, such as in steel, tracers may not be able to fully penetrate to the bottom of the sump to reveal the true solid liquid interface [4]. For this reason, melt poisoning is most effective when used in conjunction with embedded thermocouples so that both spatial and temporal data are obtained.

2.3.3 Steel Rod Measurement Technique

Another technique used to determine the sump depth is by inserting a rod into the centre of the liquid sump vertically until moderate resistance is felt and the length of the rod that is submerged is taken to be the sump depth [5]. In an experiment that involved casting a 455 mm diameter AZ31 magnesium alloy billet cast at 1.0 mm/s, Hao *et al*. [5] used an 8 mm diameter steel rod that was inserted into the centre of the billet after steady state conditions had been reached. The measured sump depth was 425 mm deep, and the predicted depth was 410 mm. Using a 0.8 fraction solid in the model gave good correlation with the experimental results, but the accuracy of the measured sump depth was uncertain [5]. Since this method is based on feel, consistent results may be difficult to obtain. Although

this method is relatively simple, it only provides the sump depth, whereas thermocouples can provide the thermal history of the ingot, and melt poisoning can provide the entire sump shape.

2.3.4 Gap Formation Measurement Technique

The experiments by Drezet *et al*. [28] included measuring the air gap between the mould wall and the solidified shell of an ingot after steady state had been reached. In one of the experiments, an 1860 × 519 mm ingot was cast at 60 mm/min using a 5XXX series aluminum alloy. A quartz rod holding two thermocouples was lowered into the melt close to the ingot surface. The rod was guided vertically by a cylinder and was also able to move by translation along the length of the mould by low friction rails. During the cast, the rod would enter the melt, and the vertical and lateral displacements were recorded by two sensors. The contraction of the ingot at the mould exit was determined by the two sensor readings and compared with the value given by a displacement sensor at the bottom of the mould. The reliability of the measurements was confirmed by showing less than ten percent discrepancy between the two independent measurement techniques [28]. An air gap of 1.5 mm at the exit of the mould was measured. The gap between the mould and the ingot of 1.5 mm was maintained for 20 mm below the mould before further contraction occurred at a constant rate. At approximately 100 mm below the mould, the ingot surface had contracted by 5 mm away from the mould wall [28]. Drezet *et al*. [28] showed that metal contraction begins when the alloy is still in its semisolid state, since at the moment the thermocouples began to pull away from the mould, it had temperature readings of 620°C, or approximately 70 percent volume fraction of solid. Although this is a very interesting technique for determining the air gap, it may not be as effective for smaller moulds, since the air gap may be too small to measure with precision.

2.3.5 Mould Thermocouples

Thermocouples have been inserted in the mould by some researchers to measure the thermal gradient across the mould wall and along the height. Hao *et al*. [5] ran experimental plant trials to validate a thermal model of direct chill casting of AZ31 magnesium billets. In their experiment, a 455 mm diameter AZ31 billet was cast at 1.25 mm/s, with a flow rate of 1.5 L/s, a pouring temperature of 676ºC, and a water temperature of 34.4ºC. Type K 1.5 mm Ø stainless steel sheathed thermocouples were used to obtain temperature readings from the ingot and the mould at a sample rate of 10 readings per second. The thermocouple was positioned 8 mm from the surface along the diameter of the billet. Two pairs of thermocouples were placed in the mould walls 100 mm and 350 mm from the top of the mould. Within each pair, one thermocouple was 3 mm from the mould hot face while the second

thermocouple was 16 mm from the hot face. It was found that the top pairs of thermocouples had a temperature reading of approximately 80ºC and 70ºC for the hot and cold thermocouple positions in the mould wall. The pair of thermocouples near the bottom of the mould both read a temperature of 60ºC. It was concluded that there was lower heat transfer at the bottom of the mould leading to lower temperatures because an air gap had formed so that contact between the billet and the mould was poor [5]. Since the pairs of thermocouples were located 250 mm apart at only two vertical locations, there is not enough resolution to determine how the air gap changes along the height of the mould wall. The mould thermocouples can provide temperatures at particular locations inside the mould wall for model validation.

2.4 Summary

The measurement techniques must be chosen and the experiment must be designed and run in order to validate the models for conventional DC casting. It is important to obtain the sump shape to compare the results with the simulations so using two independent methods, the array of thermocouples and the melt poisoning technique, together will allow the experiment to be checked for reliability. Although thermocouples do not appear to influence the environment of the liquid sump during the cast in large ingots, this may not be true for small lab-scale casts. While much research has been done in DC casting, new experiments and simulations must be performed every time different alloys, casting parameters, and mould shapes are used [4]. Once the validation is complete for conventional DC casting, the same process will be used for co-casting of aluminum alloys. In the following chapter, the design of the experiments used to validate the CFD model is discussed.

Chapter 3
Experimental Apparatus and Methods

The objective of the experiments performed during this study was to obtain temperature profiles and a sump profile in the ingot as it cools and solidifies during direct chill casting under a wide range of casting conditions using a number of different alloys. The results were used to validate computational fluid dynamics model simulations performed by Dr. Baserenia at the University of Waterloo [29]. To collect data for the temperature contours of the ingot during a cast, a row of thermocouples spanning the width of the mould were lowered into the mould. Multiple experiments were required to test how changing aluminum alloy, casting speed, cooling water flow rate, and superheat affect the sump depth and shape during a cast. DC casting experiments were performed at Novelis Global Technologies Inc., Kingston, Ontario.

A data acquisition (DAQ) system was used to collect data from the thermocouples as well as the displacement transducer, and the velocity transducer attached to the casting table. A melt poisoning technique was used to determine the sump profile in the ingot. Radiographs were performed on the solidified ingot to confirm the location of the thermocouples inside the ingot.

The lab-scale DC caster located at Novelis Global Technology Centre (NGTC) in Kingston, Ontario, consisted of a 95 mm × 227 mm open aluminum mould cooled by a water manifold that surrounded the mould as shown in Figure 3-1. During a cast, molten aluminum flowed from a nearby furnace, down a launder, into the tundish, down the feeder tube, through the diffuser, into the mould where it was cooled and exited as a solid ingot. The molten aluminum was initially cooled by the primary cooling of the water jets from the manifold that hit the outer perimeter of the mould wall, and then from secondary cooling as the water ran down the side of the ingot after it exited the mould. The starter block was on the end of a hydraulic piston that lowered the ingot into the casting pit in the floor at a constant rate. There were pre-existing displacement and velocity transducers attached to the starter block base plate. These were used to measure the position of the starter block and the casting speed during the casting experiment.

In this chapter, the alloys used in the two experiments as well as the hardware and software required to run the experiments are described. The procedure used to make the thermocouple assemblies are discussed along with the differences and improvements made to the first experiment design for the second experiment.

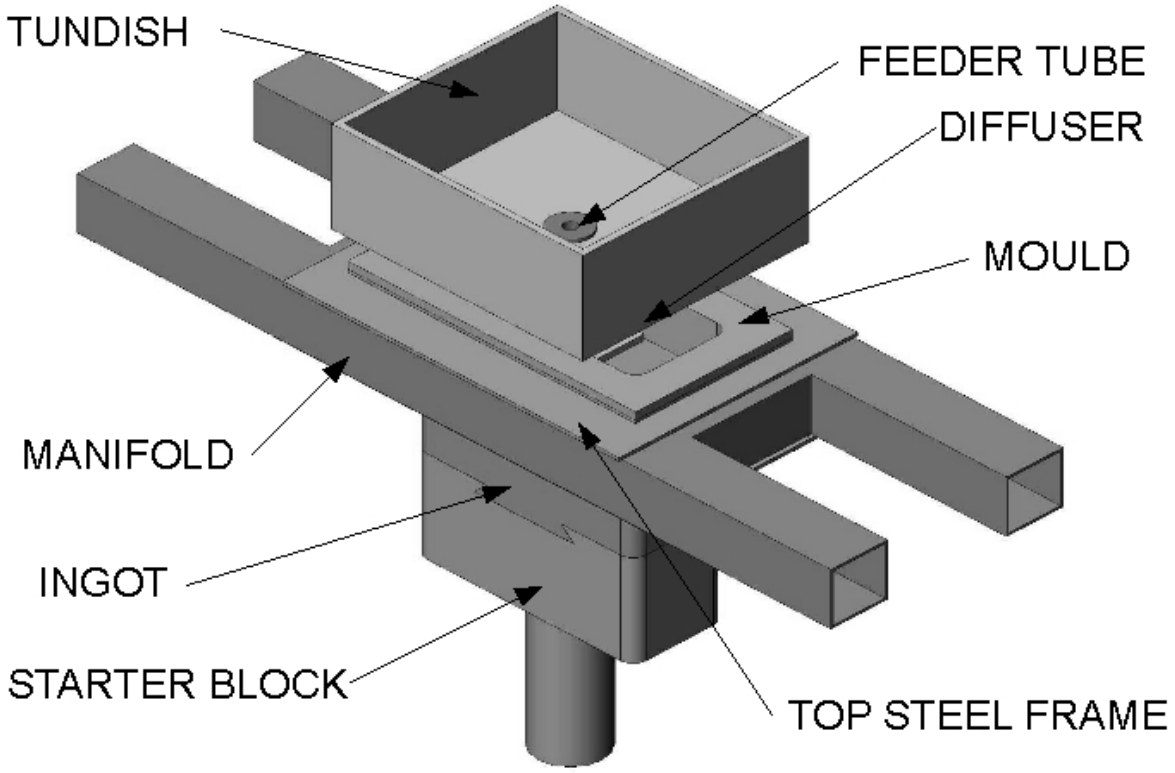

Figure 3-1: Solid model of the lab-scale DC caster at Novelis.

3.1 Experimental Materials

The properties of aluminum alloys can vary widely from one alloy to another [30]. To ensure the CFD model can give accurate DC casting simulations for aluminum alloys with different properties, three different alloys were used for the experiments: AA3003, AA4045, and AA6111. Table 3-1 and Table 3-2 show the material properties and nominal compositions of the aluminum alloys used in the experiments. Table 3-3 shows the spectrographic compositions of the alloys used in the experiments. These vary slightly from the nominal compositions since each batch of alloy will have a specific composition within the nominal range. These three alloys were chosen since they are commonly used in the casting industry, including co-casting. AA3003 and AA6111 are often used as core alloys, since they solidify over a higher temperature range, while AA4045 is used as clad alloy, since it is a brazing alloy that solidifies at lower temperature ranges and will not melt the semi-solid core alloy during co-casting [31].

Table 3-1: The material properties of the aluminum alloys used in the experiment **[30][31]**.

Alloy	Solidus Temperature [°C]	Liquidus Temperature [°C]	Thermal Conductivity at 25°C [W/m·°C]
AA3003	636	655	193
AA4045	571	600	172
AA6111	606	652	205

Table 3-2: The nominal compositions of the alloys used in the experiment (wt. %) **[30]**.

Alloy	Si	Fe	Cu	Mn	Mg	Cr	Zn	Ti
AA3003	0.6	0.7	0.05-0.20	1.0-1.5	--	--	0.2	-
AA4045	9.0-11.0	0.8	0.30	0.05	0.05	-	0.1	0.20
AA6111	0.7-1.1	0.40	0.50-0.9	0.15-0.45	0.50-1.0	0.10	0.15	0.10

Table 3-3: The spectrographic compositions of the alloys used in the experiment (wt. %) **[31]**.

Alloy	Si	Fe	Cu	Mn	Mg	Cr	Zn	Ti
AA3003	0.23	0.60	0.08	1.07	-	-	-	0.01
AA4045	9.88	0.15	-	-	-	-	-	0.02
AA6111	0.75	0.20	0.63	0.14	0.88	-	-	0.05

3.2 Experiment Apparatus

3.2.1 Data Acquisition System

Figure 3-2 shows a diagram of the data acquisition system used in the casting experiments. The data acquisition system was purchased from National Instruments (NI) and consisted of a SCXI-1000 4 Slot Chassis, SCXI-1102 32 Channel Thermocouple Amplifier, and a SCXI-1303 32 Channel Terminal. The SCXI-1000 powered and controled the SCXI modules and a SCXI bus used analog and digital signals to allow the modules to communicate with one another [32]. The SCXI-1102 Channel Thermocouple Amplifier had a maximum sampling rate of 333 kilo-samples per second with cold junction compensation on each channel. Filters were required because output voltage signals from the thermocouples were often low, in the range of millivolts, making them susceptible to ambient electrical noise [33]. The channel thermocouple amplifier had 2 Hz low-pass filters on each channel that attenuate

higher frequency noise so that the higher frequency noise was removed thereby providing a smoother signal [34]. Each channel could be programmed to sense inputs of ±100 mV or ±10 V. The SCXI-1303 32 Channel Terminal allowed the wires from the thermocouples to be connected or disconnected from the data acquisition system using screw terminals. For cold junction compensation, the terminal also included an onboard temperature sensor.

A data acquisition program was written using LabView [35]. This program was used to provide an interface between the National Instruments data acquisition system and the computer and to record the temperatures and voltages and output the results to a text data file suitable for post-processing using an Excel spreadsheet.

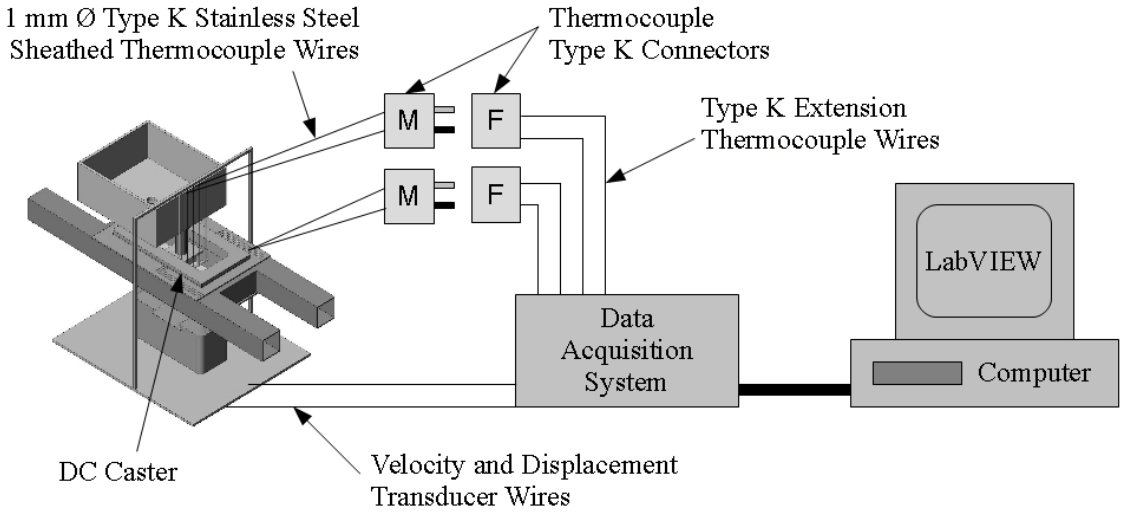

Figure 3-2: A schematic of the experimental data acquisition system.

3.2.2 Thermocouple Array Assembly of the First Set of Casting Experiments

Type K, chromel-alumel, thermocouples were chosen due to their capability of measuring temperatures of up to 1250°C. The thermocouples were sheathed with 304 stainless steel in order to provide rigidity as well as to protect the two fine 0.18 mm diameter chromel-alumel wires from alloying and dissolution in the molten aluminum. The thermocouples had a diameter of 1 mm with an exposed welded bead to ensure fast reaction time.

The length of each type K stainless steel sheathed thermocouple wire was 600 mm. The first 300 mm was cast into the ingot after the casting process reached steady state. The remaining length was used to keep the connectors, wires, and thermocouple lowering assembly a safe distance above the mould and molten metal.

In the initial casting experiments, the individual thermocouples were cut from a spool of thermocouple wire and a thermocouple bead was made by hand on one end using the following procedure. Before stripping the sheath, the thermocouple wire was clamped between two pieces of wood in a vice. The wood prevented the deformation of the sheath when the thermocouple was clamped since a flattened thermocouple would not fit into the stripping tool. Only a short length, 10 mm to 20 mm, of the thermocouple was exposed for stripping. The longer the exposed thermocouple was, the more likely the sheath buckled during the stripping operation or the sheath even became twisted and jammed in the stripping tool.

Both ends needed to be stripped to ensure the wires were not twisted by the stripping tool, since twisted wires inside the sheath formed a second junction and caused temperature reading errors. After both ends of the thermocouple wires were exposed, the magnesium oxide powder insulation was removed from the wires as shown in Figure 3-3. The alumel and chromel wires were then twisted together on one end of the thermocouple to form a junction, care was taken to keep the wires inside the sheath straight and separated. The twisted ends were then cut until only about 3 mm of wire was left exposed and then cleaned with alcohol. The tip was dipped into ASTM B813 WSF 100 flux before welding with a water torch. The water torch was an oxyhydrogen torch which used hydrogen and oxygen gases it produced through the electrolysis of water to create a high temperature flame. The flame was approximately 15 mm long and nearly invisible in a well lit room. Brazing goggles were worn during welding to protect the eyes. The tip of the twisted wire was placed into the hydrogen flame of the water torch and removed once a molten bead of metal formed on the end of the sheath as shown in Figure 3-4.

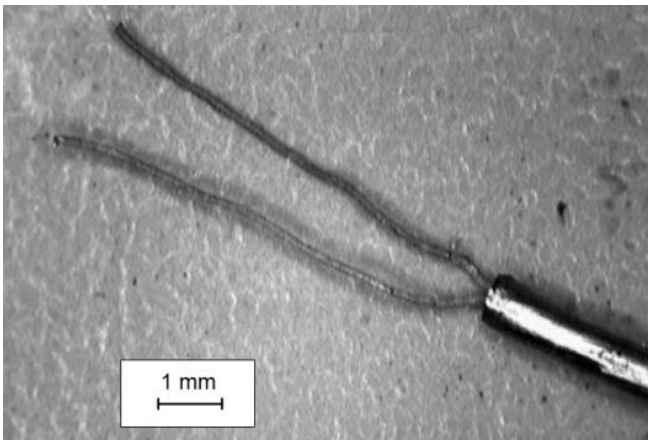

Figure 3-3: Exposed thermocouple wires stripped of the 304 stainless steel sheath.

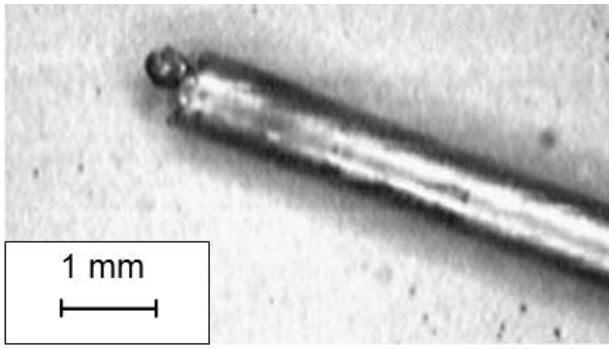

Figure 3-4: A handmade thermocouple bead after welding.

Each thermocouple was tested using a digital thermometer to ensure it was functioning properly. As shown in Figure 3-5 and Figure 3-6, an array of seven thermocouples was made to measure the time temperature history within the ingot during casting. Figure 3-5 shows the row of thermocouples in the mould where 1 mm of clearance was maintained between the spacer and the mould on both sides. To keep the thermocouples in place, the thermocouples were inserted through a 304 stainless steel strip of metal 1.3 mm thick, with drilled holes to position and hold each thermocouple. By selecting a spacer material to be the same steel as the thermocouple sheath, the weld bond would be stronger than with mixed metals. The thermocouples protruded 10 mm past the spacer so that the junctions were not too close to the steel sheet spacer which might interfere with the flow of molten aluminum around the thermocouple bead. Pulsed laser Nd:YAG (neodymium-doped yttrium aluminium garnet) beam spot welding was used to fix the thermocouples in place on the spacer. Because laser welding has a small concentrated heat affected zone with high rates of heating and cooling, it is a good choice for welding small components such as stainless steel sheathed thermocouples.

Before laser spot welding the thermocouples to the spacer, the sheath and spacer were cleaned with acetone, and the residual water and acetone was removed with alcohol. The row of thermocouples in the spacer is shown with the welding jig in Figure 3-6. Each thermocouple was welded on both sides of the sheath. A welding jig was designed to keep the thermocouples spaced properly and ensuring that all the thermocouples protruded past the spacer an equal distance. The laser beam welder with the thermocouple assembly and jig is shown in Figure 3-7. The jig held the thermocouples at a 45 degree angle to allow the laser to melt the thermocouple sheath and spacer simultaneously. A 5 ms laser pulse with an energy of 11.9 J was the setting used to make the weld. Argon shielding gas delivered at a flow rate of 368 litres per hour through nozzles directed at the site of the weld was used to prevent oxides from forming and reduced embitterment of the weld. The finished assemblies were extremely delicate and had to be treated very carefully to avoid the fine wires, bead, and spot welds from breaking.

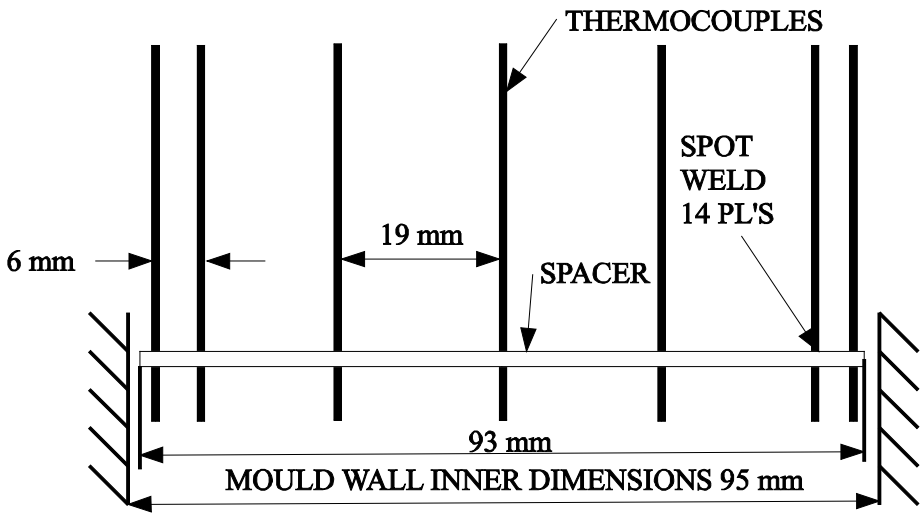

Figure 3-5: The thermocouple spacing and arrangement.

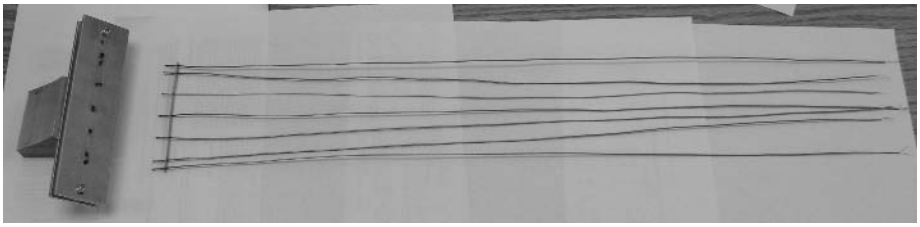

Figure 3-6: The thermocouple assembly and the welding jig.

Figure 3-7: Pulsed Nd:YAG laser welding system used to spot weld the thermocouples to the steel spacer.

Every cast had three sets of thermocouples entering the mould with a spacing of 50 mm between each set as shown in Figure 3-8. A threaded rod was used to stabilize the thermocouples and prevent the jet of molten aluminum from the diffuser from pushing the thermocouples away from the centre of the mould. Spacing of 50 mm between each set of thermocouples was chosen so that as one set exits the mould, another set enters the molten metal. Due to symmetry, pairs within each set of thermocouples could be compared with one another. Having three sets of thermocouples allowed a standard deviation to be calculated.

Figure 3-9 shows the experimental setup at Novelis in Kingston, Ontario. This was the first series of experiments run where three sets of thermocouples were fed into the mould in each cast. Type K male and female connecters were used to reduce setup time between casts. These connecters were attached to 24 gage type K thermocouple extension wire, which were then screwed into the terminals of the data acquisition system.

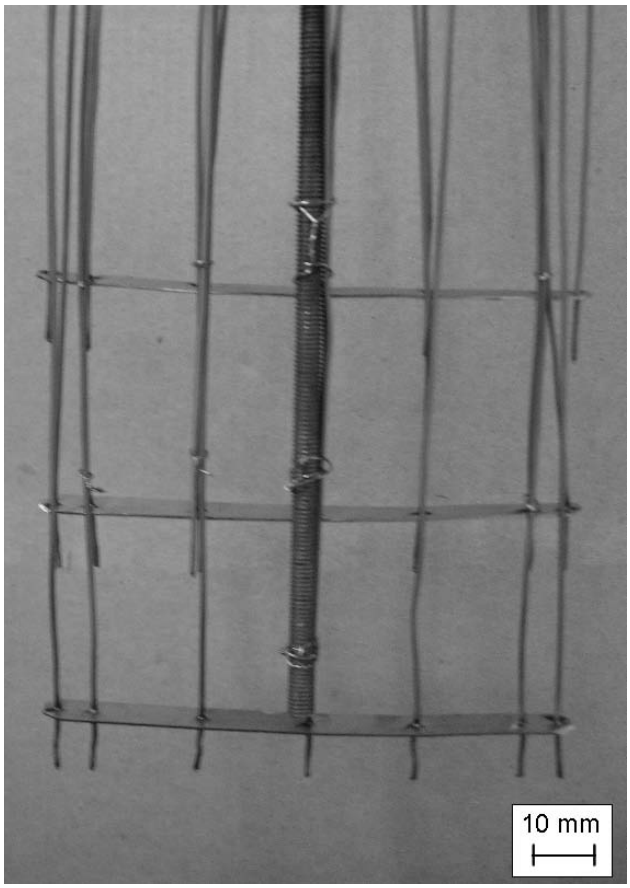

Figure 3-8: Three sets of thermocouples arrays were spaced 50 mm apart in the casting direction and held in place using a 3.2 mm Ø threaded steel rod.

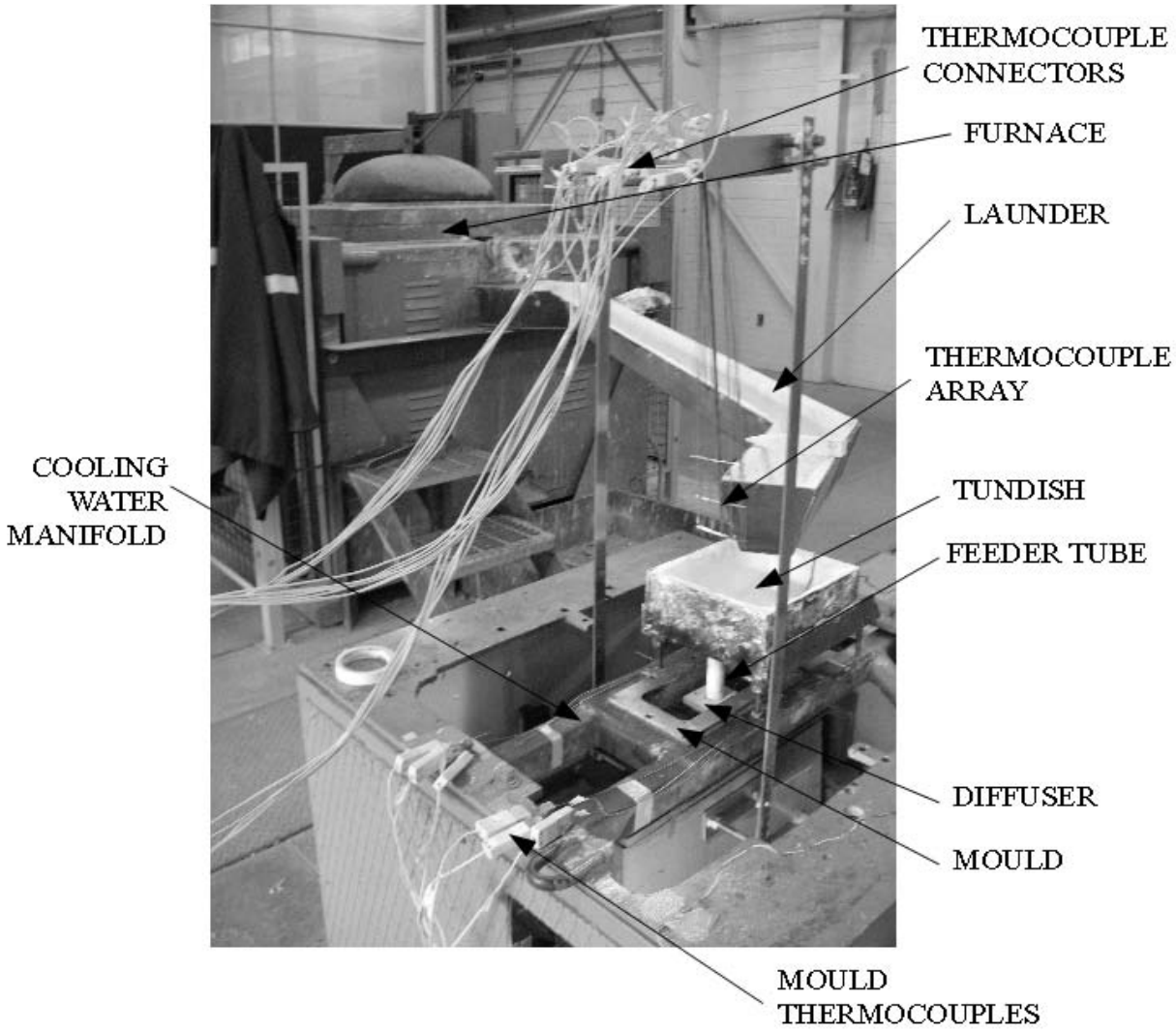

Figure 3-9: The DC casting experimental set up at Novelis in Kingston.

3.2.3 Thermocouple Array Assembly for the Second Set of Casting Experiments

Experience with the operation and performance of the initial thermocouple array during the first set of casting experiments showed that there were a number of deficiencies in the design of the apparatus. There were a significant number of thermocouples which failed because the handmade thermocouple beads did not survive direct contact with the molten aluminum or the thermal strains in the cooling ingot. In addition, there was clearly significant fluid drag generated by the array of thermocouple wires which resulted in the array being pushed well out of the desired position in the ingot by the fluid motion in the sump. Therefore, a number of changes were made to the experiment design and thermocouple assemblies to improve the results and limit the effect the thermocouples had on the fluid flow in the sump during the experimental cast.

All of the type K stainless steel sheathed thermocouples with 1 mm (0.04 in.) diameter sheaths and exposed beads were replaced by type K stainless steel thermocouples with 1.59 mm (0.062 in.) diameter sheaths and grounded pre-made thermocouple beads. A picture of a premade thermocouple is shown in Figure 3-10. Figure 3-11 shows a schematic of the cross sectional views of an exposed and a grounded thermocouple bead. The stainless steel sheath of the grounded thermocouples covers the bead and this protects the bead from direct contact with the molten aluminum which can dissolve or damage the fine thermocouple wires. The thicker, pre-made grounded thermocouples were better than the thermocouples used in the first experiments, because the thermocouple beads and fine wires were protected from the molten aluminum by the stainless steel sheath and were less likely to fail during casting. Having thermocouples machine-made also made the thermocouple behaviour more consistent with one another than welding the thermocouple junctions manually. Magnesium oxide insulation is more effective with larger diameter probes meaning the 1.59 mm diameter thermocouples are able to survive at higher temperatures [36]. The response time of the thermocouples increased from 0.16 seconds with the 1 mm diameter ungrounded probe to 0.19 seconds with the 1.59 mm diameter grounded probe. This was not considered a significant increase according to Figure 3-12, because both probe diameters were relatively small [36] and the response time was still 2.5 times faster than allowed by the 2 Hz low pass filter used in the data acquisition system.

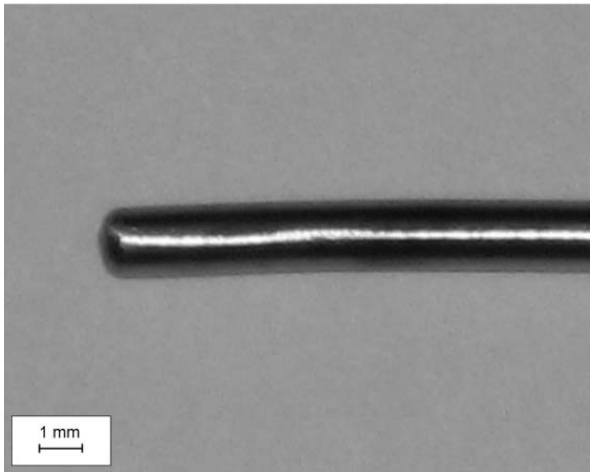

Figure 3-10: Premade type K grounded stainless steel sheathed thermocouple bead.

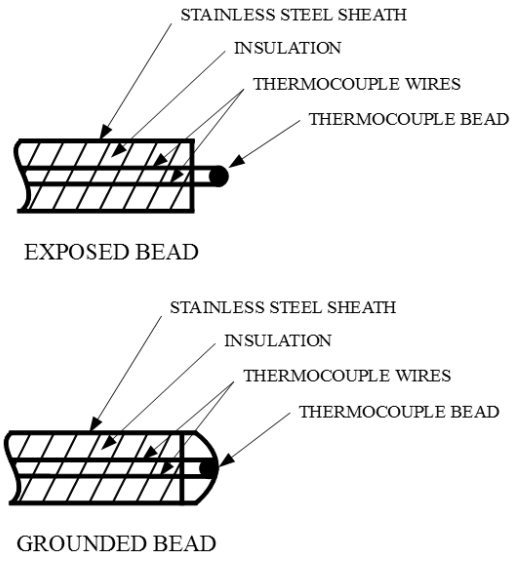

Figure 3-11: Cross section of an exposed and grounded thermocouple bead.

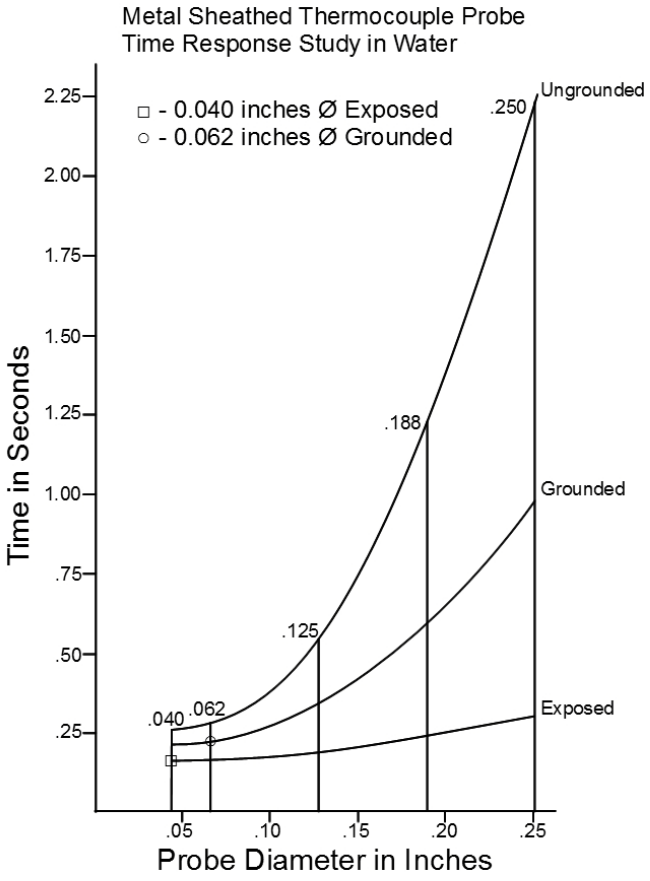

Figure 3-12: Thermocouple response time (taken from **[36]**).

The thermocouple wires were 600 mm long with type K male connectors attached to the ends. Similar to the first experiment, the first 300 mm was cast into the ingot allowing time for the casting process to reach steady state and the remaining length was used to keep the connectors and wires a safe distance above the hot mould and molten metal. All of the thermocouples were tested with a digital thermometer to ensure they were functioning properly. Rather than using flat steel spacers, shorter round spacers made from 3.2 mm diameter 12L14 carbon steel rods were used instead to keep the thermocouples positioned correctly. The 12L14 carbon steel was chosen due to its high machinability, which was required to drill fine holes through the rod for the thermocouples. The spacer was also 4.1 mm shorter than the original spacer design so that aluminum would be able to flow between the spacer and the mould. A cylindrical spacer provided more rigidity and was less prone to warping under the high temperatures during the cast than the first sheet metal spacer design. Figure 3-13 shows the row of thermocouples in the mould where 3 mm of clearance was maintained between the spacer and the mould on both sides.

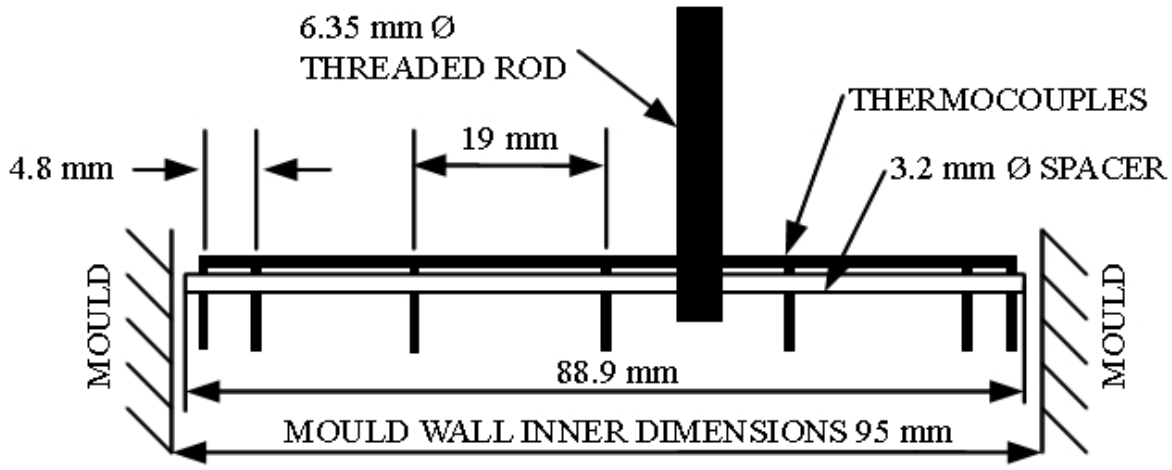

Figure 3-13: The thermocouple spacing and arrangement for the second experiment.

Holes with a diameter of 1.59 mm were drilled though the steel rod so that the thermocouples would be held in place when inserted though them. The thermocouples protruded 10 mm past the spacer so that the flow of molten aluminum around the thermocouple bead would not be hindered. A 6.35 mm Ø threaded rod was offset 9.5 mm from the centre so that it did not interfere with the centre thermocouple. The threaded rod was used to prevent the jet of molten aluminum exiting the diffuser from pushing the thermocouples away from the centre of the mould. Unlike the previous design, the threaded rod on the second experiment ran the entire length of the ingot and was secured on both ends so that the entire

thermocouple assembly with the spacer was fixed in place. On the bottom, the threaded rod was inserted through a hole in a t-shaped steel sheet, shown in Figure 3-14. Two nuts on the rod on both sides of the t-shaped steel were used to hold the rod and steel sheet together. The t-shaped steel sheet metal rested on the starter block and was fit snugly in the mould in the casters starting position. The shape prevented the bottom of the threaded rod from moving, but still allowed molten aluminum to flow around the t-shaped piece into the starter block dove tail. As the aluminum solidified around the rod, the end of the threaded rod was fixed in place permanently ensuring that the thermocouples entered the mould vertically. The top of the threaded rod was secured to the thermocouple holder so that the rod remained in its vertical position.

A 3.2 mm Ø hole was drilled through the centre of the 600 mm long threaded rod. This hole allowed the steel rod spacer to be inserted and held in position 300 mm above the starter block. Figure 3-15 shows a thermocouple assembly. Only one hex nut was required since it tightened the spacer against the hole in the threaded rod, thus securing it in place. Having the hex nut placed above the thermocouples rather than beside them allowed more room for aluminum to flow around the thermocouples. The symmetry of the thermocouple positions on the spacer allowed the three outer pairs of thermocouples to be compared with one another.

Unlike the first experiments, the thermocouple array used in the second experiments had only one set of seven thermocouples entering the mould rather than three sets of seven thermocouples. The advantage of using only one set was to limit the number of thermocouple wires in the mould during the experiment, hence limiting the impact the measurement devices had on the fluid flow in the sump during the experiment. The thermocouple wires were bent in such a way that all the wires could be tied down to the spacer using steel twist tie wires as it ran along the spacer and up the threaded rod. Having all the wires tied to the threaded rod and running up to the type K miniature connectors was deemed to be beneficial since the thermocouple wires would not form a wall-like barrier in the mould as the first experiment design had. By minimizing the effect of the wires on the measurement, better data can be expected. Like the first experiment, the type K connecters were attached to 24 gage type K thermocouple extension wires, which were then connected to the terminals of the data acquisition system.

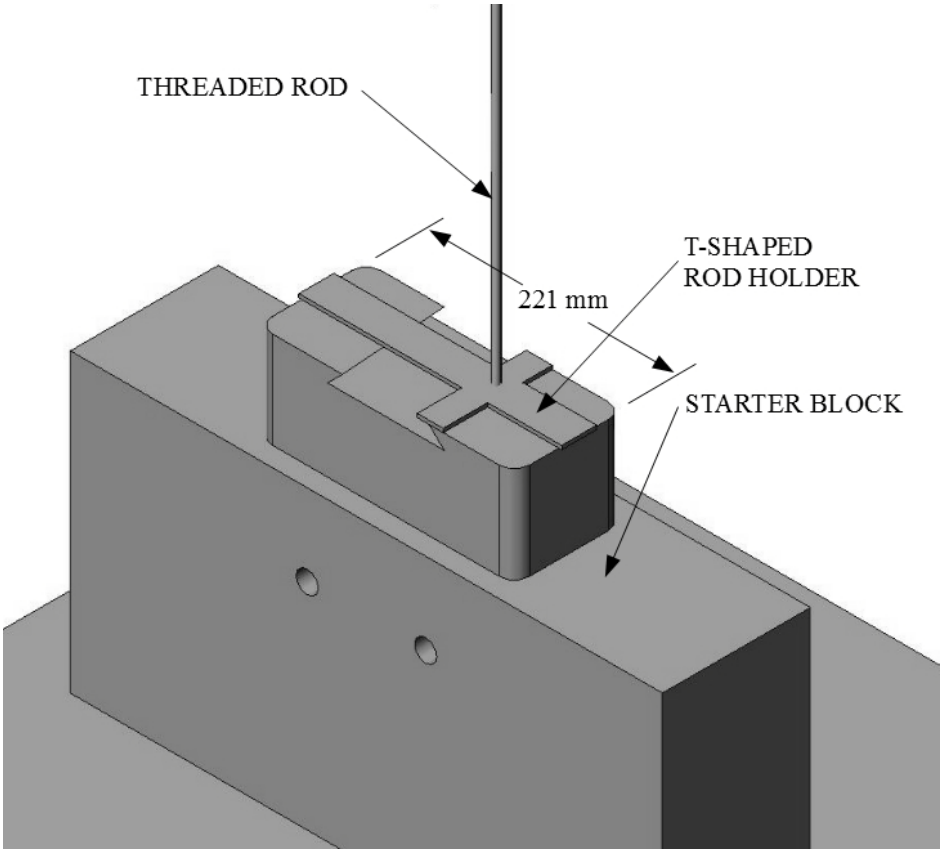

Figure 3-14: The t-shaped rod holder is positioned on the starter block.

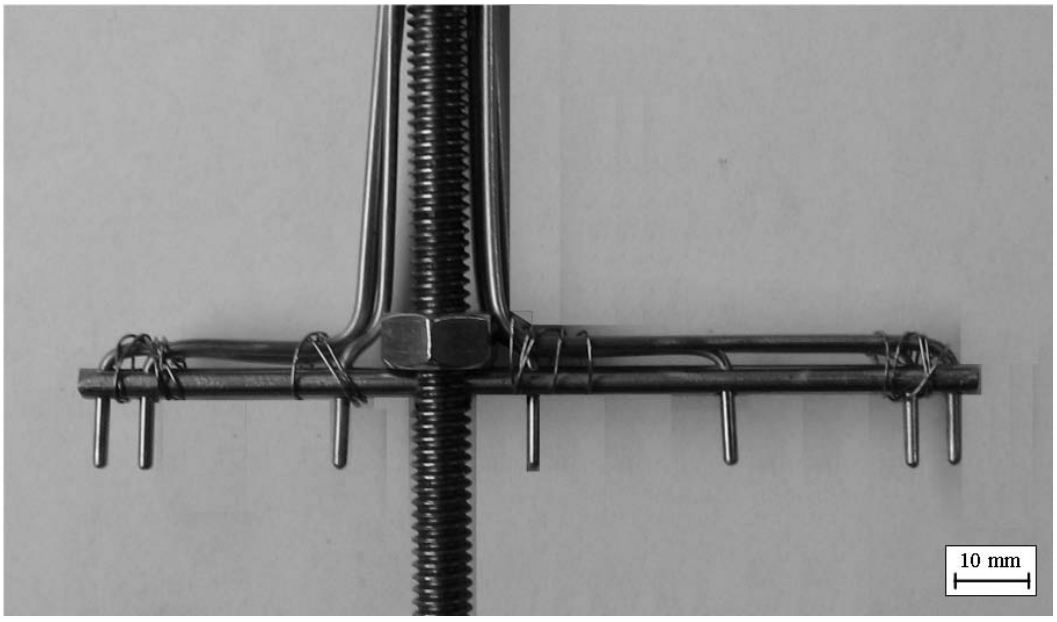

Figure 3-15: Thermocouple array for the second series of experiments.

3.2.4 Tundish Modification

For these experiments, it was necessary to move the tundish towards one side to allow the thermocouples to be inserted in a location close to the centre of the ingot. The feeder tube and diffuser were kept in the same location at the centre of the mould. Figure 3-16 shows a front section view of the DC caster with the tundish offset. A new hole was drilled for the feeder tube, while the existing hole was plugged. The thermocouples were lowered near the centre of the wide face of the mould, 75 mm from the closest narrow face of the mould. The thermocouples were far enough away from the cooling effects of the narrow face that a simplified two-dimensional assumption may be used for the resulting thermal contours rather than a more complex three-dimensional assumption.

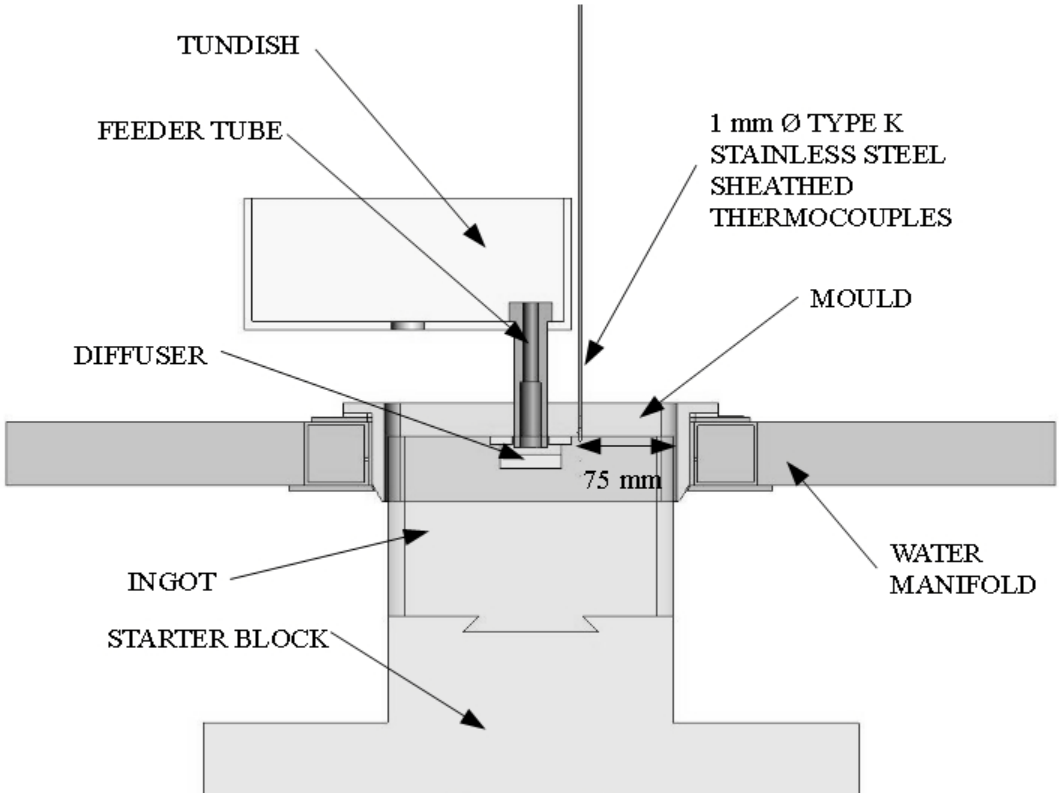

Figure 3-16: The DC caster with the tundish shifted left to allow thermocouples to enter the mould near the centre of the mould.

3.2.5 Thermocouple Stand

It was necessary for the thermocouples to be lowered into the mould at the same rate as the starter block descended so that the voltage outputs for the displacement and velocity transducers could be used to determine the temperature at a particular position and time during the cast. For this reason, a thermocouple stand was attached to the starter block and used to lower the sets of thermocouples into

the mould as shown in Figure 3-17. Two 12.7 mm Ø threaded rods were inserted through the existing holes in the starter block. The threaded rods were fixed in place by tightening hex nuts against the starter block. Two steel strips 1000 mm long, 25.4 mm wide, and 3 mm thick were used to support the thermocouple connector tray. The thermocouple lowering stand was kept in a vertical position by bracing the assembly at the bottom using steel supports. The tray centered 600 mm above the mould was made from sheet steel and the two threaded rods were inserted through one of the steel strips, through the tray, and then through the second steel strip. The entire assembly was adjustable in both the vertical and horizontal positions and held in place by hex nuts. The tray allowed a place for the thermocouple connectors to rest and to ensure they did not fall into the mould and sump during the cast.

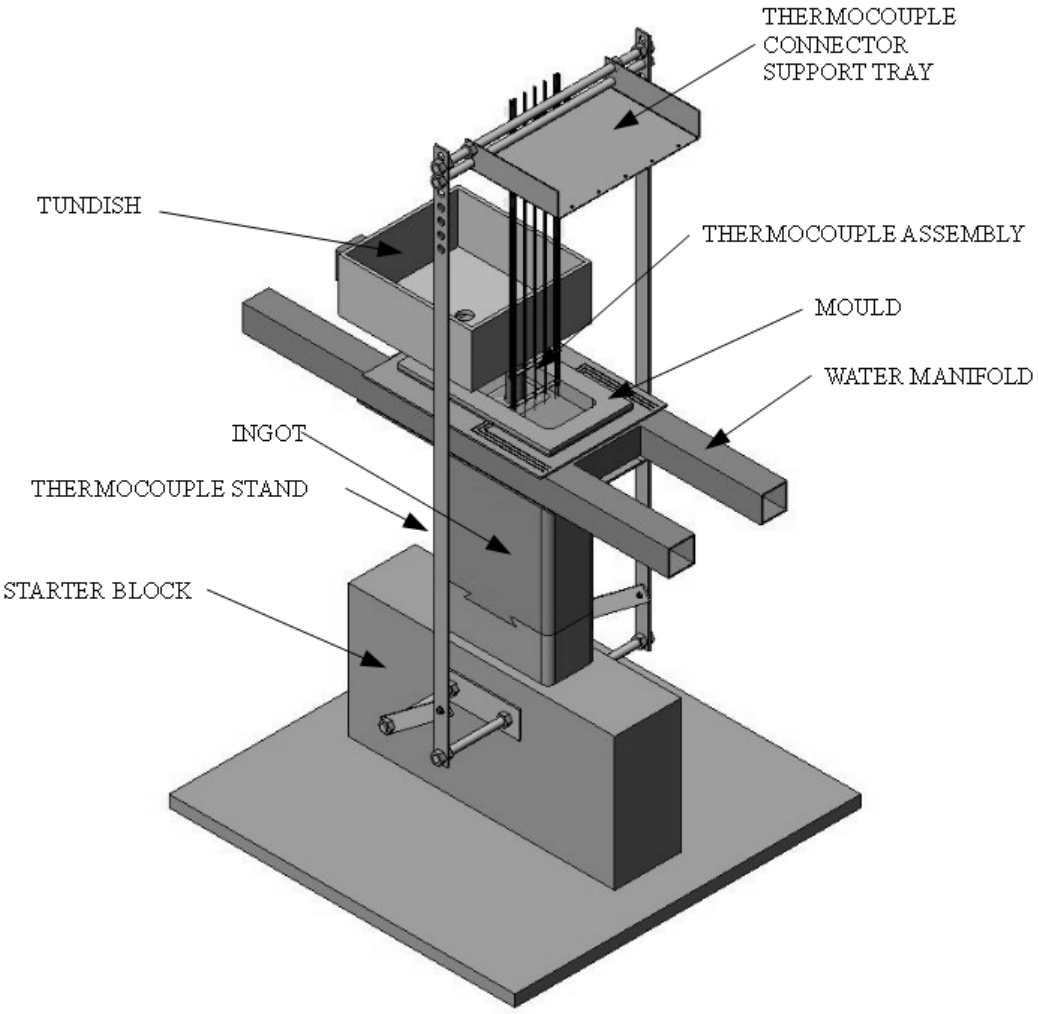

Figure 3-17: The thermocouple lowering stand on the DC caster.

3.2.6 Melt Poisoning

A measuring technique known as melt poisoning was also used to find the sump profile. Because this measurement technique was independent of the thermocouples, it provided a second method to confirm the validity of the thermocouple readings. It also provided a continuous outline of the thin shell and sump profile which was not attainable with only seven discrete thermocouples, especially the shell. Melt poisoning involved pouring about a half litre crucible of 50% aluminum-50% zinc molten alloy heated to the pouring temperature into the mould during a cast. The zinc mixed throughout the molten material in the sump very quickly as the ingot solidified and caused a sudden change in solidification microstructure that was used to delineate the sump shape. To reveal the sump, a 10% solution of sodium hydroxide was applied on a sectioned face of the ingot to etch the surface. The zinc reacted with the sodium hydroxide solution and turned black thereby revealing the sump profile. To ensure the molten aluminum zinc mixture did not affect the results of the thermocouples, it was heated to the same pouring temperature as the melt and poured into the cast only after all the thermocouples had solidified into the ingot.

3.2.7 Mould and Other Thermocouple Locations

In addition to the 21 thermocouples used in the first experiments to measure the temperature contours in the ingot, three thermocouples were inserted into the mould on the outer wide face of both sides of the mould on the same plane at which the thermocouples are being lowered, i.e., 75 mm from the inner length of the mould. The purpose of the mould thermocouples was to help validate the mould wall temperatures for the CFD simulations. Figure 3-18 shows a cross sectional view of the mould where the mould thermocouples are positioned 13 mm apart, with the top thermocouple 32 mm from the top of the mould. The thermocouples were located 3 mm away from the inner surface of the mould because drilling any deeper into the wall would risk damaging the mould.

Other thermocouple data that were recorded during the experiment included the tundish temperature, the cooling water inlet temperature, and the water temperature coming off the ingot during casting. For the tundish temperature, the thermocouple was placed near the feeder tube hole at the bottom of the tundish. It was important not to have the thermocouple inserted directly into the feeder tube hole as there may be a greater risk of freeze off in narrow spaces. The water inlet temperature was measured by placing the thermocouple inside one of the manifold water outlet holes. The thermocouple was bent so that it exited with the other three mould thermocouples. The water outlet temperature was measured by attaching a thermocouple to the starter block such that the water coming off the ingot fell onto the head of the thermocouple probe.

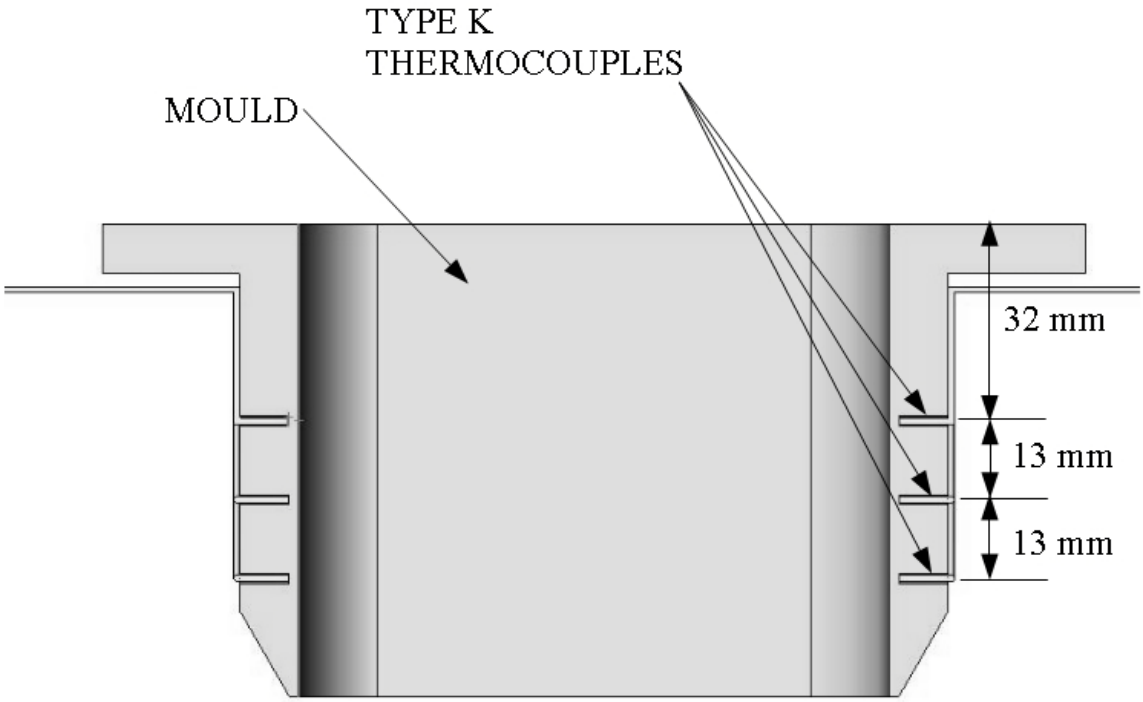

Figure 3-18: Cross section showing placement of the six mould thermocouples.

3.2.8 Thermocouple Channel Numbering

The thermocouples were numbered in a consistent manner in all casting experiments. The first set of thermocouples was numbered from 1 through 7, the second set was numbered from 8 through 14, and the third set was numbered from 15 through 21. The numbering system for the first series of experiments is shown as a section view of the direct chill caster in Figure 3-19 and the numbering for the second series of experiments is shown in Figure 3-20. The mould thermocouples were numbered from 22 through 27, the water inlet and outlet temperatures were numbered 28 and 29 respectively. The tundish temperature was numbered 30, while the displacement and velocity were numbered 31 and 0, respectively. These numbers corresponded to the terminal numbers on the data acquisition system and the same numbering system and were used in plots to define the location of the thermocouple.

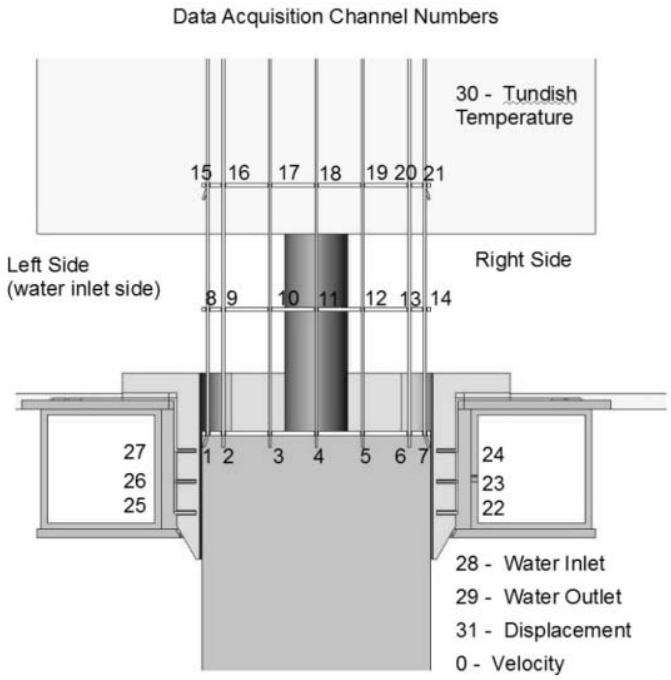

Figure 3-19: Channel numbering for the first series of experiments.

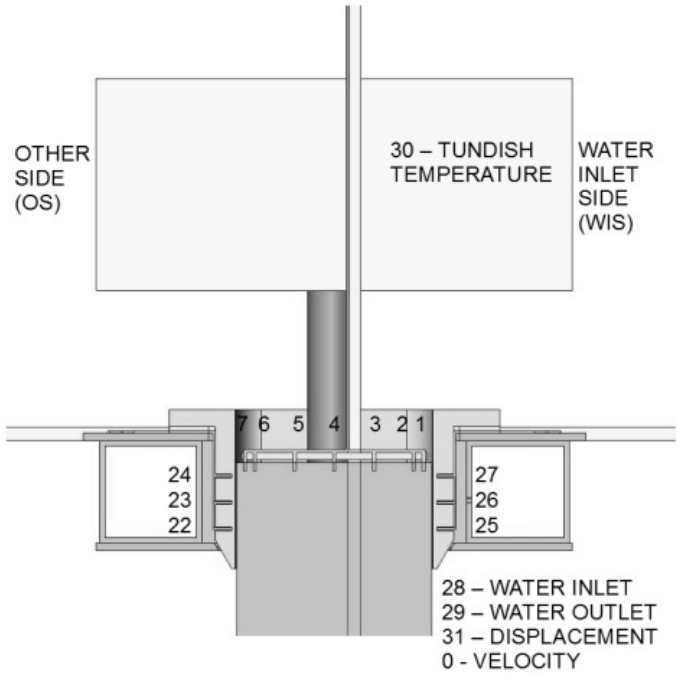

Figure 3-20: Channel numbering for the second series of experiments.

3.3 Calibration of the Transducers and Thermocouples

3.3.1 Displacement and Velocity Transducers

To measure the velocity and displacement of the starter block as it moved down during casting, a 20 AWG polyvinyl chloride insulated solid copper hook-up wire was used to connect the data acquisition system to the pre-existing starter block displacement and velocity transducers. Before running the experiments, the experimental equipment and data acquisition system were tested and calibrated for precision and accuracy. The pre-existing velocity transducer on the DC casting machine was tested to confirm that the velocity varies linearly with voltage by raising and lowering the starter block at different speeds. The pre-existing displacement transducer was also tested to confirm that the voltage varies linearly with distance. The results are plotted in Figure 3-21, Figure 3-22, and Figure 3-23. The measurements were used to derive calibration equations for converting the voltage signals into velocities and displacements. To convert the voltage to displacement in millimeters and casting speed in millimeters per second, the following formulas were used:

$$\text{Displacement [mm]} = \text{Voltage} \times (-194.6025) - 122.7883 \quad (\mathbf{3.1})$$

$$\text{Velocity [mm/s]} = \text{Voltage} \times 0.5265 - 0.0579 \quad (\mathbf{3.2})$$

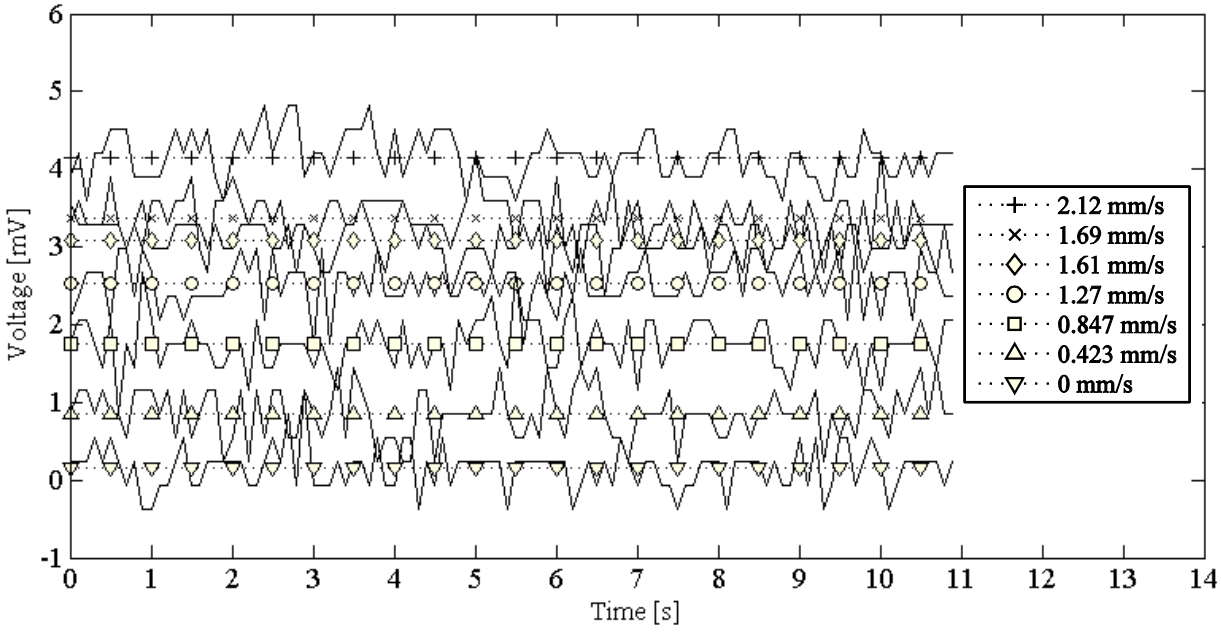

Figure 3-21: Measured velocity transducer voltage versus time for five different casting speeds.

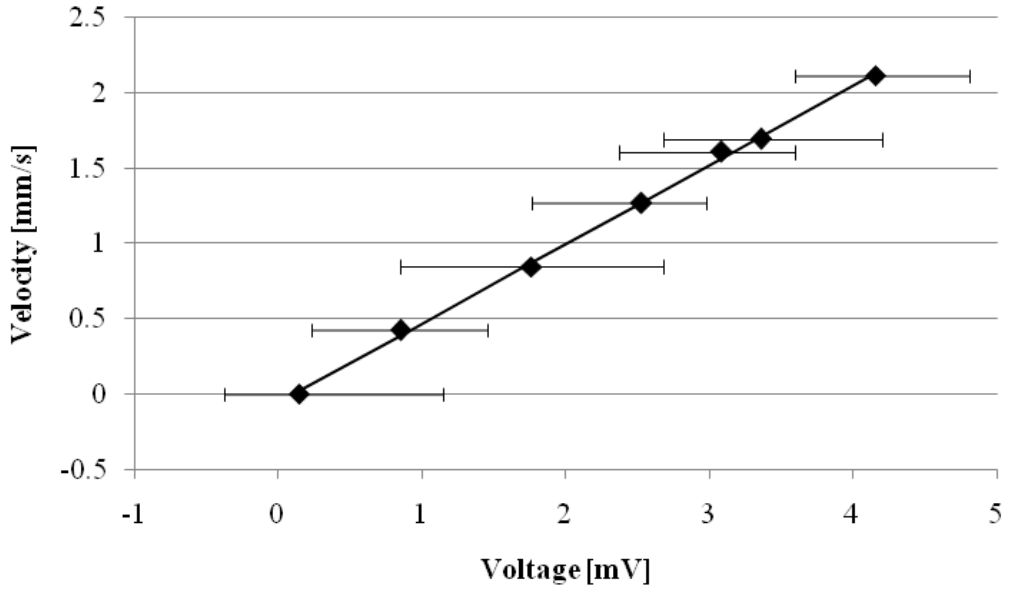

Figure 3-22: Measured voltage transducer voltage versus casting speed.

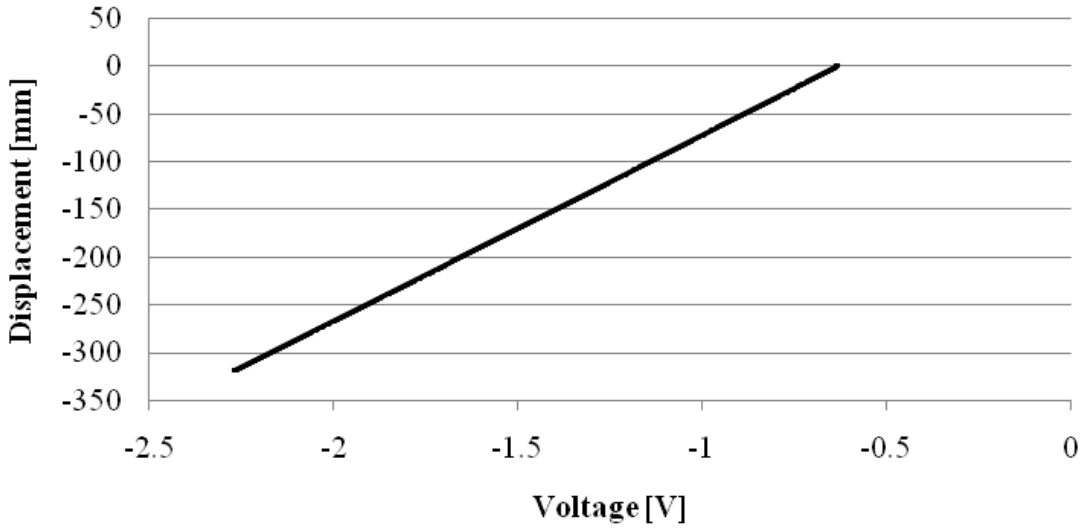

Figure 3-23: Measured displacement transducer voltage versus position of starter block with respect to the mould.

3.3.2 Thermocouples

In order to test the accuracy of the data acquisition system and the thermocouples, it was necessary to test the experimental equipment against known properties such as the boiling and melting points of an element [37]. Pure aluminum has a melting point of 660°C. Pure aluminum in a crucible was heated to 800°C in a furnace where it became liquid. Immediately after removing the crucible from the furnace

and setting it on a insulated table to cool, a thermocouple was inserted into the molten metal to obtain a cooling curve. A representative result is shown in Figure 3-24. It can be seen that where the line plateaus is the melting temperature of aluminum. For approximately 130 seconds, the metal released latent heat at a recorded temperature of 656°C until it finally solidified. The National Instruments SCXI 1102 32 Channel Voltage Input Module has a cold junction sensor accuracy of ±1.0°C and for type K thermocouples, a measurement accuracy of ±0.7°C for temperatures between 0°C and 500°C and a measurement accuracy of ±1°C between 500°C and 1000°C [34]. The type K thermocouple connectors have an uncertainty of ±0.5°C [38]. The stainless steel sheath type K thermocouples and extension wire have an accuracy of ±2.2°C or ±0.75%, whichever is greater [36]. The voltage to temperature conversion has an uncertainty of 0.8°C [38]. The root square sum (RSS) of the uncertainty of the cold junction sensor, the measurement accuracy of the input module, the thermocouple and extension wire, the connectors, and the voltage to temperature conversion is approximately ±7.5°C. Detailed calculations are found in Appendix A. Since the recorded temperature of 656°C is only 4°C less than the actual temperature, it is an acceptable result, because it is within the equipment's uncertainty range.

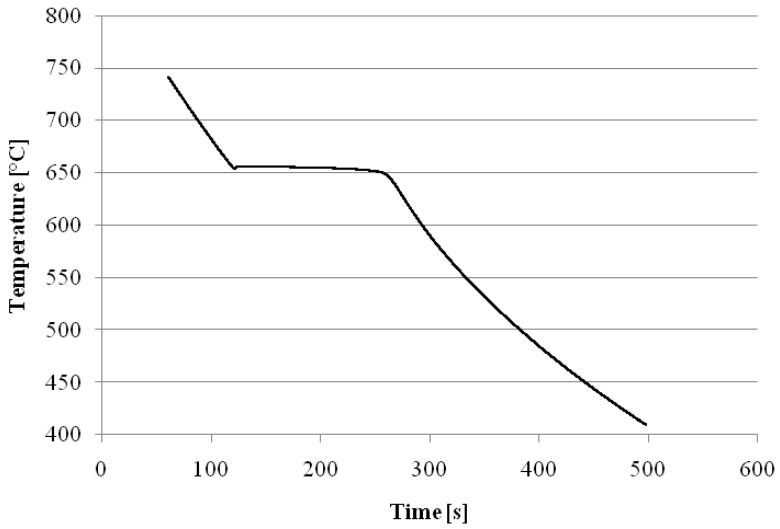

Figure 3-24: The cooling curve of pure aluminum.

To gain confidence of the accuracy and precision of the thermocouples and the data acquisition system, 54 thermocouples were tested in both ice water at 0°C and boiling water at 100°C. The allowable uncertainty of the thermocouples is ±2.2°C and the measurement accuracy of the input module is ±0.7°C. The total uncertainty of the measurement is the root square sum of the uncertainty which is ±3.5°C. Detailed calculations are shown in Appendix A. The results of the tests are shown in

Figure 3-25 and Figure 3-26. An ice bath was created using ice chips mixed with water. The mean temperature was found to be -0.23°C, and is well within the allowable uncertainty of ±3.5°C. The standard deviation of the thermocouples is only 0.03°C for the ice water test. The boiling water test result is also within the allowable uncertainty yielding a mean temperature of 98.6°C and a standard deviation of 0.33°C. From testing the thermocouples in molten aluminum, ice water, and boiling water, it can be concluded that although the results are slightly bias in the negative direction, the precision and accuracy are well within the experimental equipment's allowable uncertainty range.

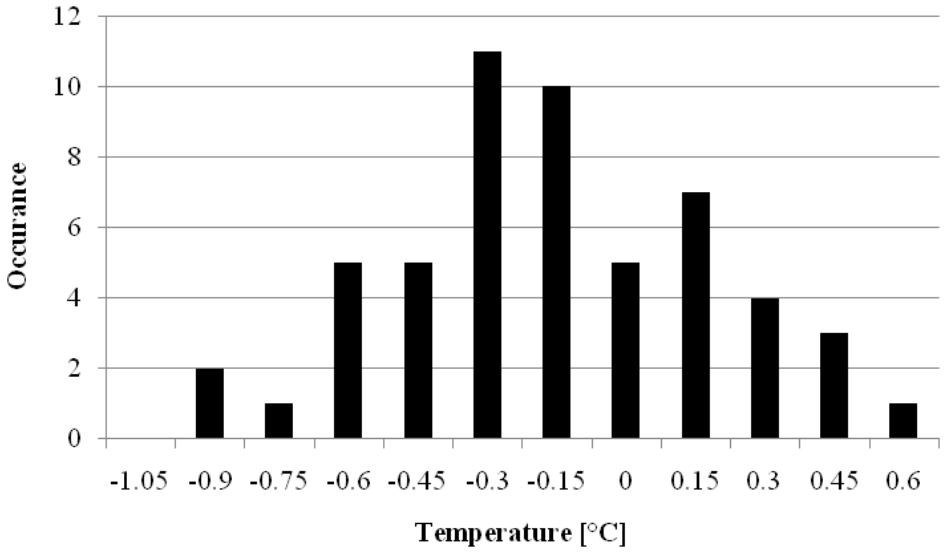

Figure 3-25: The temperature distribution of thermocouple readings in ice water.

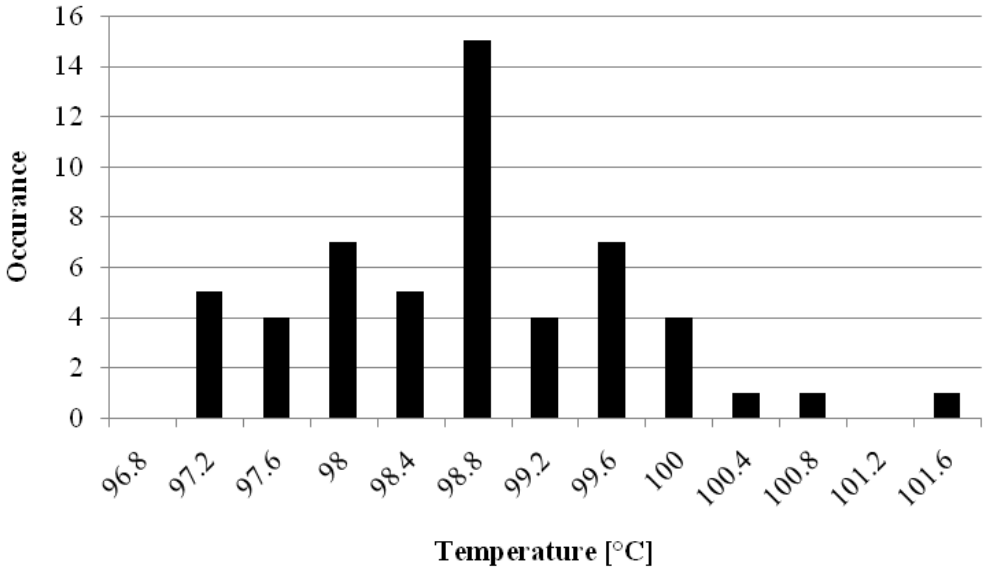

Figure 3-26: The temperature distribution of thermocouple readings in boiling water.

3.3.3 Water Flow Rate

The water flow rate used to cool the ingot during casting was measured to check the reliability of the gauge. Typically, the flow rate gauge is set to 1.5 litres of water per second. To verify the actual flow rate, the time it took to fill a 10 litre bucket was taken. Seven trails were taken and a water flow rate average was 1.79 litres per second with a standard deviation of 0.05 litres per second. Although the gauge underestimated the water flow rate, the actual flow rate was known for the experiments since the gauge was always set to 1.5 litres per second.

3.4 Experimental Procedures

3.4.1 Experiments Performed

Two series of casting experiments were performed. The first set of experiments consisted of eight casts. The casting parameters used for these experiments are listed in Table 3-4. The original thermocouple array design with 1 mm Ø type K stainless steel thermocouples with exposed beads and three sets of seven thermocouples were used to obtain three sets of ingot temperature data per cast. A 3.2 mm Ø threaded rod was used to hold the thermocouple arrays steady during the casting (casts 4 through 8).

The purpose of these casting experiments was to determine the effects of alloy, casting speed, water flow rate, and pouring temperature on the sump profile. To do this, the variables were changed one at a time so that any changes could be compared with one another. Having data from additional variables provided more methods to check the reliability of the computational fluid dynamics simulations.

Table 3-4: The casting parameters used in the first series of casting experiments.

Cast #	Material	Casting Speed	Water Flow Rate	Pouring Temperature	Melt Poisoning
1	AA3003	1.91 mm/s	1.79 L/s	700 °C	No
2	AA3003	1.69 mm/s	1.79 L/s	700 °C	No
3	AA3003	2.54 mm/s	1.79 L/s	700 °C	No
4	AA3003	1.91 mm/s	2.69 L/s	700 °C	Yes
5	AA6111	1.73 mm/s	1.79 L/s	700 °C	No
6	AA6111	1.61 mm/s	1.79 L/s	700 °C	Yes
7	AA6111	2.12 mm/s	1.79 L/s	700 °C	No
8	AA6111	1.61 mm/s	1.79 L/s	730 °C	No

The second series of experiments consisted of nine casts. The casting parameters used during these experiments are listed in Table 3-5. The revised thermocouple arrays made with pre-made 1.59 mm Ø

type K stainless steel thermocouples with grounded beads were used. Only one array of seven thermocouples was used in each cast. A 6.35 mm Ø threaded rod offset 9.5 mm from the centre to hold the thermocouple arrays steady during the cast was used during the casts. These casts used an improved thermocouple array design and the results were used in order to validate the results of the first series of experiments, to test a third alloy, AA4045, as well as to provide more reliable data for the computer simulated models. Casts 3, 6, and 9, for the three different alloys AA3003, AA6111, and AA4045, respectively, were cast without any thermocouples in the mould to act as control samples. Being able to compare the melt poisoned and etched sumps of the ingots with and without the thermocouples, the effect the thermocouples might have on the sump shape may be determined.

Table 3-5: The casting parameters used in the second series of experiments with the improved thermocouple array design.

Cast #	Material	Casting Speed	Water Flow Rate	Pour Temperature	Melt Poisoning
1	AA3003	1.69 mm/s	1.79 L/s	700 °C	Yes
2	AA3003	2.33 mm/s	1.79 L/s	700 °C	Yes
3	AA3003	2.33 mm/s	1.79 L/s	700 °C	Yes
4	AA6111	1.61 mm/s	1.79 L/s	700 °C	Yes
5	AA6111	2.12 mm/s	1.79 L/s	700 °C	Yes
6	AA6111	2.12 mm/s	1.79 L/s	700 °C	Yes
7	AA4045	1.69 mm/s	1.79 L/s	640 °C	Yes
8	AA4045	2.12 mm/s	1.79 L/s	640 °C	Yes
9	AA4045	2.12 mm/s	1.79 L/s	640 °C	Yes

3.4.2 Casting Procedure

After setting up the thermocouple stand, the thermocouple assemblies, connecting the hookup wires to the velocity and displacement transducers, installing all necessary thermocouples, and connecting the thermocouples and hookup wires to the terminals in the data acquisition system. The starter block was moved to its starting position in the mould. Measurements of the position of the starter block relative to the mould as well as the starting distance of the thermocouple tips on the arrays relative to the bottom of the starter block were then made. This enabled the position of the thermocouples to be tracked as the starter block was lowered during the cast.

The starter block and the mould must be free from water so that when molten aluminum contacts the starter block in the mould, there will be no water to vaporize and cause steam explosions. Water vapour from contact with molten aluminum is very dangerous since molten aluminum may be ejected creating

a dangerous working environment. Prior to casting, the inside wall of the mould was coated with lard to provide a thin lubricated layer of oil for the aluminum to flow over. The lard protected the inner surface of the mould from direct contact of molten aluminum, extending the life of the mould.

When all was ready for the cast, the cooling water was turned on and left to run for three minutes to allow it to reach a steady-state temperature of approximately 9°C. At this point, the data acquisition system was turned on and recording of data started. The lab technicians, Rick Lees and Peter Rice, ran the DC caster at NGTC in Kingston, Ontario. The furnace was then tipped to allow molten aluminum to flow down the launder into the tundish and down the feeder tube into the mould. When the molten metal level in the mould was approximately 25 mm from the top of the mould, lowering of the starter block was commenced. Meanwhile, the array of thermocouples was lowered towards the mould by the thermocouple lowering stand. After the starter block had moved down 300 mm, the casting process was well into its steady-state condition and the thermocouples entered the mould and penetrated the liquid surface of the molten aluminum. After all the thermocouples had solidified into the ingot, a mixture of 50% molten aluminum and 50% molten zinc, heated to the same pouring temperature as the melt, was poured into the melt in the mould. The casting process was stopped after a predetermined length of ingot had been cast.

3.4.3 Foundry Safety

Safety is an extremely important aspect of running the direct chill casting experiments. Safety equipment included wearing foundry safety clothing, safety glasses, a hardhat with a face shield, steel toed work shoes, and gloves. Materials worn were made of natural fibers such as cotton because they do not melt on exposure to molten aluminum spatter as do some synthetic fiber clothing. This safety equipment offered some protection against possible spatter of molten aluminum as it allowed time for the aluminum to solidify and cool before reaching skin.

There were more than 30 wires going to the data acquisition system, which could create tripping hazards. It was necessary to secure the wires to the floor with tape or to have an overhead crane hold the wires so that they did not interfere with the workers and technicians during the casting experiment.

3.5 Post-Processing of Measurements

3.5.1 Radiograph of Ingots

After the experimental casts were performed, the ingots were sectioned and then x-rayed to determine the exact location of the thermocouples in case the thermocouples had moved from their original positions. The x-rays were performed by Peter Wales at NGTC in Kingston, Ontario. The x-rays were also capable of revealing the sump profile of the ingot if it was melt poisoned due to the differences in radiographic absorptivity with and without zinc. Since the entire ingot could not be x-rayed at the same time due to size limitations, a lead marker was placed 250 mm from the bottom of the ingot to act as a point of reference when the x-rays of the thermocouples were taken. The wide side of the ingot was x-rayed first to determine how much the thermocouple array moved along the length of the mould. When x-raying the section across the narrow side of the ingot, the x-rays could not penetrate through 222 mm of aluminum and still create clear radiographs. To solve this problem, the ingot was cut in half parallel to its narrow face so that the x-rays only needed to travel through 111 mm of aluminum.

The radiographs were developed on a film size of 356 mm × 432 mm on a type AA film. A DN x-ray unit was used with a low focus setting. For a 111 mm thick aluminum part, a setting of 140 kV and 10 mA was used with an exposure time of 2 minutes and 10 seconds at a distance of 914 mm from the surface.

The developed radiographs were at a 1:1 scale so the positions of the thermocouples along both faces of the ingot could be measured directly from the film. The radiographs were important for the first series of experiments, because the thermocouples and threaded rod acted as a cantilever and were pushed well out of position by the jet of molten aluminum. The x-rays were not crucial for the second set of experiments since a threaded rod ran the entire length of the ingot allowing very little room for the thermocouple array to shift.

3.5.2 Determining Thermocouple Bead Position

Since it was not possible to see if the thermocouples moved out of position once they submerged in the molten aluminum during the experiments, it was necessary to confirm the location of the thermocouples in the ingot after the cast. A combination of taking measurements of the radiograph films and taking measurements of the ingot was used to confirm the location of the thermocouples. The radiographs provided a one-to-one scale of the thermocouples in the ingot from both the view of the wide face and the narrow face.

A ruler was used to measure the distance of the tip of the thermocouple bead to the edge of the ingot. To aid in the location of the thermocouples, the ingot was also used since the spacer was visible on one or both sides of the ingot. This occurred due to the spacers being long so that aluminum had difficulty enveloping the entire spacer near the edge and also due to the slight lateral movement of the thermocouple assembly during the cast. These spacers were used to confirm the vertical height of the thermocouple beads to the starter block. The distance of the thermocouples from the edge was measured to determine whether the thermocouples assembly was shifted.

As a final check, the raw temperature and displacement data were used to confirm the vertical positions of the thermocouples. The raw data gave one reading every tenth of a second for the thermocouples as well as the displacement of the starter block. To determine when each thermocouple entered the molten aluminum, the position of the thermocouple was recorded at the moment the temperature had risen to 200°C, indicating that the thermocouple had touched the surface of the molten aluminum. In some cases, the thermocouple arrays went into the mould tilted upwards, one end of the spacer entered first and the other end entered later. To ensure that the thermocouples were aligned in such a way that meaningful comparisons could be made when the cooling curves were plotted, the raw data of each thermocouple were shifted higher or lower in the Excel spreadsheet such that all the thermocouples reached 200°C at the same time. Since the spacing of the spacer was fixed, the locations of the thermocouples beads were known by using the information from the radiograph films, the measurements from the ingots, and the raw data.

3.5.3 Sectioning and Etching

To determine the sump profile, the melt poisoned ingots were sectioned with a band saw and then etched. The ingots were sectioned by Rick Lees at NGTC in Kingston, Ontario. Figure 3-27 shows the top view of a sectioned ingot where all the dimensions are in millimetres. By sectioning along the length and width, at various distances from the edge, the changing shape of the sump profile was observed as the sections moved from the centre towards the edge. Once each section was inscribed with a sharp tool to indicate the alloy, cast number, and cross section distance from the edge, the parts were ready to be etched.

A 10% concentration of sodium hydroxide, NaOH, solution [39] was used to etch the melt poisoned sections where the zinc left a black spot on the surface. Rick Lees and Ed Luce performed the etching at NGTC in Kingston, Ontario. The parts were placed in a basket which was gently lowered into the sodium hydroxide bath and left for fifteen minutes. It was important to do this in a well ventilated area. Gloves, lab coats, and safety glasses should be worn when handling sodium hydroxide or parts that

have been in contact with the chemical because it is highly corrosive and will cause serious burns on the skin.

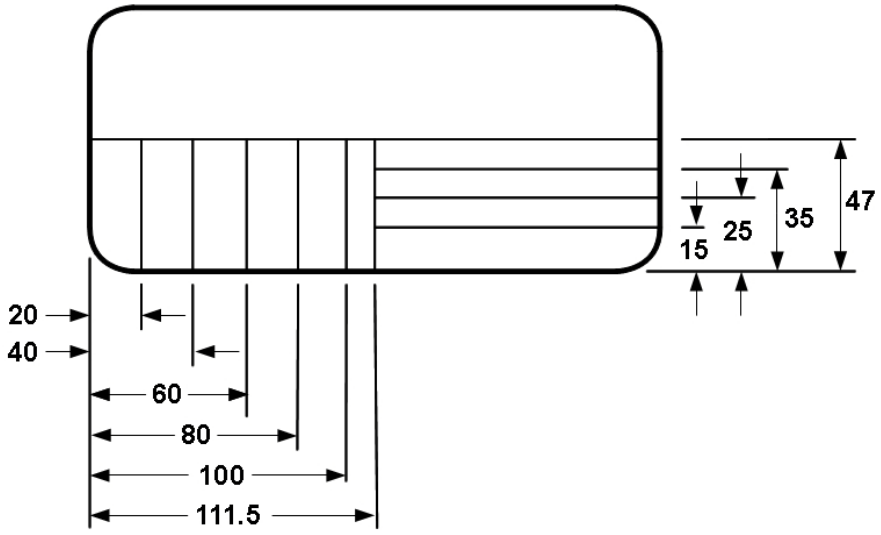

Figure 3-27: Locations of the ingot sections (dimensions in mm).

Once the parts were finished etching, they were removed from the sodium hydroxide bath and rinsed thoroughly with water. The parts were then air dried as wiping them with towels would smudge the etched surface. The sump was then revealed and photographs and measurements of the sump depth and shape were taken.

3.5.4 Sump Microstructure

The microstructure of the melt poisoned sump interface was used to determine how closely the solid liquid interface of the sump profile represented the liquidus temperature of the aluminum alloy. If the interface between the etched zinc mixture and the aluminum alloy was relatively smooth with short dendrites and little mixing of zinc into the alloy below the sump, it would indicate that the sump profile closely represented the liquidus temperature. The sectioned ingot that had been melt poisoned with zinc was used to determine the microstructure. A sliced section that intersected the centre of the ingot was taken and the bottom of the sump was cut out as a 20 mm by 20 mm sample that was approximately 10 mm thick. The bottom of the sump at the centre of the mould was used since the dendrites would be growing parallel to the casting direction and heat transfer. Further away from the centre, the sump interface was no longer perpendicular to the cast direction and caused the dendrites to grow on an angle so that only a small portion of the dendritic structure may be seen when a micrograph cross section was taken.

3.5.4.1 Mounting

The specimen was placed in a plastic cup 25 mm in diameter and 25 mm deep with the surface of interest placed face down. A two component epoxy was used to cold mount the specimen. The epoxy was created by mixing 30 grams of Struers EpoFix Resin and 4 grams of EpoFix Hardener and then poured into the plastic container with the specimen. After 12 hours, the resin hardened and the mounted specimen could be removed from the cup [40].

3.5.4.2 Grinding and Polishing

Once the part was removed from the cup, it was necessary to grind the surface to remove any resin covering the part as well as large surface defects. The specimen was ground by holding it parallel against the grinding belt for approximately 10 seconds. Since aluminum is a soft metal, the specimen should not be pressed against the grinder with great force since it could cause a deep deformation layer [41].

Progressively finer SiC paper was used on the polishing wheel to create a smoother surface. Using a 400-grit SiC paper the specimen was held firmly against the polishing wheel for one minute with water continuously running to ensure the surface was lubricated and to wash away debris. All the scratches on the surface should be aligned in one direction or more polishing was required. Before using a finer SiC paper, the specimen was cleaned before every polishing step where the fineness of the polishing surface was increased. This avoided contamination and leftover debris from scratching the part. The specimen was placed face down in a beaker of alcohol, which was then placed in an ultrasonic bath and left for approximately 2 minutes. Next, an 800-grit SiC paper was used, this time holding the specimen in such a way that the scratches would be created perpendicular to the existing scratches. When the scratches were aligned in the new direction, it was cleaned again in the ultra sonic bath. A 1200-grit coarse SiC paper was used, and finally a 1200-grit fine SiC paper was used.

To achieve a smoother surface, Aerosol Diamond Spray was used on a one micron Leca diamond cloth. Instead of using water as lubrication, a diamond lapping oil microid extender was placed on the Leca diamond cloth. The specimen was checked periodically to ensure the specimen surface was still lubricated with oil. If not, more diamond lapping oil was added. The polishing took approximately three minutes. Following another ultrasonic bath, the specimen was polished using a colloidal silica polish on a 0.04 micron cloth. The specimen should be polished after 3 minutes and no defects should be visible to the naked eye. Once the surface was rinsed with alcohol and dried with compressed air, the specimen was ready to be etched.

3.5.4.3 Etching

The polished specimen was etched by placing it face down in a Petri dish of Keller's Etchant [39] for twenty seconds. This was done under a fume hood with gloves and safety glasses. The etchant consisted of 190 mL of H_2O, 2 mL of HF, 2 mL of HCL, and 5 mL of H_3NCl_3. Once the etching was finished, the specimen surface was rinsed with alcohol and dried with compressed air [40].

3.5.4.4 Microscope

The specimen was viewed and photographed under an optical microscope at various magnification. The interface between the aluminum alloy and the melt poisoned region was the primary area of interest. The dendritic structure provided information on how closely the interface represented the liquidus temperature of the alloy. This information may be confirmed by comparing the results of the raw thermocouple data and the shape of the etched sumps.

3.6 Summary

The experimental method, apparatus, and procedures were discussed in this chapter. It was shown that the thermocouples and data acquisition system operated well within the equipment's uncertainty range so there is confidence that the measurements are reliable. The experimental and post-processing of measurement techniques described in this chapter was used in the casting experiments. The results and of the experiments and the analysis of the data is presented in the following chapter.

Chapter 4
Experimental Results and Discussion

4.1 Temperature Measurement Techniques

Challenges presented in the first series of experiments were corrected allowing the design of the experiments to be improved for the second series of casting experiments. This section summarizes the different techniques used in order to obtain more reliable and consistent temperature measurement data.

4.1.1 Positioning of the Thermocouples in the Ingots

An example of how unsupported thermocouples of Cast 3 from the first series of experiments behaved is shown in Figure 4-1. The jet of molten aluminum leaving the diffuser pushed all three sets of thermocouples towards the edge of the ingot and out of their intended positions closer to the centre of the mould. The sets of thermocouples were held more securely in place during a cast by securing them to a 6.35 mm Ø threaded steel rod that was held in place at the top by the thermocouple support tray. The results can be seen in Figure 4-2 where all three sets were held in the desired position within the ingot throughout the cast. X-rays shown in Figure 4-3 illustrates the benefits of using a stabilizing rod. The initial sets of thermocouples without support were pushed about 40 mm out of position and twisted by the fluid in the molten sump while the later stabilized sets remained parallel with the direction of casting.

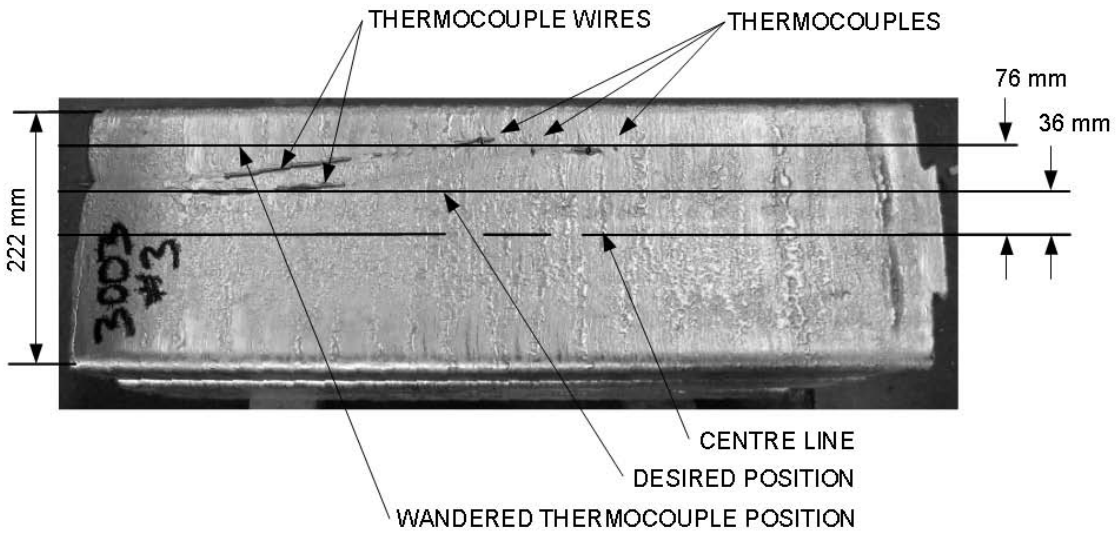

Figure 4-1: Thermocouples were pushed to the edge of the ingot by the jet of molten metal from the diffuser.

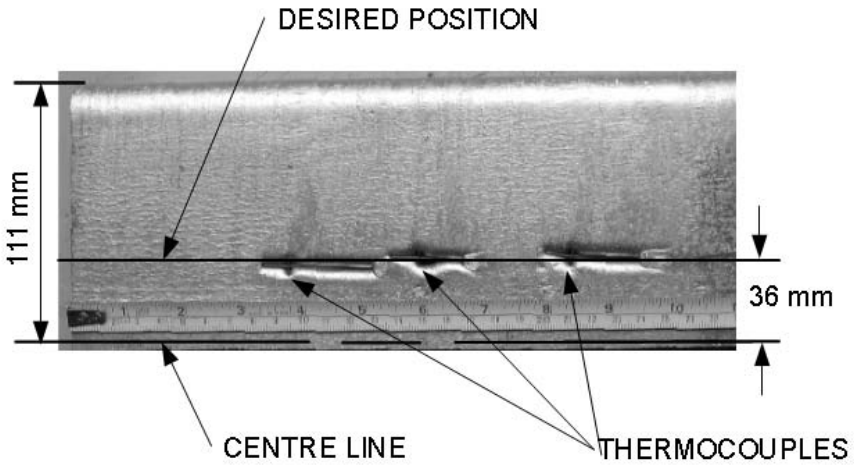

Figure 4-2: The threaded steel stabilizer rod added positional stability by holding the thermocouples in line during casting.

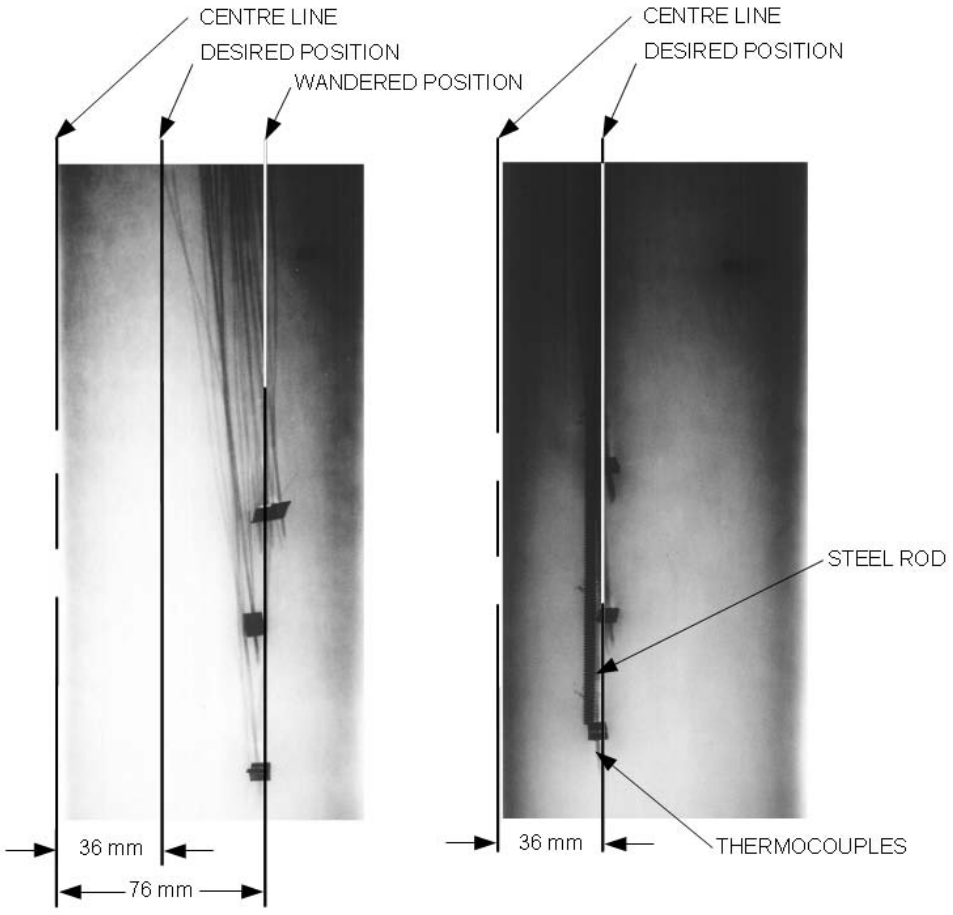

Figure 4-3: X-rays of Series 1, Cast 3 (left) section without thermocouple array support and Cast 5 (right) with a stabilizer rod.

Recognizing the deficiencies in the thermocouple array support system used in the first series of experiments, the thermocouple array support system was redesigned and modified so that the thermocouple wires would have less impact on the fluid flow in the sump and so that the positional accuracy of the thermocouple beads within the ingot would be improved. The number of thermocouples from the first to the second series of experiments was reduced from 21 thermocouples to 7. The first series used three sets of thermocouples as shown in Figure 3-8 while the second series of experiments used only one set as shown in Figure 3-15. To minimize the effect of flow disturbance of molten aluminum in the sump, the thermocouple wires were routed up and tied to the threaded rod rather than 21 thermocouple wires spread across the width of the mould forming a wall. Offsetting the stabilizing rod from the centre improved the quality of the measurements by not disturbing the flow of aluminum around the centre thermocouple. In addition, as shown in Figure 4-2 and Figure 4-3, the positional accuracy of the thermocouple beads was improved by anchoring the bottom of the rod at the starter block and the top of the rod at the thermocouple support tray.

The importance of spacer design is illustrated in Figure 4-4. The first series of experiments utilized a flat steel plate with holes drilled in it to keep the thermocouples spaced properly while the second series of experiments used a 3.2 mm Ø steel rod. It can be seen that the flat spacers disturbed the flow of aluminum especially near the ingot surface and there was poor wetting between the sheets and the aluminum, while the rod shaped spacer was more streamlined.

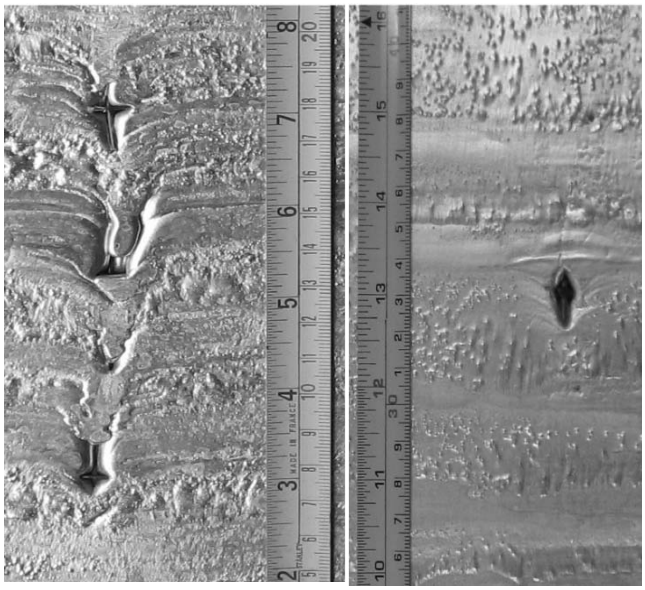

Figure 4-4: Flat sheet metal spacers used in the AA3003 Series 1 Cast 1(left) and the simple rod used in the Series 2 Cast 2 (right) may be compared.

Another advantage of using a rod spacer over a flat sheet spacer is illustrated in the x-rays of Figure 4-5. The stainless steel flat spacers tended to lose their strength and deform under the high heat shifting the thermocouples out of position. The carbon steel rod spacers used in the second series of experiments provided more rigidity.

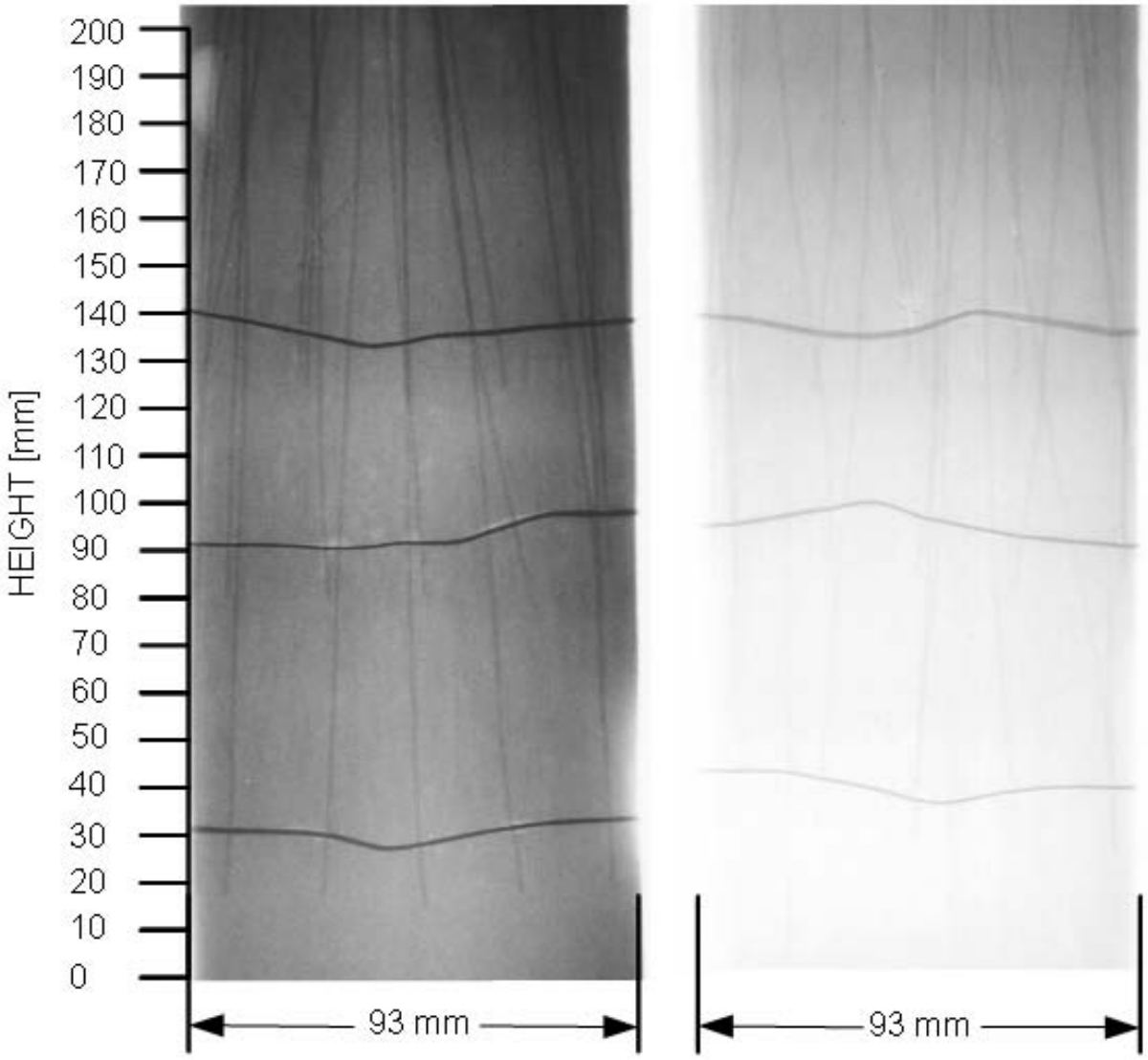

Figure 4-5: Series 1 Cast 1 (left) and Cast 3 (right) show deformed sheet metal spacers.

4.1.2 Thermocouple Consistency

The proper selection of thermocouples was critical to the success of obtaining consistent data from the thermocouples and to avoid thermocouple failure. Both series of experiments used stainless steel sheathed type K thermocouples. The cooling curves shown in Figure 4-6 demonstrated how the

manually made thermocouples from the first series of experiments performed inconsistently and unpredictably, with the thermocouple alternating from failing to functioning throughout the experiment. In this example, thermocouple 1 failed entirely while thermocouple 2 exhibited unexpected behaviour while in the solidified ingot at about 275°C. Human error and inconsistency was greater when welding thermocouple beads manually, whereas premade thermocouples from the supplier used in the second series ensured that the thermocouples behaved consistently. The contrast of measurements shown in Figure 4-7 from the second series of experiments showed an improved consistency of the measurements over Figure 4-6 from the first series of experiments.

Using grounded thicker thermocouples of 1.5 mm Ø in the second series allowed the thermocouples to survive at high temperatures. The 1 mm Ø thermocouples with the exposed beads from the first series of experiments were prone to failure, whether from the dissolution of the exposed bead or the reduced effectiveness of the magnesium oxide insulation in very thin thermocouples.

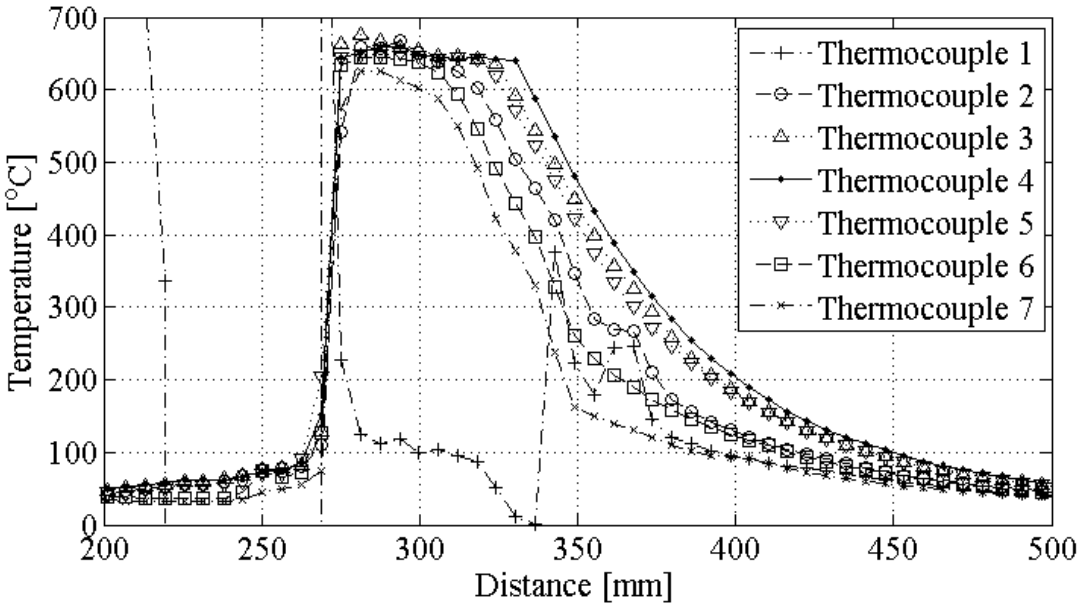

Figure 4-6: Manually made thermocouple beads exhibited a high incidence of inconsistent performance.

The design corrections made to the second series of casting experiments improved the robustness and consistency of the temperature measurements. In the balance of this chapter, data obtained from the second series of experiments were used for analysis preferentially over the data obtained from the first series of experiments.

4.2 Measured Cooling Curves

A typical measured cooling curve from an array of implanted thermocouples is presented in Figure 4-7 where AA6111 was cast at 1.61mm/s with a pouring temperature of 700°C. Distance on the x-axis represents the displacement of the starter block from its starting position inside the mould. The entry of the thermocouples into the melt was identified by the sharp temperature rise and occurred at 290°C in Figure 4-7. Although the pouring temperature measured in the tundish was 700°C, the maximum measured temperature in the sump was only 654°C. This temperature discrepancy was due to the high cooling rate of the molten aluminum in the water cooled mould so any hot aluminum that entered the mould mixed with the cooler aluminum already in the sump. As expected, the edge thermocouples, 1 and 7, were the first to cool down from the liquidus temperature of 647°C. The outer thermocouples, 2 and 6, cooled down next and were followed by the inner thermocouples, 3 and 5. Thermocouple 4 at the centre remained at the liquidus temperature the longest and was the last to cool. Due to the symmetry of the thermocouple positions across the width of the mould, each pair of thermocouples adjacent to the centre thermocouple showed very similar cooling curves. This indicated that the cooling of the ingot and positioning of the thermocouples was symmetrical.

To demonstrate how the depth of the sump was estimated based on the cooling curve, the centre thermocouple from Figure 4-7 is shown in Figure 4-8. The depth of the sump was estimated by finding the distance between the metal level and the liquidus temperature position, the point where rapid cooling began. The same method was used for the other six thermocouples to determine the sump shape at discrete horizontal positions within the ingot.

A detailed view of the centre thermocouple's cooling curve from Figure 4-8 is shown in Figure 4-9. When the thermocouple first entered the molten aluminum, it was in the liquid region and the temperature fluctuated and rose to a maximum value as it passed by the jet of molten aluminum leaving the diffuser. Soon afterwards, it cooled to the liquidus temperature and plateaued during the phase transformation from liquid to solid. The temperature dropped rapidly in the solid region as it was cooled by the water.

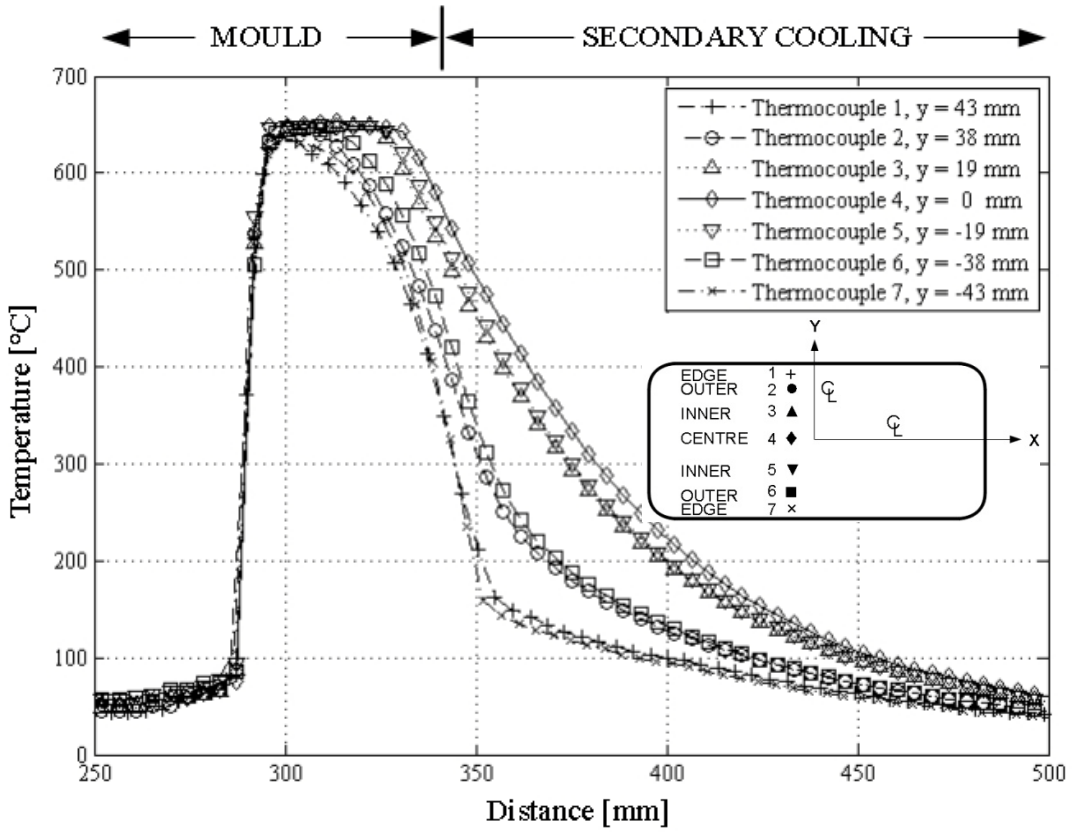

Figure 4-7: Typical cooling curves for AA6111 cast at 1.61 mm/s (water flow rate = 1.79 L/s).

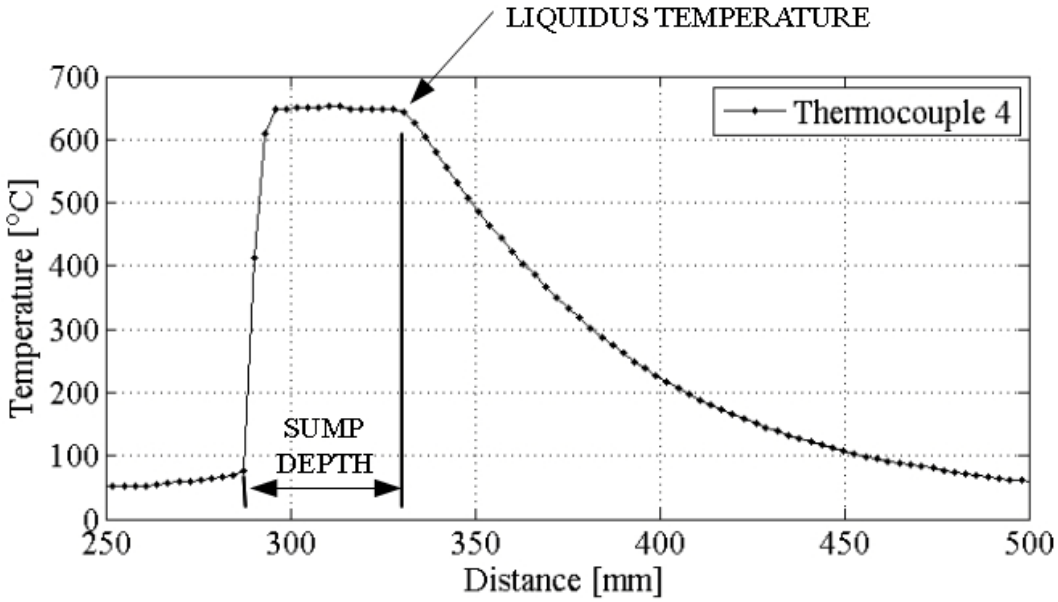

Figure 4-8: The sump depth is the distance from the metal level to the point of solidification.

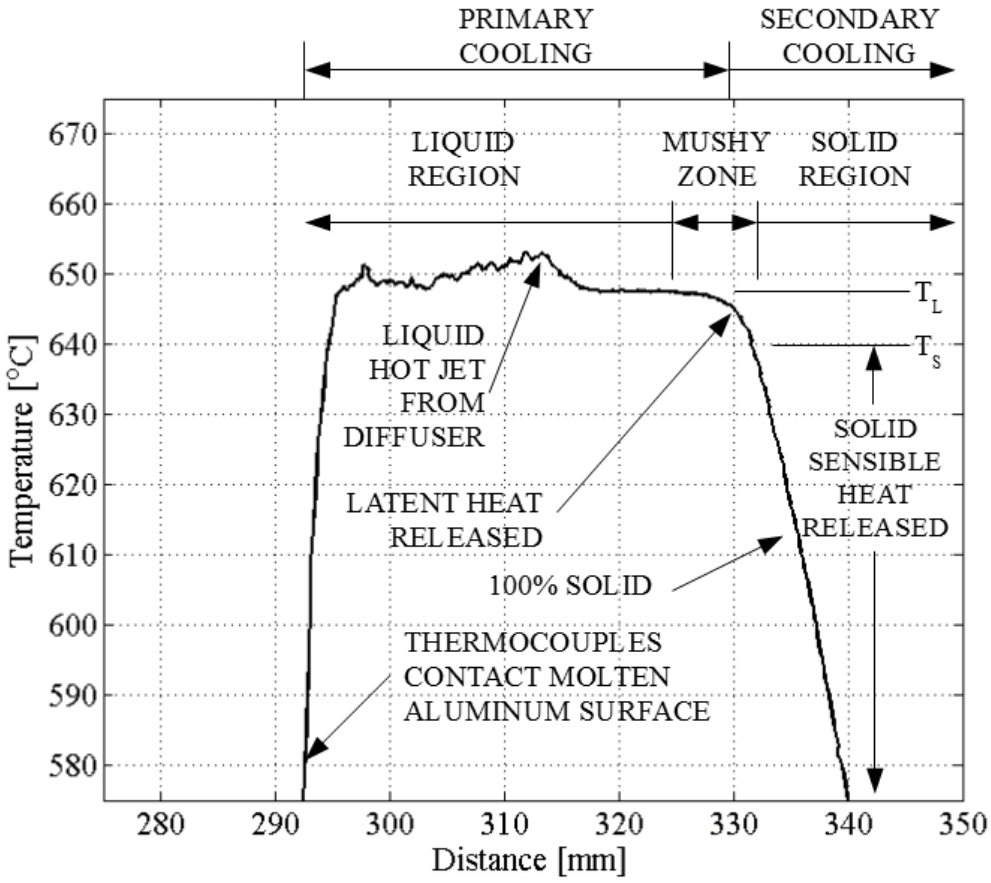

Figure 4-9: Temperatures in the liquid sump measured by the centre thermocouple #4 for an AA6111 ingot **[42]**.

The unidirectional solidification of a pure metal is shown in Figure 4-10 to illustrate the sudden change in thermal gradient at the solid-liquid interface due to the release of latent heat of fusion. On the temperature versus position graph, the dot located at the liquidus temperature, T_L, on the cooling curve shows the location of the sump interface. At this point, the incoming energy, the heat flux in the liquid, q_L, and the latent heat evolution, $\rho \times \Delta h_f \times v$, is balanced by the heat released by the heat flux in the solid, q_S, where ρ [kg/m³] is the density of the metal, Δh_f [J/kg] is the specific latent heat of fusion, and v [m/s] is the casting speed. The terms, k_L and k_S [W/m°C] are the thermal conductivities of the liquidus and solidus regions, respectively. The sudden change in the temperature gradient, dT/dz, is due to Δh_f which only starts at T_L. At the solid-liquid interface marked by the vertical dashed line labeled T_L, the metal was primarily liquid so the latent heat evolution term was relatively high and caused a large change in the thermal gradient during solidification. The large change in the thermal gradient allowed dT/dz to be used to accurately identify T_L. In an alloy, the latent heat of fusion is released over the

temperature range between T_L and T_S. This results in a more gradual increase in the thermal gradient beginning at the liquidus temperature.

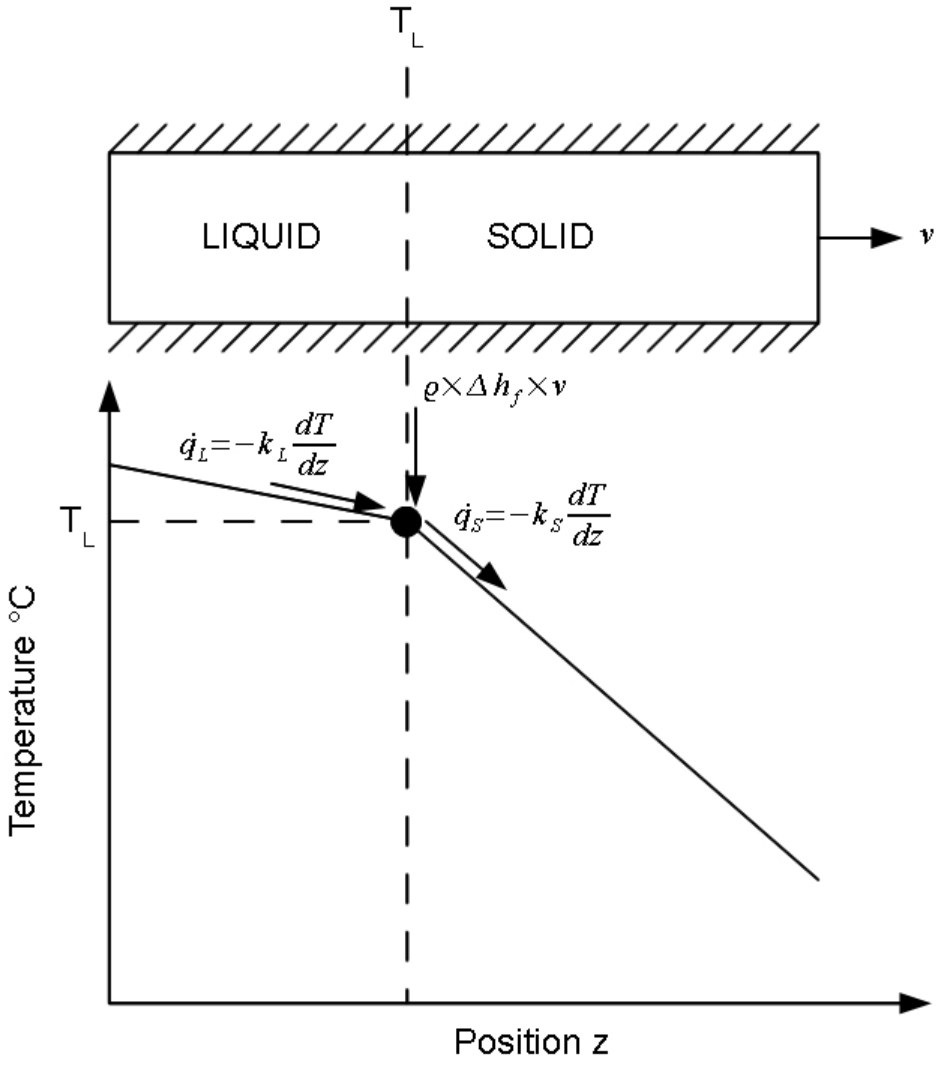

Figure 4-10: Cooling curve showing the energy balance at the solid-liquid interface **[43]**.

Plots of the temperature gradients and change in temperature gradient over distance were used to determine the liquidus and solidus of the cooling curves generated by the thermocouples are shown in Figure 4-11. The derivative, dT/dz, is the temperature gradient and was calculated by dividing the change in temperature, T, by the change in distance, z. Due to the noise encountered during the signal processing, a central difference approximation was used on the thermal gradient to generate a smoother plot that was easier to analyze. The sharp drop seen in Figure 4-11 indicated the release of latent heat and that the ingot was being cooled rapidly in that region. The point at which the temperature gradient dropped rapidly and the point it began to rise again were marked by two vertical lines and the distance

separating the lines was the length of the mushy zone, which was estimated to be 8 mm. These two vertical lines intersected the cooling curve at two different temperatures and were used to estimate the liquidus and solidus temperatures, in this case for AA6111, the temperatures were 647°C and 608°C, respectively. A close up view of the changing thermocouple gradient in Figure 4-11 is shown in Figure 4-12. It should be noted that 608°C was not the true solidus temperature, as it still had approximately 15% liquid; however, the already diminishing contribution of the release of latent heat was masked by the much larger effects of secondary cooling so the lower solidus temperature predicted by ThermoCalc and FactSage of 497°C and 520°C, respectively, was not captured [22]. A central difference of the second derivative, d^2T/dz^2, was taken to detect any change in temperature gradient over distance, which may occur as a result of phase changes in the aluminum alloy during solidification. However, no significant changes were observed beyond cooling below the solidus temperature.

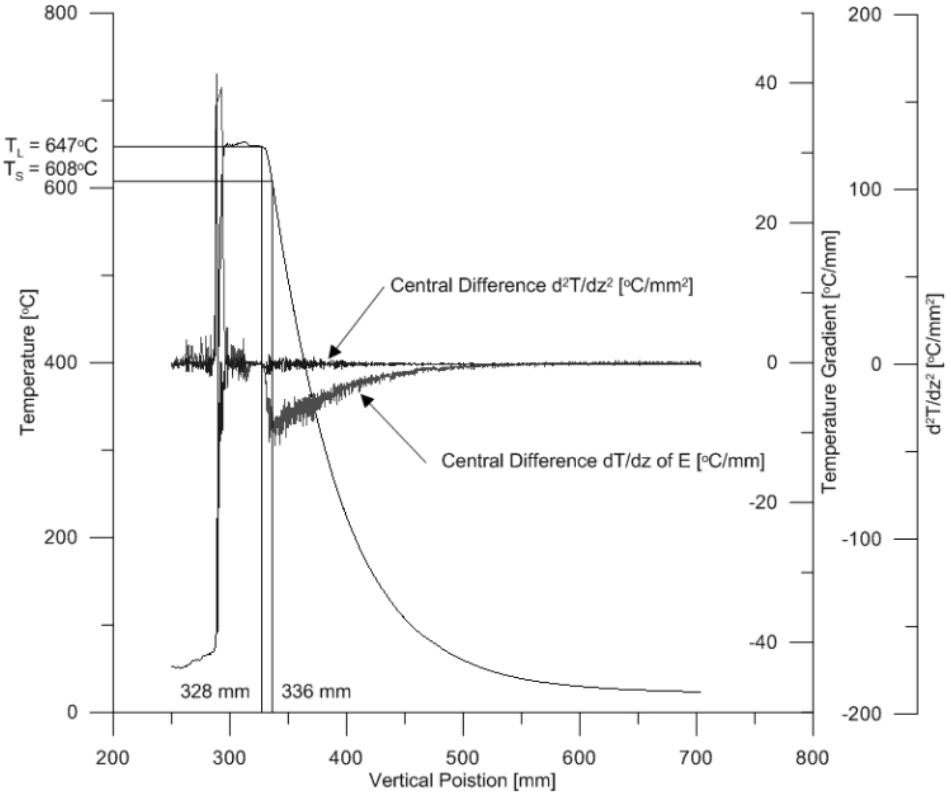

Figure 4-11: AA6111 cooling curve and temperature gradient plotted against displacement **[22]**.

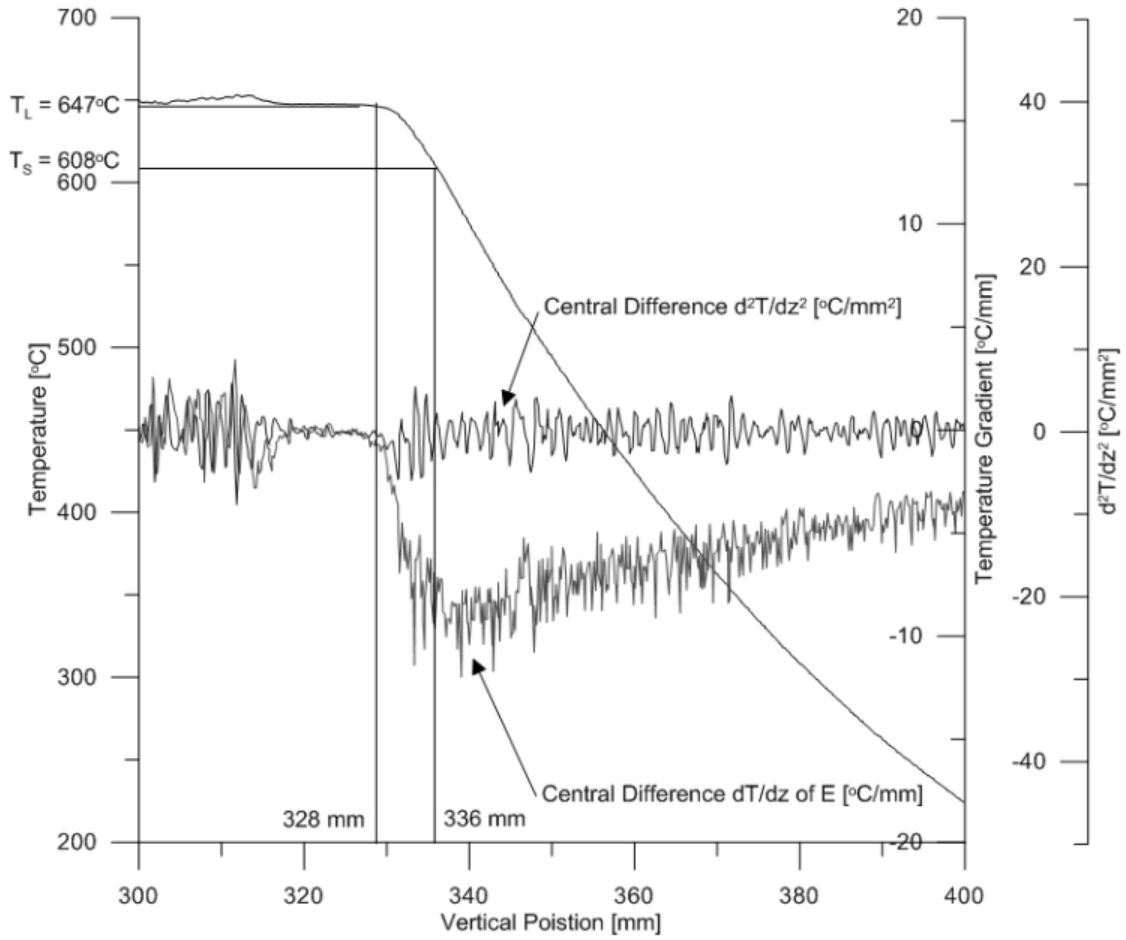

Figure 4-12: A close up view of the AA6111 cooling curve and temperature gradient plotted against displacement.

Although the liquidus and solidus temperatures were estimated by plotting the temperature gradient with the cooling curve, it was necessary to check the results against the predicted temperatures. To do so, two different programs were used, ThermoCalc was used to produce a mass fraction solid versus temperature graph using the Scheil equation, shown in Figure 4-13, and FactSage was used to generate an equilibrium phase diagram, shown in Figure 4-14. The spectrographic compositions from Table 3-3 of the alloys AA3003, AA6111, and AA4045 were used to create the plots in Figure 4-13 and Figure 4-14. The predicted liquidus and solidus temperatures are labeled in Figure 4-13. The equilibrium phase diagram of AA6111 shown in Figure 4-14 had Mg varying along the x-axis. A vertical line drawn at 0.88% Mg, the spectrographic composition of Mg found in AA6111, intersected the liquidus and solidus borders and horizontal lines were drawn at those intersections to predict the liquidus and solidus temperatures.

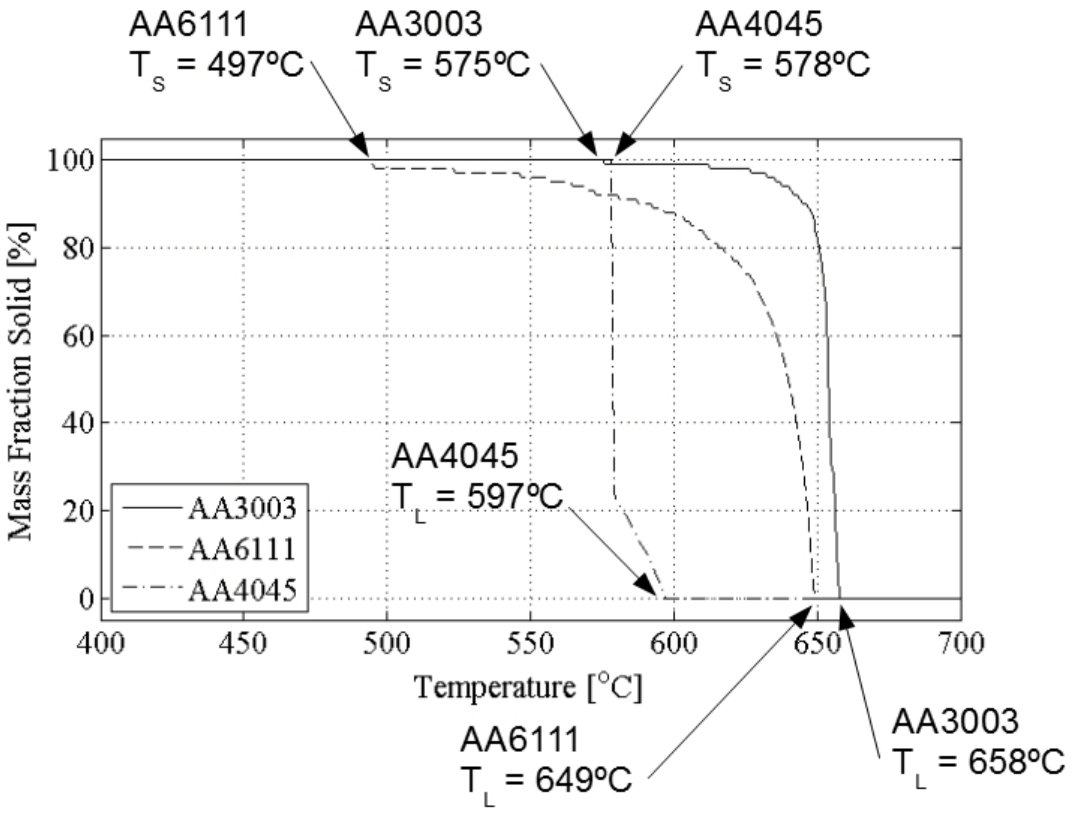

Figure 4-13: Mass fraction solid of alloys during solidification predicted by Thermocalc using the Scheil equation **[44][29]**.

The same analysis was done on AA3003 and AA4045 and are shown in Figure 4-15 through Figure 4-20. Excellent correlations between the predicted results of ThermoCalc and FactSage was seen in both liquidus and solidus temperatures. Experimental results for the liquidus temperature had excellent correlation with the predicted values, but the solidus temperature showed deviations of 16°C to 111°C. This discrepancy may be explained by the fact that the thermocouples were not sensitive enough to detect the release of latent heat when there was less than 15% mass fraction of liquid. For example, the thermocouple estimated the solidus temperature of AA3003 to be 628°C because only about 3% of liquid remained; however, it is possible to have liquid remaining at 590°C according to FactSage predictions. In reality, the effect of primary and secondary cooling was so high that the latent heat released by the last 3% of liquid was masked.

The excellent correlation between the measured liquidus temperature against the two independent prediction methods showed that plotting the thermal gradient and matching the position at which the slope changed with the cooling curve to find the mushy zone was a reliable method for estimating the liquidus temperature of an alloy.

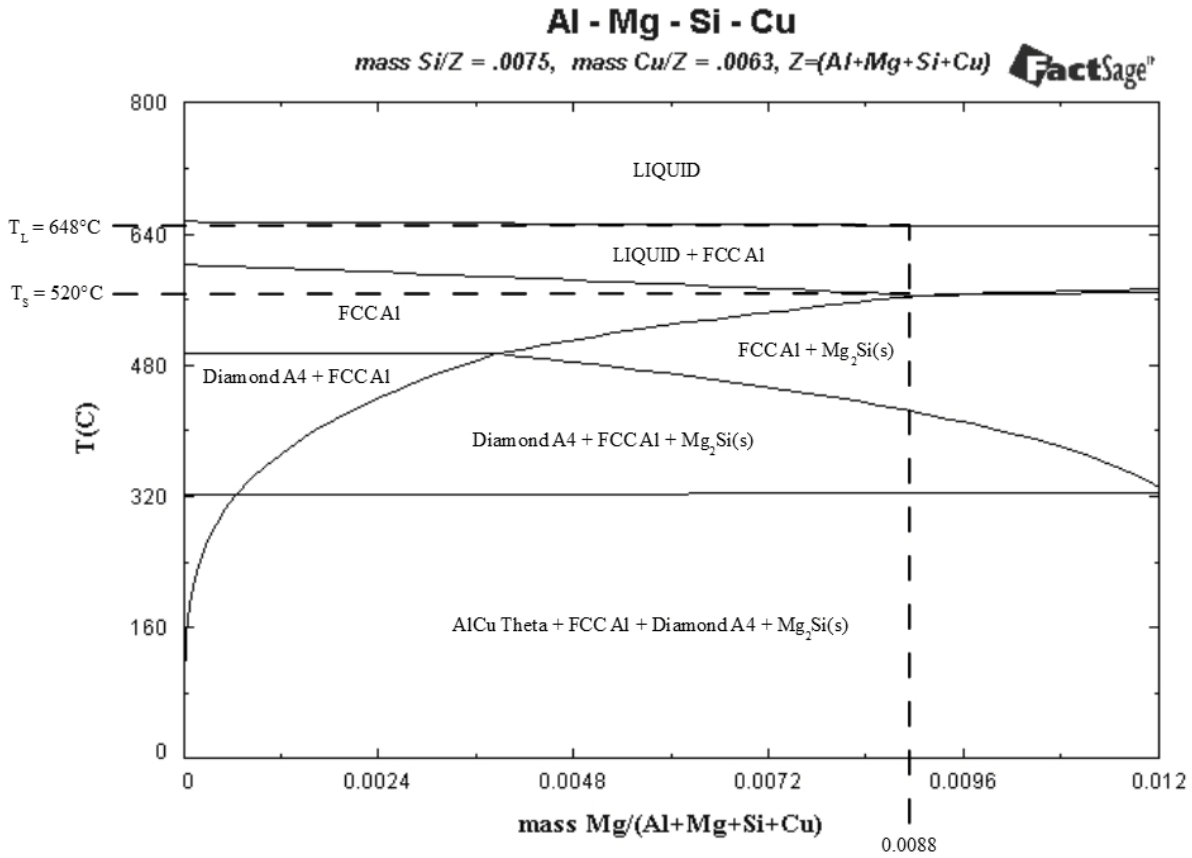

Figure 4-14: Equilibrium phase diagram of AA6111 to predict the liquidus and solidus temperatures using FactSage **[45][46]**.

Plots of the temperature gradients and change in temperature gradient over distance and equilibrium phase diagrams for AA3003 and AA4045 are shown in Figure 4-15 through Figure 4-20 and were used to determine the liquidus and solidus of the cooling curves generated by the thermocouples. In AA3003, the liquidus temperature, T_L, was estimated to be 654°C while the solidus temperature, T_S, was estimated to be 628°C. In AA4045, the liquidus temperature, T_L, was estimated to be 591°C while the solidus temperature, T_S, was estimated to be 562°C. [47]

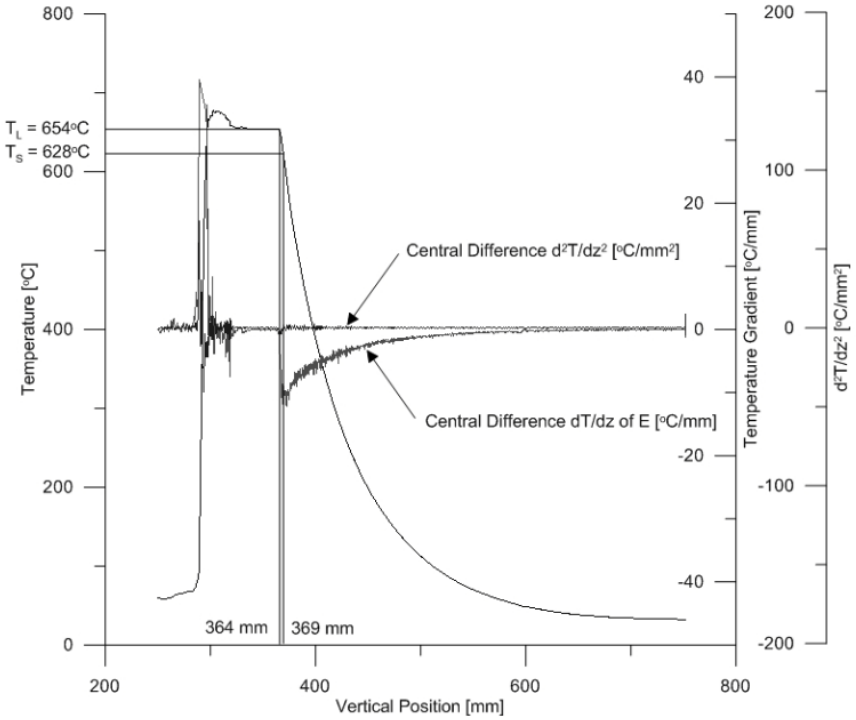

Figure 4-15: AA3003 cooling curve and temperature gradient plotted against displacement **[22]**.

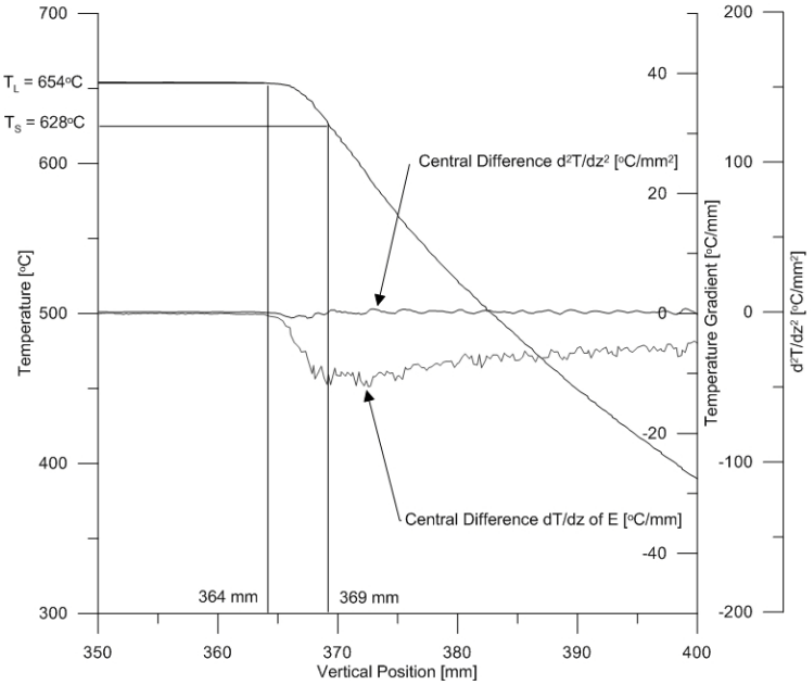

Figure 4-16: A close up view of the AA3003 cooling curve and temperature gradient plotted against displacement **[22]**.

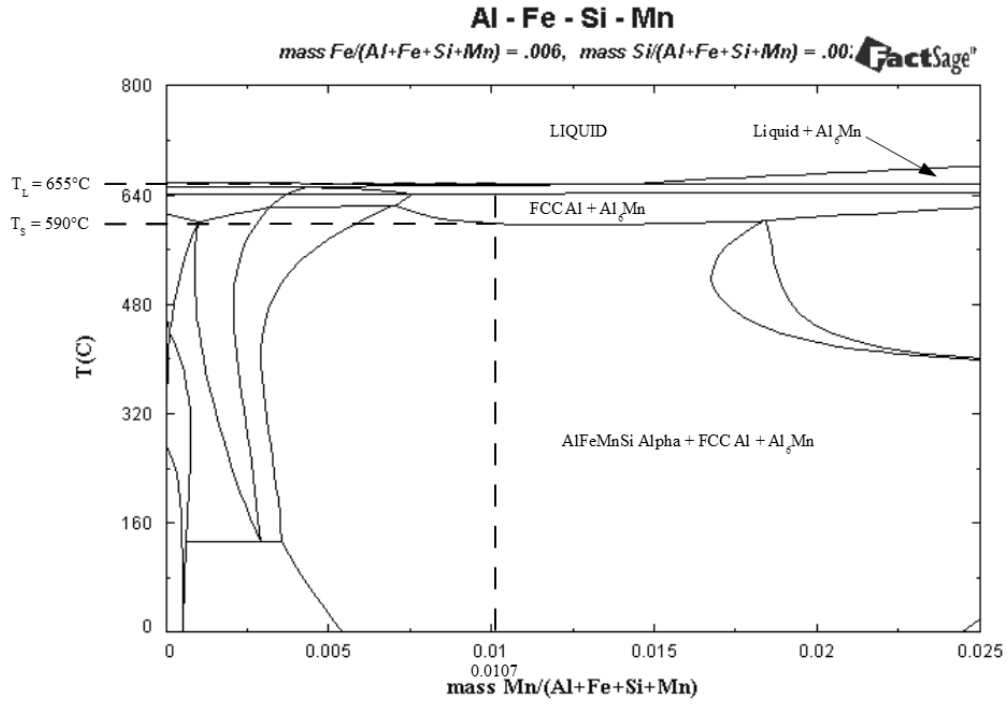

Figure 4-17: FactSage equilibrium phase diagram of AA3003 to predict liquidus and solidus temperatures **[45][46]**.

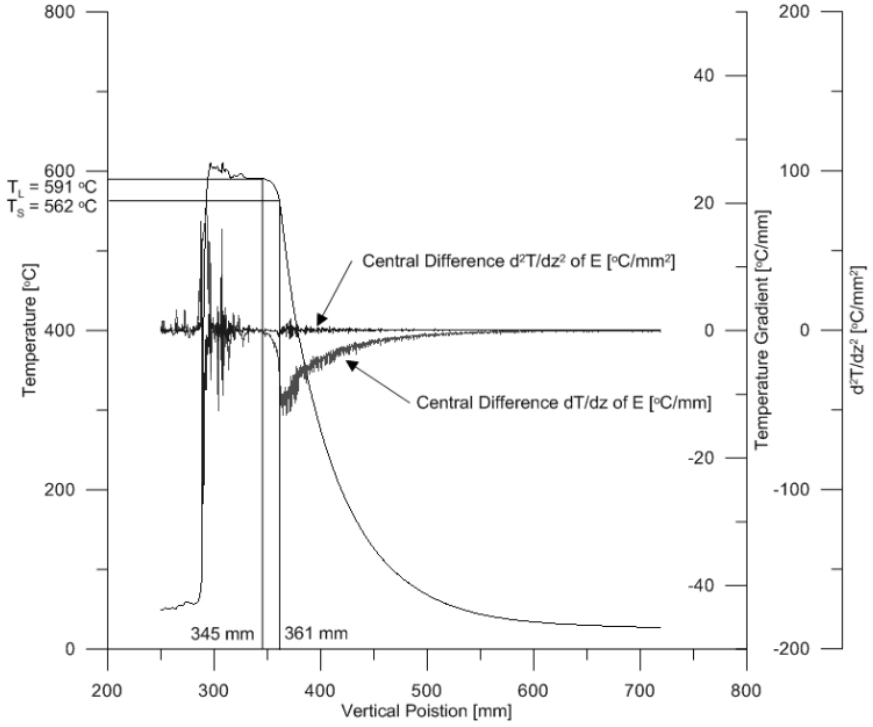

Figure 4-18: AA4045 cooling curve and temperature gradient plotted against displacement **[22]**.

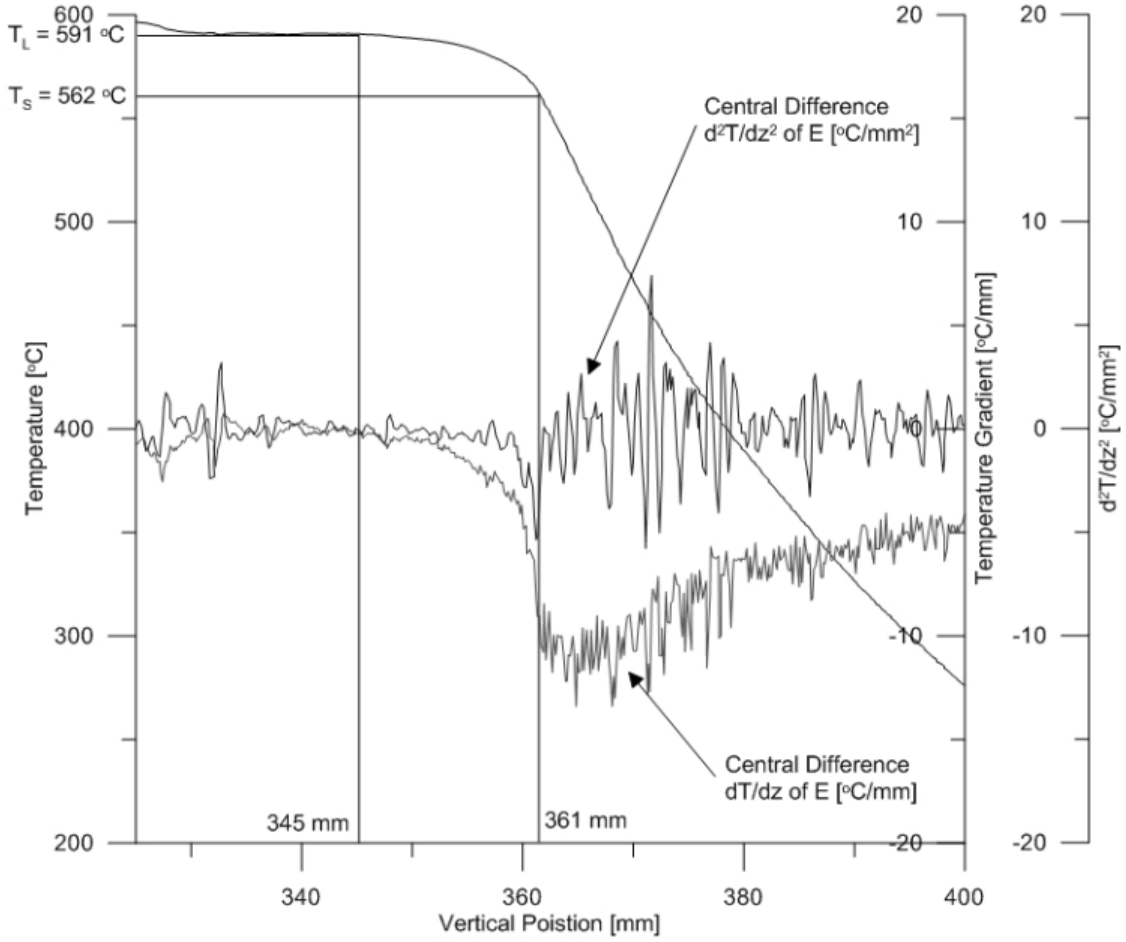

Figure 4-19: A close up view of the AA4045 cooling curve and temperature gradient plotted against displacement **[22]**.

AA3003 and AA4045 equilibrium phase diagrams predicted by FactSage are shown in Figure 4-17 and Figure 4-20. These phase diagrams were then used to predict the solidus and liquidus temperatures of the alloys. The liquidus temperature, T_L, was predicted to be 655°C while the solidus temperature, T_S, was predicted to be 590°C in AA3003. Similarly, the liquidus temperature, T_L, was predicted to be 595°C while the solidus temperature, T_S, was predicted to be 577°C in AA4045. A summary of the results of the experimental and predicted liquidus and solidus temperatures are compared in Table 4-1. The FactSage and ThermoCalc predictions correlated very well and the thermocouple measurements had excellent correlation for the liquidus temperatures and provided approximate solidus temperatures.

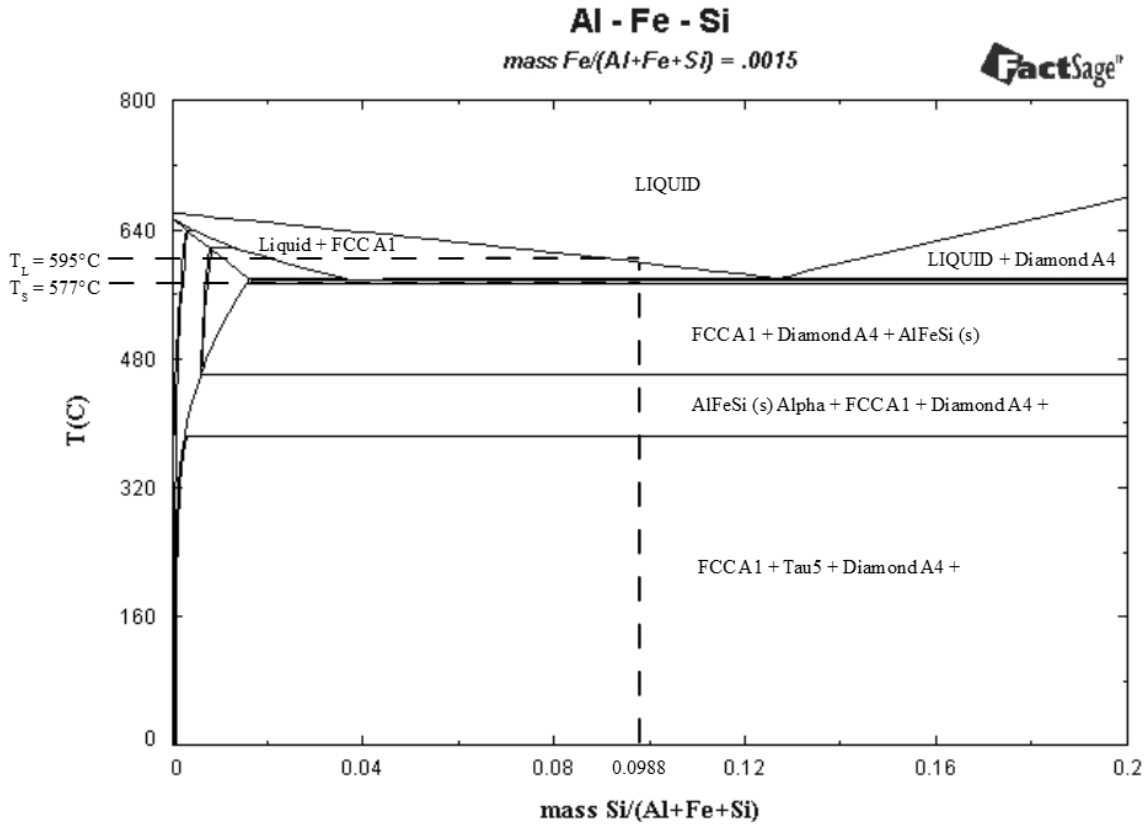

Figure 4-20: FactSage equilibrium phase diagram of AA4045 to predict liquidus and solidus temperatures **[45][46]**.

Table 4-1: The measured and predicted liquidus and solidus temperatures are compared.

	AA3003		AA6111		AA4045	
	T_L	T_S	T_L	T_S	T_L	T_S
Equilibrium Phase Diagram using FactSage	655°C	590°C	648°C	520°C	595°C	577°C
Scheil Predictions using ThermoCalc	658°C	575°C	649°C	497°C	597°C	578°C
Thermocouple Measurements	654°C	628°C	647°C	608°C	591°C	562°C

4.3 Sectioned Melt Poisoned Ingots

Using the cooling curves of the seven thermocouples was one method used to estimate the sump depth and shape at discrete horizontal positions within the ingot, but sectioning and etching the melt poisoned ingots provided a second independent method of determining the sump depth and shape. By comparing the results of the two methods, the dependability of the results would be high if the outcome of the two methods matched closely.

Figure 4-21 and Figure 4-22 show the cross sections of the etched sump of the narrow and wide face, respectively, for an AA3003 ingot cast at 2.33 mm/s. The Al-Zn melt poisoned sump is clearly delineated by the black soot left after etching in the NaOH solution. The metal level was determined using the thermocouple data as a guide. As shown in Figure 4-9, the entry of the thermocouples into the melt was identified as the time or distance at which the thermocouple data rose rapidly to the melt temperature, approximately 20 mm from the top of the mould for all of the casts. The sump, as shown in Figure 4-21 and Figure 4-22, had two distinct regions, a thin primary shell near the mould walls and the remaining sump profile in the middle of the ingot. The thinner shell against the mould wall was caused by the lower heat transfer rates from the primary cooling and the thicker shell resulted from the high rate of heat transfer from the secondary cooling by the water in direct contact with the ingot.

Remelting of the primary shell can be seen on the narrow and wide faces in Figure 4-21 and Figure 4-22 and appear as periodic variations in the etched microstructure near the ingot surface. This periodic behaviour was caused when a gap of the order of microns in thickness formed between the mould wall and the aluminum ingot. The heat transfer through the gap was significantly lower than the heat transfer through the mould. Hence, the newly solidified shell periodically remelted and oscillated during the cast [1]. As the gap was reduced, the heat transfer increased and caused the ingot surface to contract back again, thereby creating a cyclic response of the ingot surface to the mould wall.

Figure 4-23 shows an isometric view of the melt poisoned ingot illustrating the sump along the narrow and wide faces. Along the narrow face, the shell extended to the metal level surface, but this was not seen in the wide face section where the shell appeared to stop approximately 15 mm below the metal level. This was likely due to mixing of zinc into the shell during remelting. The shell at the mould wall in Figure 4-22 was thinner than the shell shown in Figure 4-21 since it was more difficult to extract heat from the centre of the ingot through the wide side than the narrow side. The isometric view of one quarter of the ingot in Figure 4-23 shows that the remelting region creates an illusion of a shallower sump depth when looking at the etched section of the wide face. The sump profile in the wide face was constantly increasing in depth due to the combined influence of secondary cooling of the wide end faces whereas the sump depth towards the centre of the wide face was flat and had a constant depth because cooling was essentially two dimensional. Cooling from the end faces was too far away and the sump depth was determined primarily from secondary cooling of the wide faces only [22]. For these reasons, only the cross sections of the narrow face of the ingot were used for analysis and comparisons of the sump depths.

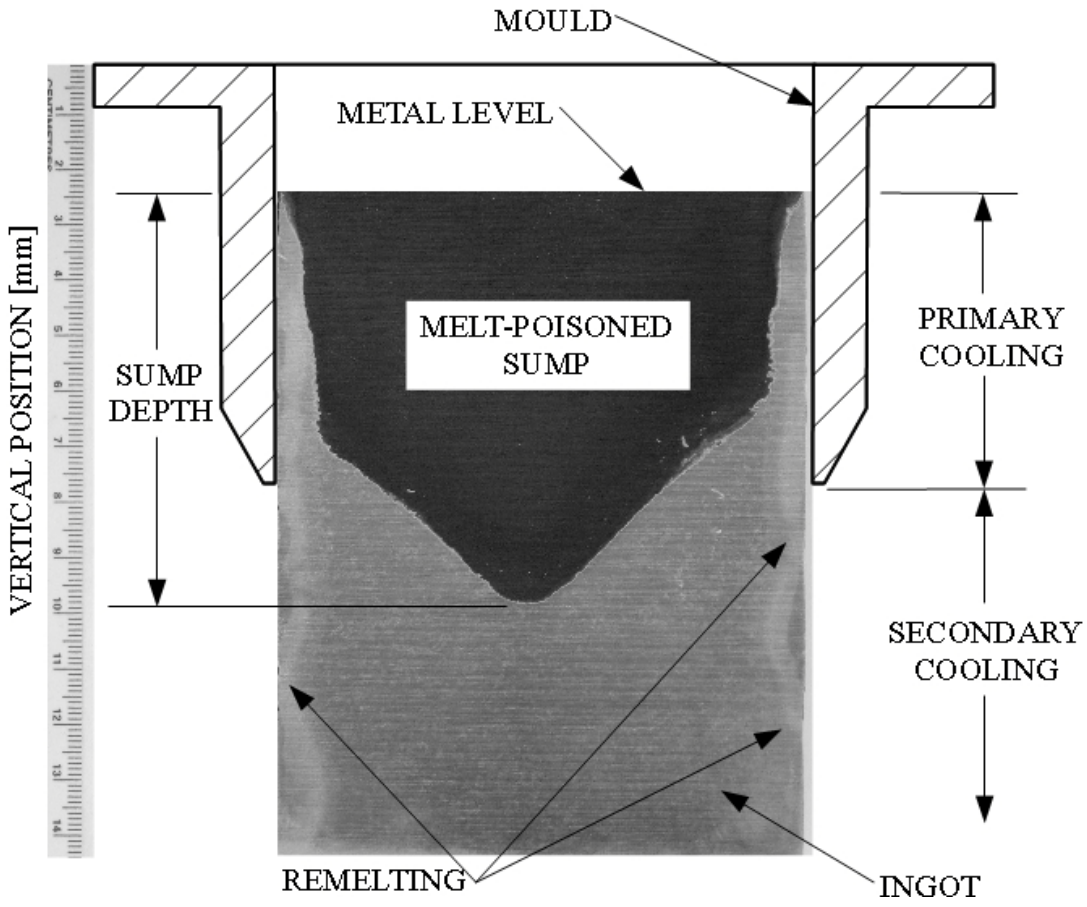

Figure 4-21: Narrow face centre cross section of AA3003 ingot from Series 2 Cast 2 cast at 2.33 mm/s.

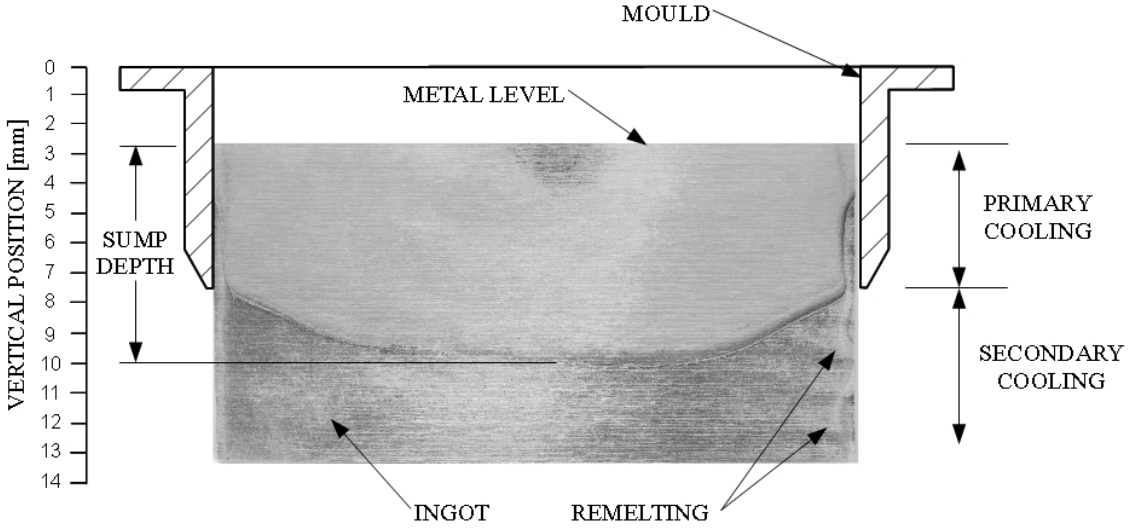

Figure 4-22: Wide face centre cross section of AA3003 ingot from Series 2 Cast 3 cast at 2.33 mm/s.

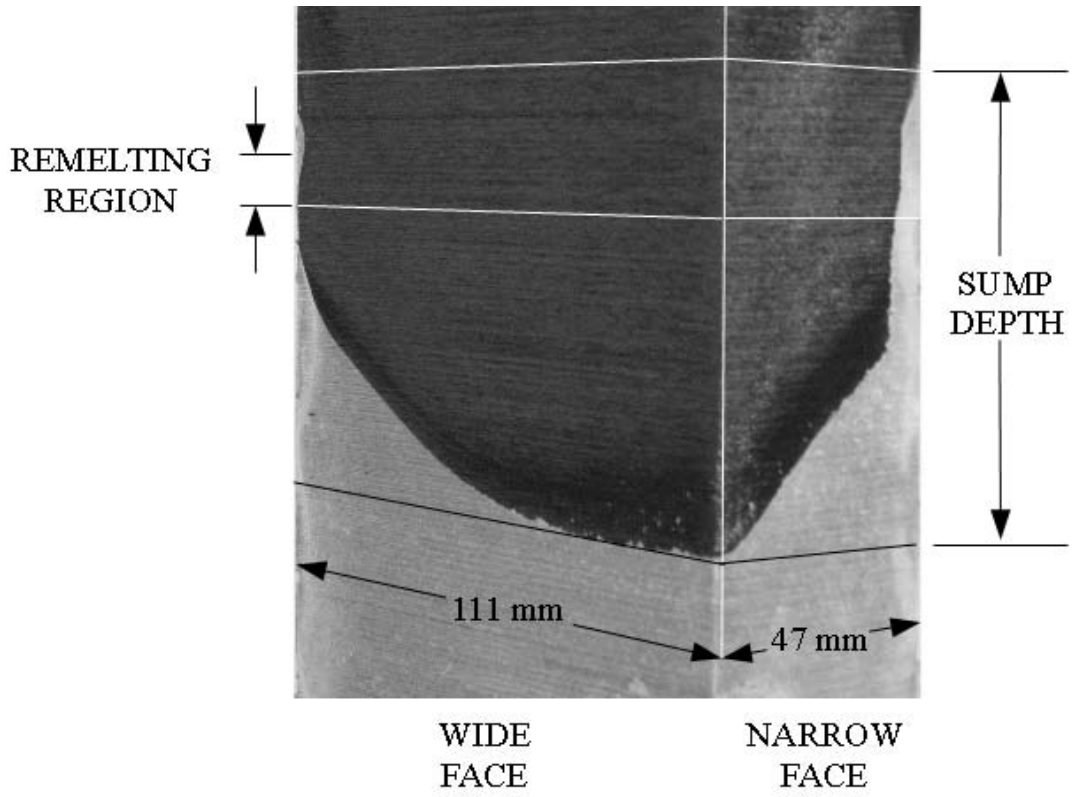

Figure 4-23: Isometric view of sectioned centre of AA3003 ingot from Series 2 Cast 2 cast at 2.33 mm/s.

4.4 Comparison of Thermocouple and Melt Poisoning Results

The sump depth was estimated using thermocouple measurements and compared with the sump depths measured from the zinc melt poisoned and sectioned ingots. These etched cross sections were taken as close to the thermocouple locations as possible, 96 mm from the narrow face of the ingot. A summary of the results is shown in Table 4-2 for the alloys AA3003, AA6111, and AA4045 at different casting speeds. The first two casts for each alloy were at two different casting speeds, and as expected, a deeper sump depth occurred in the faster cast. The close correlation between the sump depths estimated by the melt poisoned ingot and the thermocouple measurements showed that both methods were reliable.

To ensure that the presence of the thermocouples did not perturb the solidification environment and hence sump depth, comparisons of the sumps between ingots with and without the thermocouples were made and are shown in Figure 4-24. The left, centre, and right pictures show AA3003 cast at 2.29 mm/s, AA6111 cast at 1.99 mm/s, and AA4045 cast at 2.03 mm/s, respectively. The left and right halves of each picture show the sump profile of the cast with and without thermocouples, respectively. Each pair of sump comparisons showed that the sump depths of the control and the sample were very

similar and indicated that the thermocouples and threaded rods did not disturb the environment in the mould significantly.

Additional melt poisoned sump depth measurements at different cross-sections along the length and width of the ingot, sectioned at the cross sections shown in Figure 3-27, for AA3003, AA6111, and AA4045 are given in Table B-1, Table B-2, and Table B-3. Although these etched sections of the ingot did not have corresponding thermocouple data, the etched sections provided additional information that can be used to validate the CFD model. In summary, the results from two independent methods showed good correlation between the experiment data from the thermocouples and the measured etched sump, which gave confidence that the data and measurements were reliable.

Table 4-2: Comparison of estimated sump depths using results from measured melt poisoned sections as well as sump depth estimated based on TC measurements.

Alloy	Cast #	Casting Speed [mm/s]	Distant From Narrow Face [mm]	Sump Depth (Melt Poisoned Measurements) [mm]	Sump Depth (Thermocouple Estimates) [mm]
AA3003	1	1.69	96	55	55
AA3003	2	2.33	96	72	74
AA6111	4	1.61	96	41	40
AA6111	5	2.12	96	62	64
AA4045	7	1.69	96	60	62
AA4045	8	2.12	96	70	73

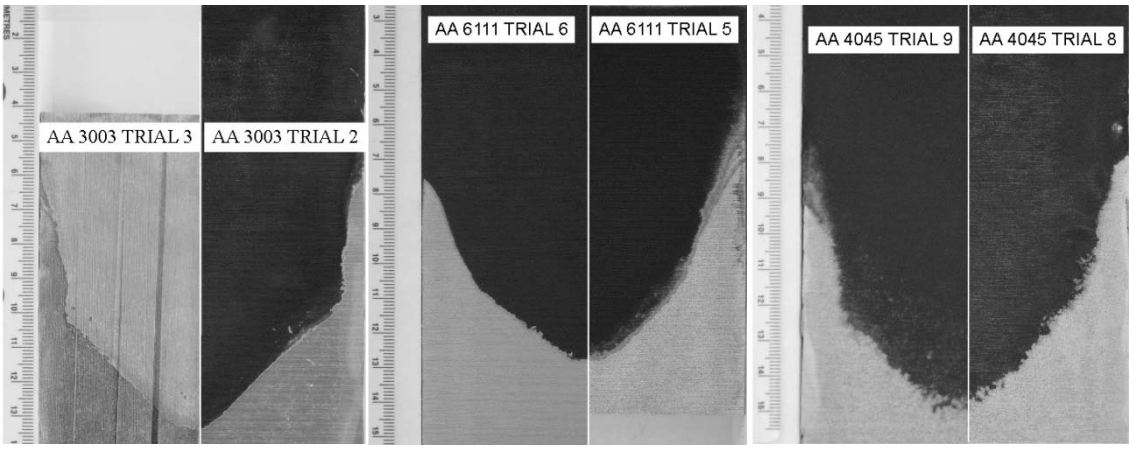

(a) AA3003 **(b) AA6111** **(c) AA4045**

Figure 4-24: Comparing the sump profiles for ingots cast with thermocouples (left) and without thermocouples (right): (a) AA3003, (b) AA6111, (c) AA4045.

4.5 Cooling Curve Comparison

In the first series of experiments, three sets of seven thermocouples spaced at 50 mm intervals were used for each cast. Figure 4-25, Figure 4-26, Figure 4-27, and Figure 4-28 compare the three sets of cooling curves for the centre, inner, outer, and edge thermocouples, respectively, for AA6111 cast at 1.61 mm/s. In Figure 4-25, the correlation between the thermocouples was close, but with the first centre thermocouple to enter the mould, thermocouple 4, the sump depth indicated by the inflection point in the measured temperature at the liquidus temperature was greater than that indicated by the subsequent thermocouples 11 and 18. This was likely due to the stabilizing threaded rod blocking the centre thermocouples of the second and third sets, while the first thermocouple to enter the molten aluminum remained unhindered. The stabilizing rod and thermocouple wire 'screen' blocked the jet of molten aluminum exiting the diffuser from directly heating the thermocouples hence the area behind the threaded rod was slightly cooler. It suggested that the thermocouple wire 'screen' and stabilizing rod affected fluid flow and heat transfer in the sump allowing solidification to occur sooner and, therefore, a shallower sump was indicated. In the second series of experiments, the stabilizing rod was offset from the centre and the thermocouple wires were run along the stabilizing rod so that the effects of the thermocouple array assembly on fluid flow and heat transfer in the sump was minimized.

For the inner, outer and edge thermocouple measurements, shown in Figure 4-26, Figure 4-27, and Figure 4-28, there was good correlation between all three sets of thermocouples. This confirmed that the cast had reached steady state conditions. The thermocouples near the edge of the ingot and closest to the direct water spray cooled more quickly than the inner and centre thermocouples, as expected.

Repeatability of the experiments is demonstrated in Figure 4-29 where the three centre thermocouple of the first series of experiments are compared with the centre thermocouple of the second series of experiment casting AA6111 at 1.61 mm/s. There were minor differences in the cooling curves between the two series of experiments indicating that the first series of casts gave reasonable data even without the improvements in the experiment design of the second series of casts.

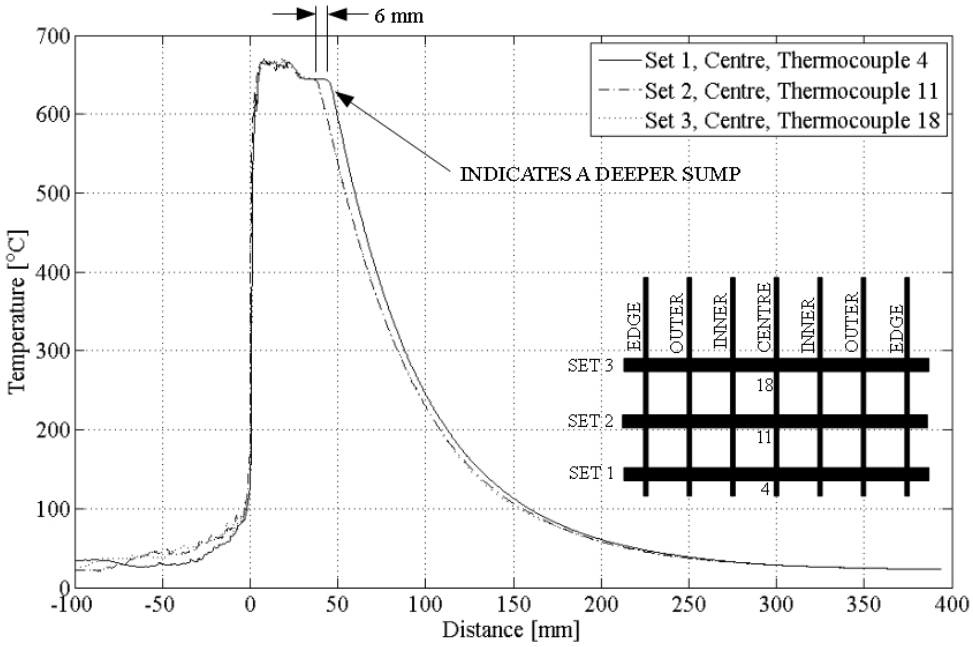

Figure 4-25: Cooling curves from the three centre thermocouples in Series 1 Cast 6 AA6111 cast at 1.61 mm/s.

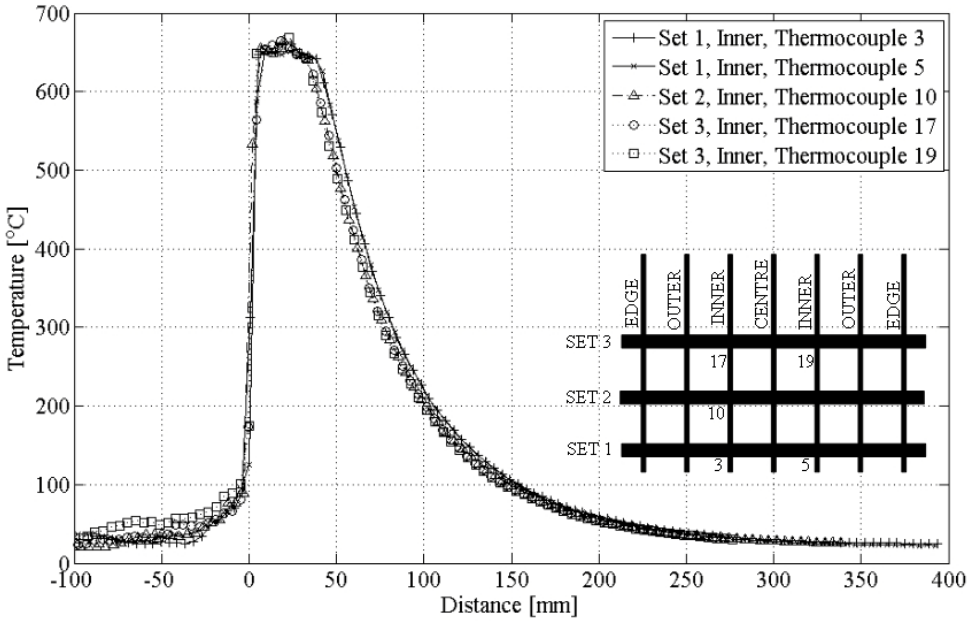

Figure 4-26: Inner thermocouples of Series 1 Cast 6 AA6111 cast at 1.61 mm/s show consistent results.

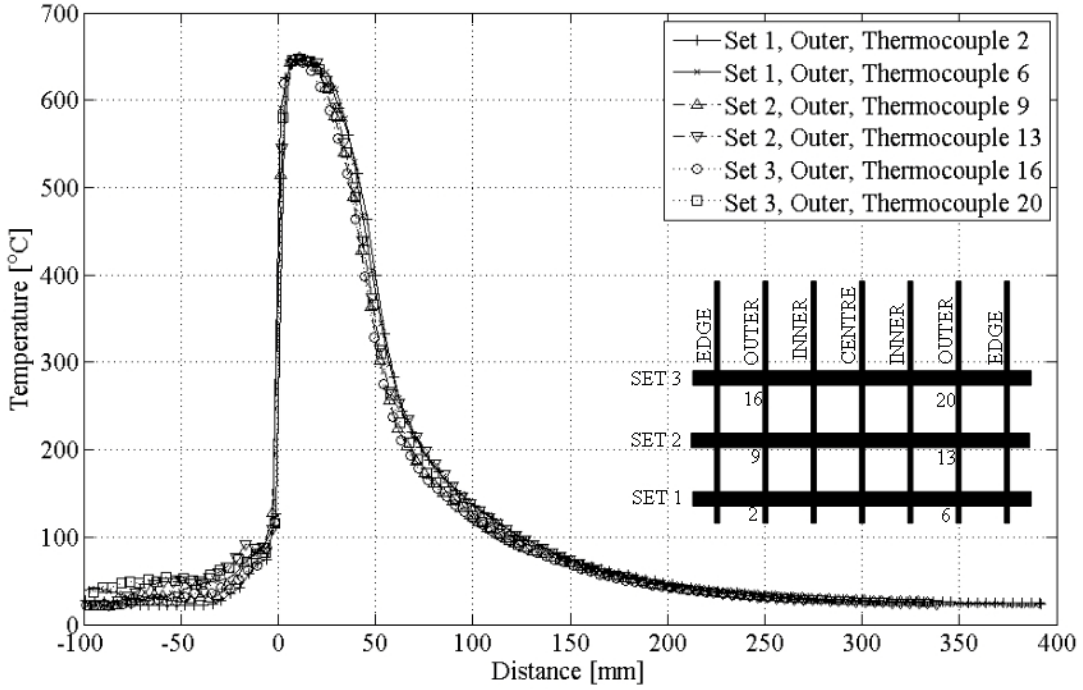

Figure 4-27: Outer thermocouples of Series 1 Cast 6 AA6111 cast at 1.61 mm/s show consistent faster cooling rates.

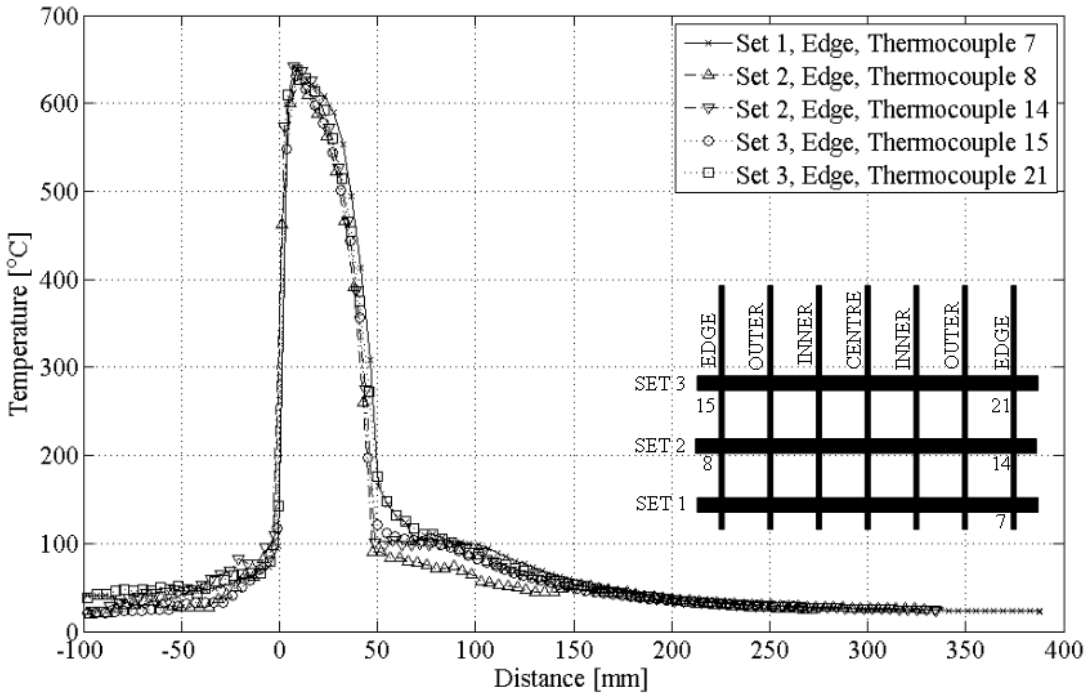

Figure 4-28: Edge thermocouples of Series 1 Cast 6 AA6111 cast at 1.61 mm/s show consistently fast cooling rates.

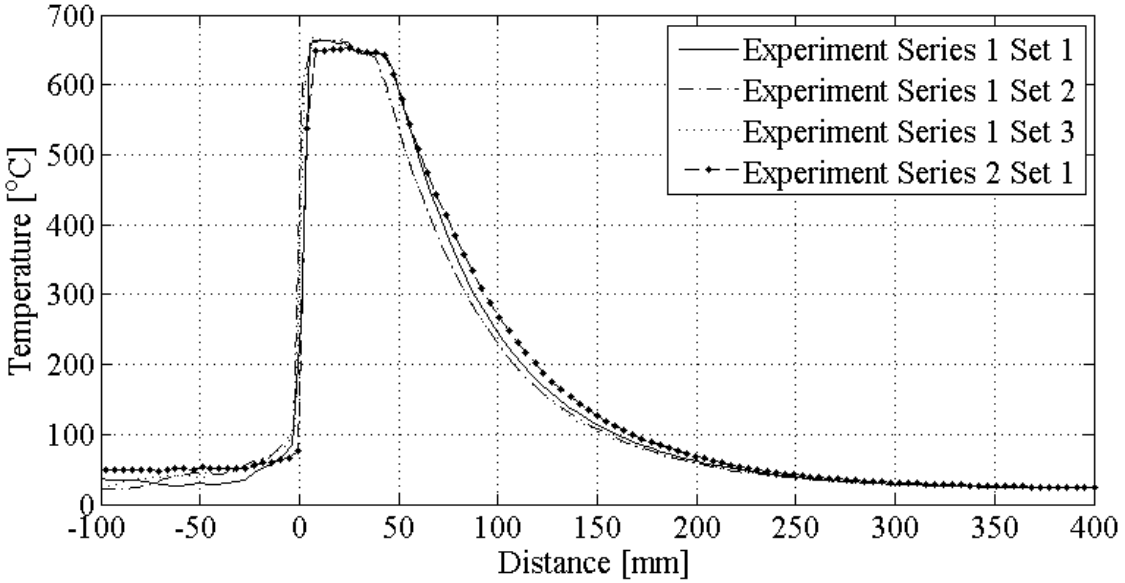

Figure 4-29: Measured temperature versus vertical position of centre thermocouples in four different casts of AA6111 at 1.61 mm/s performed using the same casting parameters.

4.6 Effects of Casting Variables

Water flow rate, superheat of the molten alloy, and the casting speed were three of the process variables that were changed one at a time to determine the effect they had on the cooling curves and sump depth. Two water flow rates through the manifold, 1.79 L/s and 2.69 L/s, were used in the first series of experiments and the results of the cooling curves of the centre thermocouples are shown in Figure 4-30. AA3003 was used in both Cast 1 at 1.79 L.s and Cast 4 at 2.69 L/s with a superheat of 700°C and a casting speed held at 1.91 mm/s. The cooling curves and indicated sump depths of 57 mm were nearly identical indicating that increasing the water flow through the water manifold rate beyond 1.79 L/s did not have a significant effect on the rate of cooling of the ingot. Under these conditions, cooling by the secondary cooling water was conduction limited, i.e., limited by the rate of conduction through the ingot, not convection at the ingot surface [22]. These results were consistent with the findings of Wells and Cockcroft [18], Grandfield *et al.* [19], and Hao *et al.* [5] as they showed that the sump depth of the casting of billets or ingots was not very sensitive to the water flow rate.

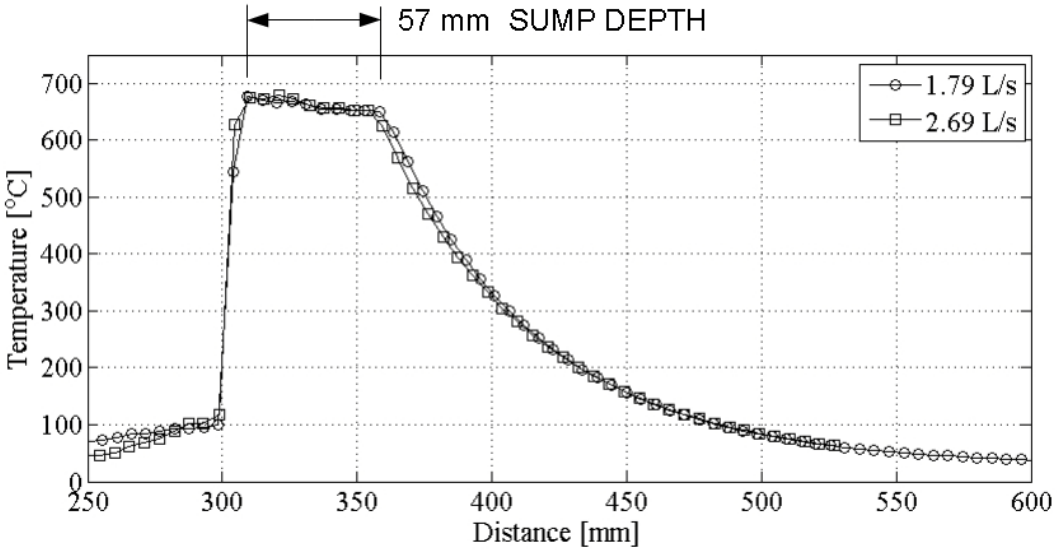

Figure 4-30: Cooling curves of AA3003 cast at 1.91 mm/s using water flow rates of 1.79 L/s (Cast 1) and 2.69 L/s (Cast 4).

Figure 4-31 compares the cooling curves of the centre thermocouples when casting AA6111 at 1.61 mm/s from Cast 6 using a superheat of 45°C and Cast 8 using a superheat of 75°C. A superheat of 75°C took slightly longer to cool and produced a sump 3 mm deeper than using a superheat of 45°C. Although changes in the superheat had more impact than the water flow rate in the manifold, the casts were not very sensitive to the superheat temperature and did not affect the depth of the sump in a considerable way, if at all. This is consistent with the findings of Larouche *et al.* [6].

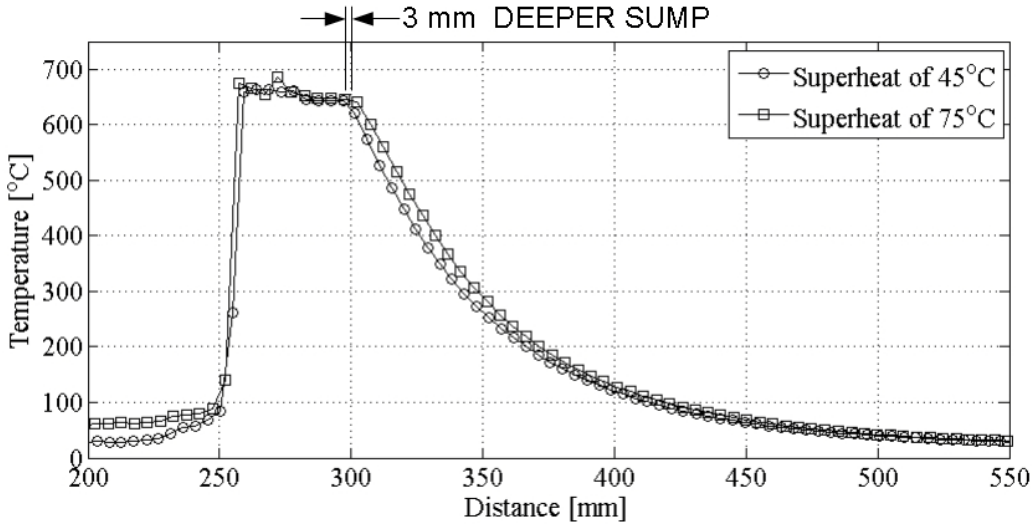

Figure 4-31: Cooling curves of AA6111 cast at 1.61 mm/s using a superheat of 45°C (Cast 6) and 75°C (Cast 8).

The effect of casting speed on the sump depth is illustrated in Figure 4-32. This figure compares the cooling curves of the centre thermocouples from Cast 6 cast at 1.61 mm/s and Cast 7 cast at 2.12 mm/s using AA6111. Increasing the casting speed increased the time required to cool the centre of the ingot resulting in a 15 mm deeper sump because the amount of sensible energy and latent heat of fusion released is proportional to the casting speed. From the first series of experiments, it was demonstrated that the casting experiments were neither sensitive to the water flow rate in the manifold nor the superheat of the aluminum alloy, but was very sensitive to the casting speed. The sump depth's sensitivity to casting speed is well known and the findings were consistent with the research of Hao *et al*. [5], Wiskel and Cockcroft [16][17], and many other researchers. Therefore, in the second series of experiments the water flow rate and superheat were kept constant for all the casts and only the casting speed was varied.

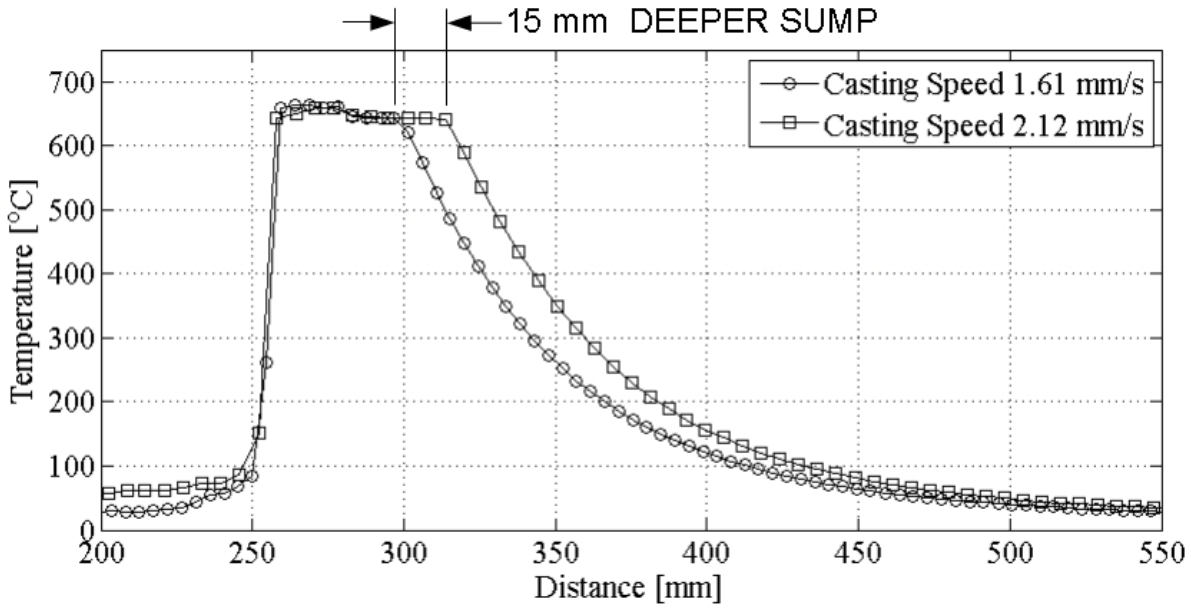

Figure 4-32: Cooling curves of AA6111 cast at 1.61 mm/s (Cast 6) and 2.12 mm/s (Cast 7).

4.7 Effect of Alloy Composition

Each of the three alloys, AA3003, AA6111, and AA4045, produced uniquely different sump profiles with the sump depth increasing with casting speed. In Figure 4-33 through Figure 4-38, the six plots show the sump profiles from the melt poisoned ingots with the positions of the liquidus and solidus measured by the thermocouples. The metal level varied slightly from one cast to another, but all were approximately 20 mm from the top of the mould.

Sump profiles of AA3003 from the second series of experiments are shown in Figure 4-33 and Figure 4-34. In both plots, the liquidus sump profile matched very closely with the sump profiles obtained from etched sumps and indicated that the two methods of determining the sump profile produced consistent and reliable results. The liquidus temperature of AA3003 was 654°C while the solidus temperature was 575°C.

Regions of remelting sometimes disturbed the shape of the shell in the mould created by the primary cooling for the cast at 1.69 mm/s, but the effects were less pronounced in the faster cast at 2.33 mm/s. For a casting speed of 1.69 mm/s, the sump was still within the mould while at a casting speed of 2.33 mm/s the sump depth increased to 18 mm below the bottom of the mould. With a slower cast shown in Figure 4-33, the shell produced by secondary cooling is significantly thicker than the shell produced by primary cooling.

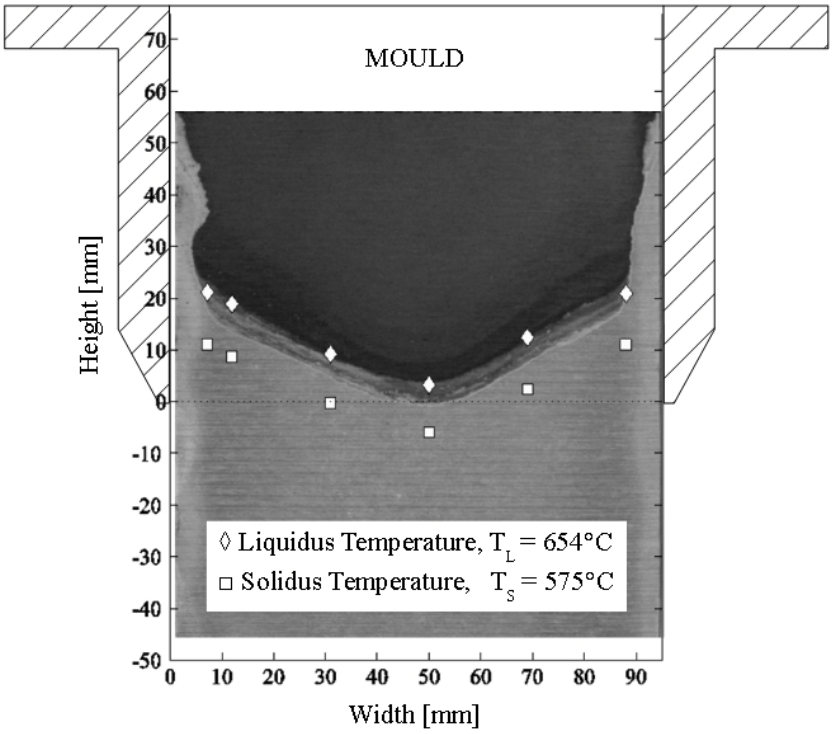

Figure 4-33: AA3003 cast at 1.69 mm/s show the locations of liquidus and solidus temperatures measured by the thermocouples superimposed onto the etched sump.

A distinct change in shell thickness due to the primary and secondary cooling can be observed in the AA3003 ingot shown in Figure 4-34. A slower casting rate produced a thicker shell than a faster casting rate since casting at 2.33 mm/s allowed less time for the ingot to cool than casting at 1.69 mm/s. In both cases, the solidus isotherm profile closely matched the shape of the liquidus profile giving a mushy

zone of approximately 9 mm thick. This showed that the cooling rate within this temperature range was relatively constant.

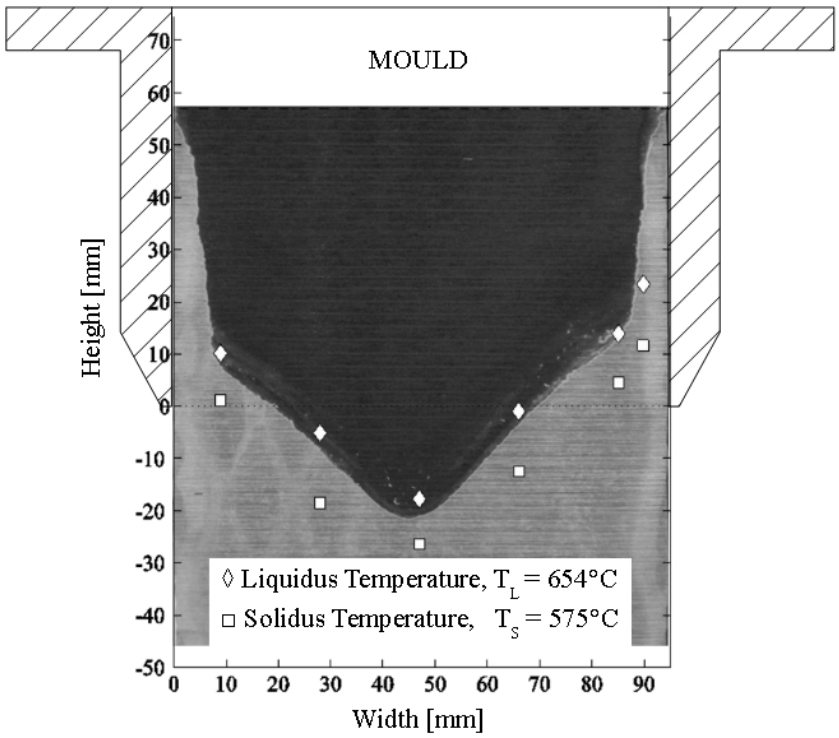

Figure 4-34: AA3003 cast at 2.33 mm/s show the locations of liquidus and solidus temperatures measured by the thermocouples superimposed onto the etched sump.

Sump profiles of AA6111 ingots cast at two different speeds, 1.61 mm/s and 1.79 mm/s, are shown in Figure 4-35 and Figure 4-36 respectively. In both cases, the liquidus isotherm locations obtained from the thermocouple data matched closely with the etched sump profiles and demonstrated that the results were reliable. The liquidus temperature of AA6111 was 647°C and the solidus temperature was 608°C.

Unlike AA3003, AA6111 showed no signs of remelting on the ingot surface and both sumps were mainly within the mould. It was noted that the shell thickness of AA6111 due to the primary cooling was significantly thicker than what was seen in AA3003. The distinction between the shell formation due to primary cooling, and the shell formation due to secondary cooling was not clear in the AA6111 ingots. It was noted that the sumps observed in the sectioned AA6111 ingots were not as deep as those seen in AA3003. This may be partially due to the fact that the casting speed used in AA6111 was slightly slower than that used in AA3003, as summarized in Table 4-2. Another cause may be that

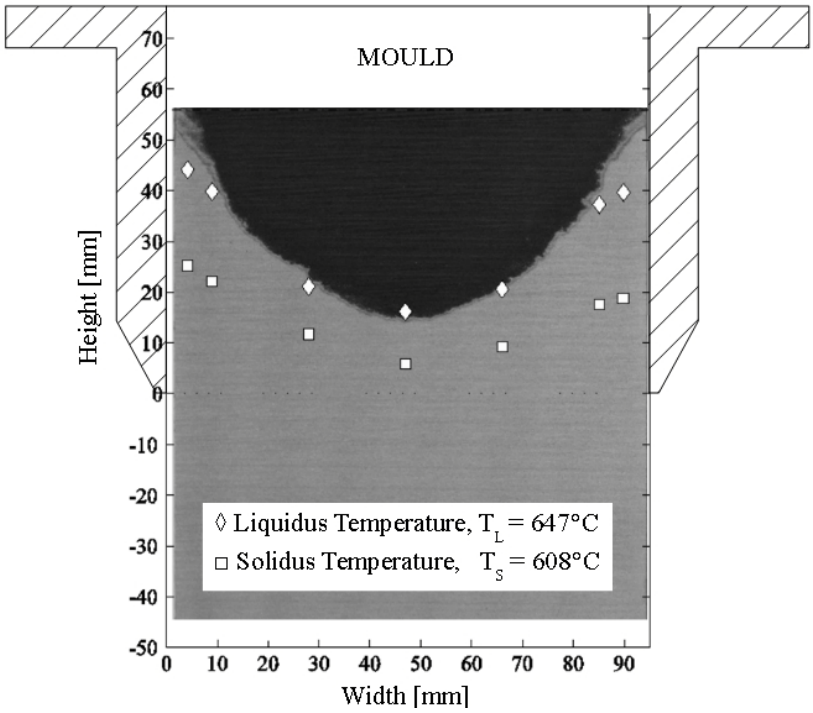

Figure 4-35: AA6111 cast at 1.61 mm/s show the locations of liquidus and solidus temperatures measured by the thermocouples superimposed onto the etched sump.

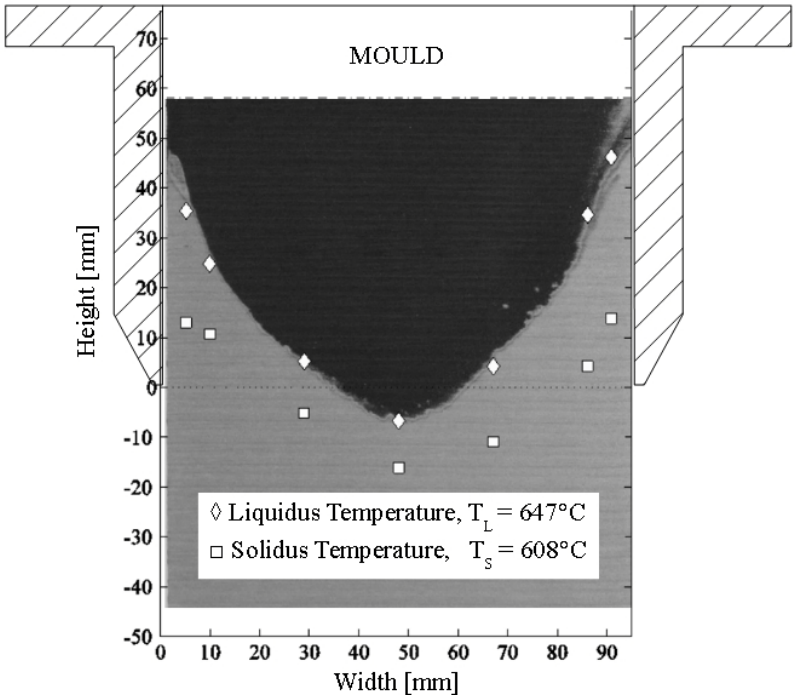

Figure 4-36: AA6111 cast at 2.12 mm/s show the locations of liquidus and solidus temperatures measured by the thermocouples superimposed onto the etched sump.

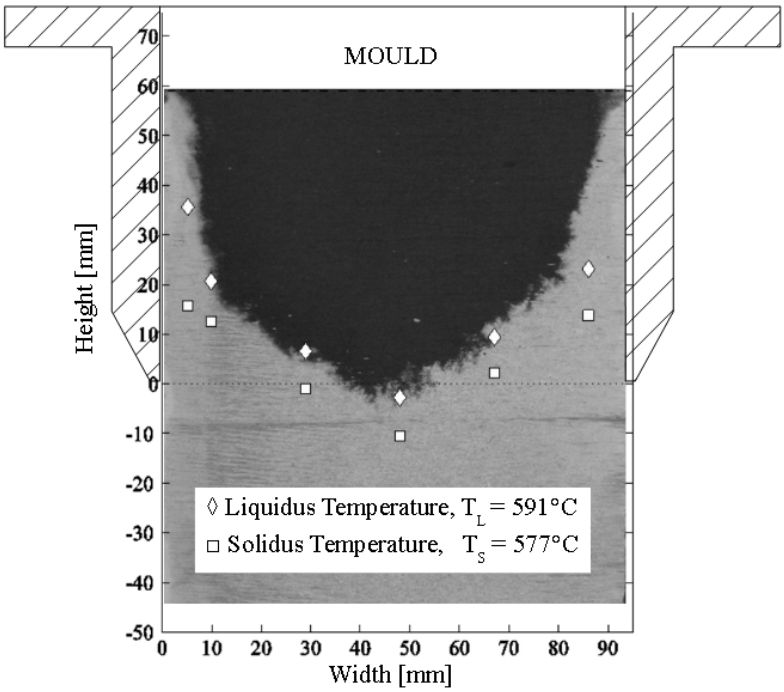

Figure 4-37: AA4045 cast at 1.69 mm/s show the locations of liquidus and solidus temperatures measured by the thermocouples superimposed onto the etched sump.

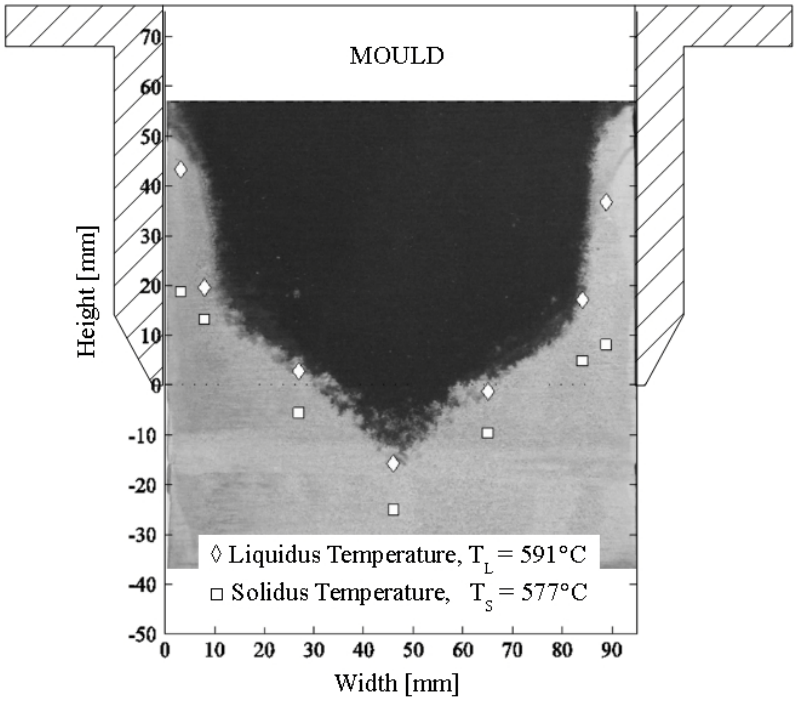

Figure 4-38: AA4045 cast at 2.12 mm/s show the locations of liquidus and solidus temperatures measured by the thermocouples superimposed onto the etched sump.

AA6111 has a higher thermal conductivity, k, than AA3003, resulting in a higher rate of heat transfer out of the AA6111 ingot. The effect of the Péclet number on the sump depth and shape is illustrated in Figure 4-39. The Péclet number, Pe, is a dimensionless number and is defined as:

$$Pe = \frac{v \cdot W}{\alpha} \tag{4.1}$$

where:
v is the casting speed [m/s]
W is the width of the ingot [m]
α is the thermal diffusivity [m²/s]

The thermal diffusivity, α, was calculated using the following formula:

$$\alpha = \frac{k}{\rho \cdot C_p} \tag{4.2}$$

where:
k is the thermal conductivity [W/m°C]
ρ is the density [kg/m³]
C_p is the specific heat capacity [J/kg°C]

Pe is the ratio of energy transport by advection versus conduction. Geometrically similar sump and isothermal contours shapes will be similar for ingots cast with the same Pe, even though they may be different alloys with different thermal diffusivities [22][47][48]. In addition, the sump depth will increase with increased Pe.

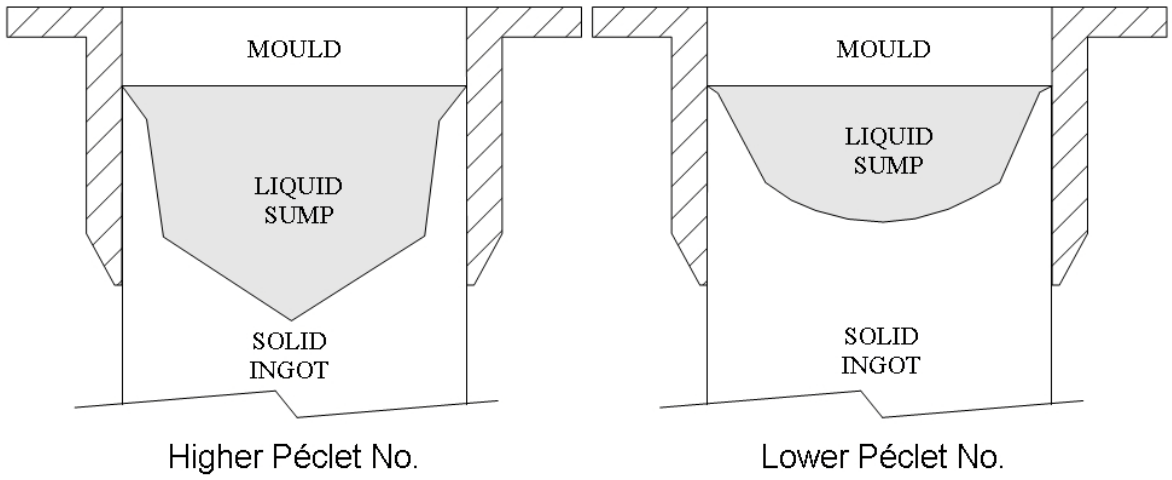

Figure 4-39: The effects of the Péclet number on the sump depth and shape **[22]**.

In Table 4-3 the thermophysical property values used to calculate the Péclet number are shown. Table 4-4 compares the Péclet number of different alloys at various casting speeds with the sump depths of all the alloys. A higher Pe number produced a thinner shell in the primary and secondary cooling region of the ingot and a deeper sump as it is dependent on the casting speed, the width of the

mould, and the thermal diffusivity of each alloy [22]. The Pe numbers of two casting speeds were compared for each alloy and it was found that deeper sumps had higher Pe numbers in all cases. The alloys were also compared and it was found that casts with similar Pe numbers produced similar sump depths, for example, AA3003 cast at 2.33 mm/s produced nearly identical sump depths as AA4045 cast at 2.12 mm/s because the Pe numbers were very similar.

Table 4-3: Thermophysical property values for AA3003, AA6111, and AA4045 used to calculate Pe.

Properties	Units	AA3003	AA6111	AA4045
k	[W/m°C]	193	205	172
ρ	[kg/m³]	2710	2710	2710
C_p	[J/kg°C]	893	897	885
α	[m²/s]	7.98×10^{-5}	8.43×10^{-5}	7.17×10^{-5}

Table 4-4: Calculated Péclet number and measured sump depth for AA3003, AA6111, and AA4045.

	Units	AA3003		AA6111		AA4045	
v	[m/s]	0.00169	0.00233	0.00161	0.00212	0.00169	0.00212
W	[m]	0.094	0.094	0.094	0.094	0.094	0.094
Pe		1.99	2.75	1.79	2.36	2.22	2.78
Sump Depth	[mm]	55	74	40	64	62	73

Using the data from Table 4-4, the sump depth versus Péclet number is plotted in Figure 4-40. A least squares regression line was drawn through the points, omitting the outlier data point from Cast 4, AA6111 cast at 1.61 mm/s. The equation of the linear regression model is:

$$\text{Sump Depth} = \text{Péclet Number} \times 23.15 + 9.58 \quad [\text{mm}] \tag{4.3}$$

The coefficient of determination, r^2, was calculated to be 0.988, where r is the linear correlation coefficient. The term r^2 may have values that range from 0 to 1 and indicates the goodness of fit of the model where a value of 1 means the regression line fits the data perfectly. The estimated Péclet numbers calculated for AA3003 and AA4045 behaved in a predictable way and had an excellent fit with the linear regression model. While AA6111cast at 2.12 mm/s had consistent Péclet numbers with the other two alloys, the slower cast of 1.61 mm/s did not. One possible explanation may be due to the unusually high rate of heat transfer in the primary cooling region. Figure 4-35 shows the shape of the sump in AA6111 cast at 1.69 mm/s, but the distinction between the primary shell and secondary shell was not as clear as in all the other casts, including AA6111 cast at a faster speed of 2.12 mm/s.

A closer look at the surface morphology shown in Figure 4-41 may provide further insight as to why AA6111 cast at a lower speed had a higher rate of heat transfer. It was noted that the surface of

AA6111 cast at 1.61 mm/s had a rougher appearance than when cast at 2.12 mm/s. According to Wells and Cockcroft [18], surface roughness had a significant impact on the boiling curve and increased the heat transfer by as much as 20% in the nucleate boiling regime. The rougher surface caused the flow of water over the surface of the ingot to become more turbulent and resulted in higher convective cooling [18]. A rougher surface was also able to break down an insulating vapor layer that would have otherwise developed between the hot ingot surface and the water flow and this increased the rate of heat transfer [18].

The Péclet number only takes the thermal diffusivity of the alloy, the casting speed, and the width of the ingot into account, but does not consider the surface morphology, which may impact the rate of heat transfer during a cast and consequently, the sump depth. The outlier, AA6111 cast at 1.61 mm/s, in Figure 4-40 may be the result of its rough surface increasing the rate of heat transfer leading to a shallower sump than expected.

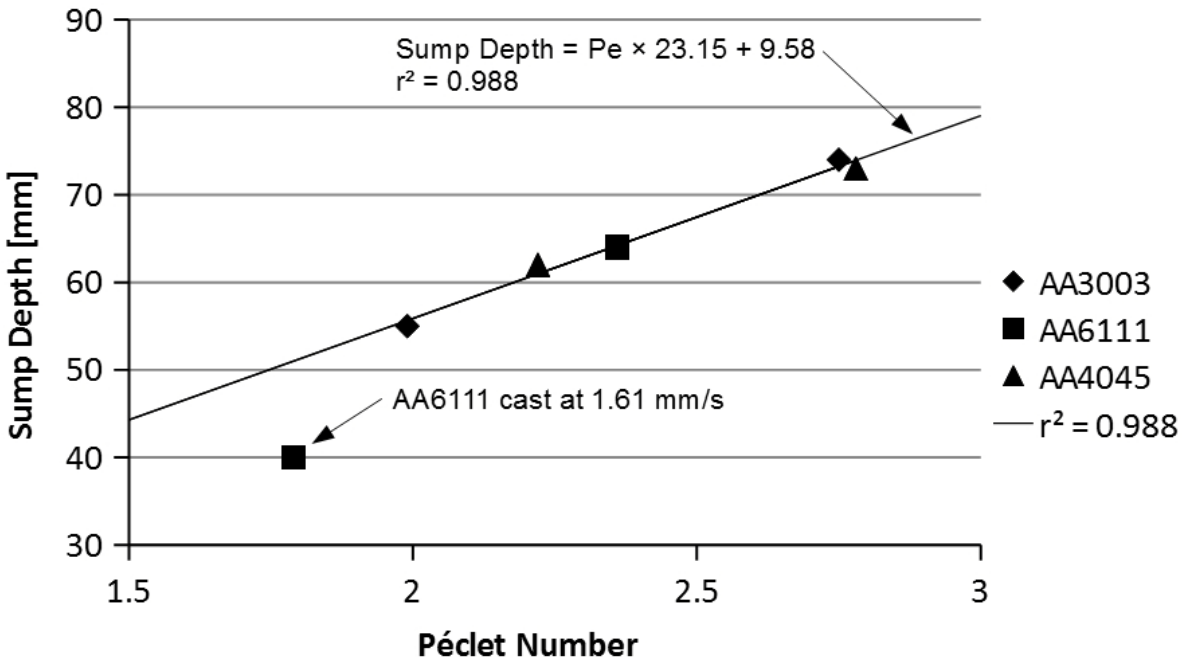

Figure 4-40: The sump depth plotted against the Péclet number and showing a line of best fit.

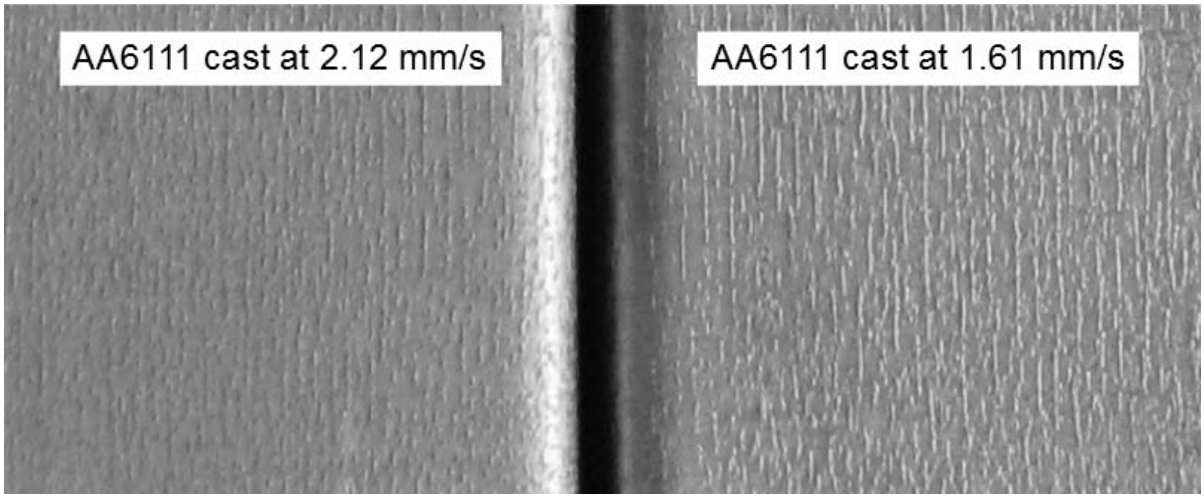

Figure 4-41: The as cast surface of AA6111 cast at 2.12 mm/s (Cast 5) and 1.61 mm/s (Cast 4).

Figure 4-37 and Figure 4-38 show the T_L and T_S thermocouple locations superimposed onto the NaOH etched sump of AA4045 cast at 1.69 mm/s and 2.12 mm/s respectively. The two methods used to determine the sump profiles match closely with one another. Although the sump shape of AA4045 was similar to that of AA3003, the outline of the sump is not as clear due to the large equaixed dendritic crystals that accumulated at the bottom of the sump. In this case, grain multiplication by dendrite arms breaking off the interface of the primary shell formed near the mould wall during the cast and these sank or were carried down to the centre of the ingot and sump where they collected around the bottom of the sump and grew as equiaxed dendritic grains making the sump appear to be shallower. The liquidus temperature was assumed to be 591°C and the solidus sump temperature was assumed to be 577°C.

The interface of the micro-etched (Keller's Etchant) sump profile of a melt poisoned AA3003 ingot was examined in more detail to investigate how deeply the zinc melt poisoned mixture penetrated into the AA3003 aluminum solidification interface. Figure 4-42 shows the location of the micrograph in Figure 4-43. The bottom of the sump was chosen because it is the flattest portion of the sump and close to the plane of symmetry. The AA3003 Al-Zn melt poisoned interface shown in Figure 4-43 exhibits cellular dendrites in the AA3003 region growing perpendicular to the interface, in the direction opposite to the direction of heat transfer. Since the Al-Zn mixture does not penetrate much past the tips of the cellular dendrites in the AA3003, the micrograph shows that the interface closely represents the liquidus sump. This result is consistent with what is seen in Figure 4-33 and Figure 4-34. The microstructure of the melt poisoned region and the alloy, AA6111 and AA4045, are shown in

Figure 4-44 and Figure 4-45, respectively. The addition of zinc provided more nucleation sites for grains and dendrites. In the melt poisoned region, smaller grains were seen in AA6111 and denser concentrations of dendrites were seen in AA4045 than in the base alloy region. The high cooling rate of AA6111 did not allow time for dendrite formation as seen in AA3003 and AA4045. Since there was little mixing between the melt poisoned region and the base alloy, the interface of all the alloys closely represented the liquidus temperature.

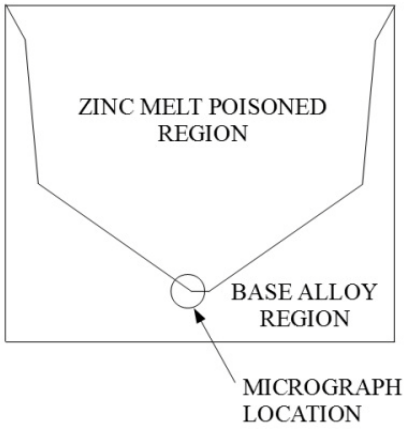

Figure 4-42: Location of the micrograph is the bottom of the sump.

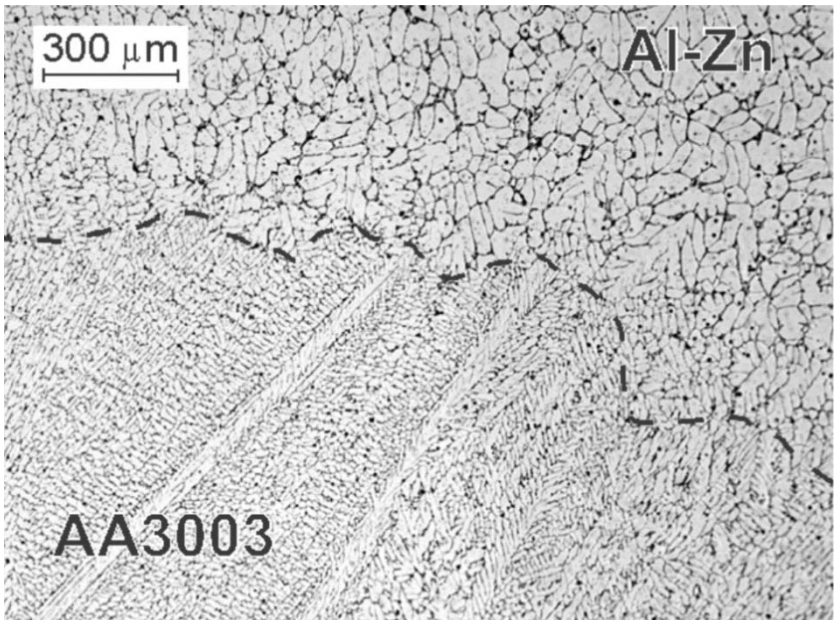

Figure 4-43: Microstructure of the zinc melt poisoned region and AA3003 interface (etched using Keller's Etchant) **[22] [39]**.

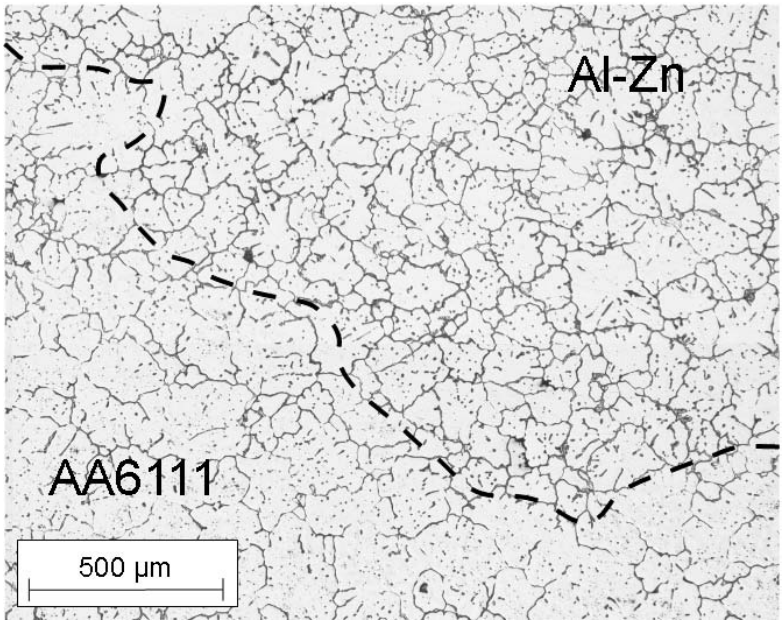

Figure 4-44: Microstructure of the zinc melt poisoned region and AA6111 interface (etched using Keller's Etchant) **[39]**.

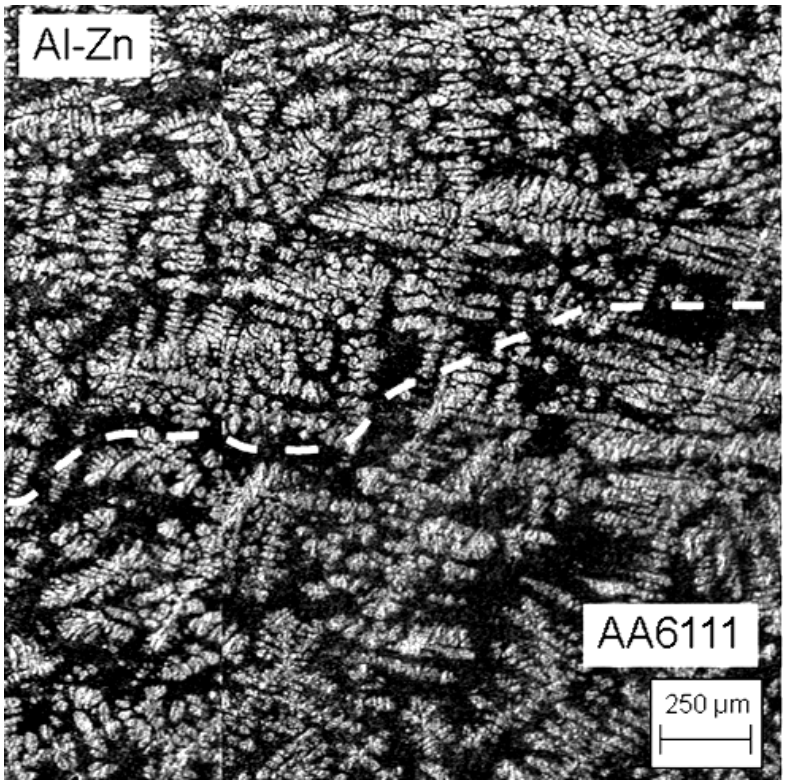

Figure 4-45: Microstructure of the zinc melt poisoned region and AA4045 interface (etched using Keller's Etchant) **[39]**.

4.8 Mould Temperature Analysis

Three thermocouples inserted in the mould wall on both sides were used to provide additional information of the boundary conditions for model validation. The results of the three thermocouples from one side of the mould are plotted in Figure 4-46 with the data taken from Cast 2 of the second series of experiments, casting AA3003 at 2.33 mm/s. The temperatures oscillate periodically in time. The first thermocouple in the mould to heat up was the top, thermocouple 24, and was followed by the centre, thermocouple 23, and finally the bottom, thermocouple 22. This meant that there was a hot region that grew near the metal level surface and moved down the side of the mould. Once the hot region moved down the mould, a new hot spot grew in its place and the cycle continued for the duration of the casting. The heating and cooling phenomenon, known as remelting, occurred in AA3003 and AA4045, but was not observed in AA6111.

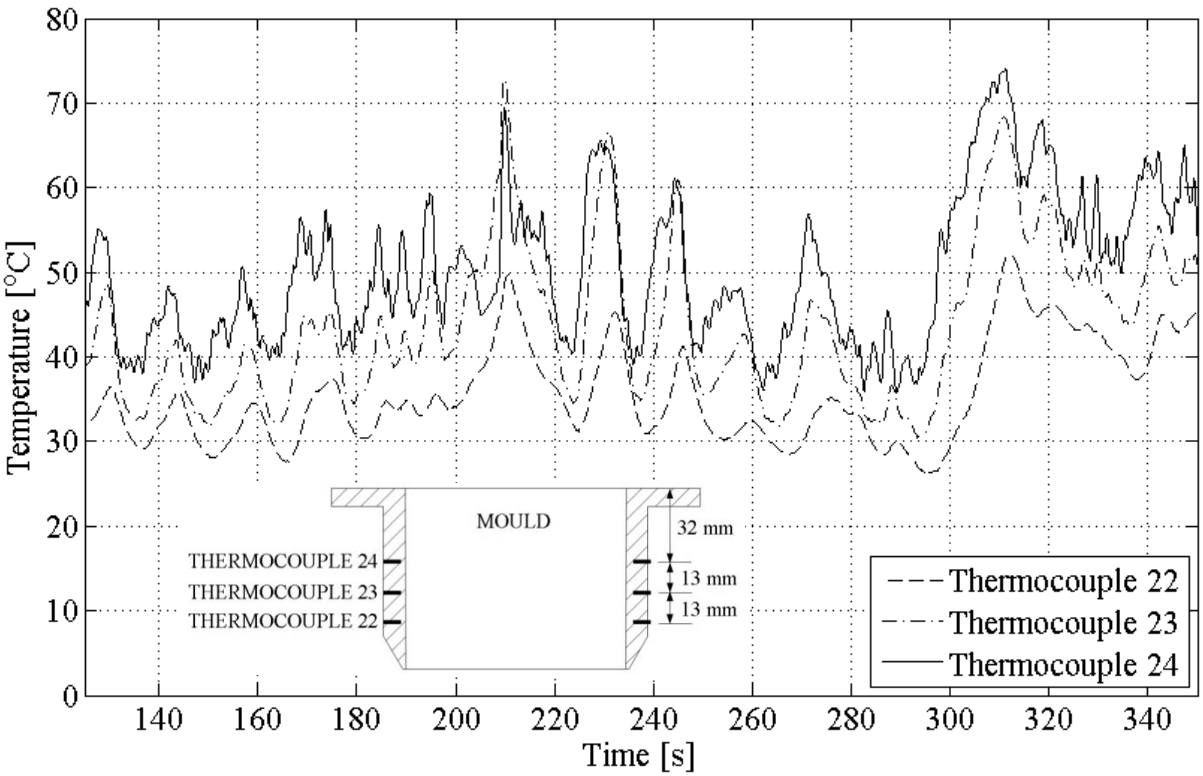

Figure 4-46: Typical mould temperature readings of AA3003.

One of the mould thermocouple data from Cast 1 of the second series of experiments is plotted in Figure 4-47. AA3003 was used in this experiment and cast at 1.69 mm/s. A fast Fourier transform (FFT) was used to determine the frequency of the cycles and the results are shown in Figure 4-48. The highest magnitude of the Fourier amplitude was the dominant frequency of the cast, in this case,

0.06 Hz. This frequency translated to 16.67 s. At a casting speed of 1.69 mm/s, this corresponded to a cycle spacing of 28 mm. This spacing was confirmed from Figure 4-49, where a picture of the ingot surface showed the spacing between the remelting bands to be approximately 28 mm.

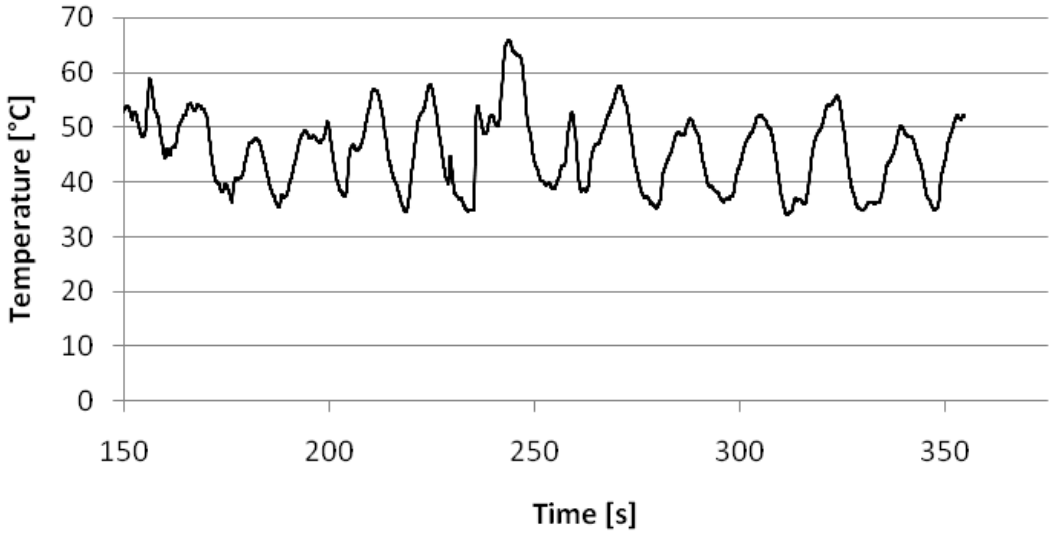

Figure 4-47: Mould temperature oscillations of Cast 1 casting AA3003 at 1.69 mm/s.

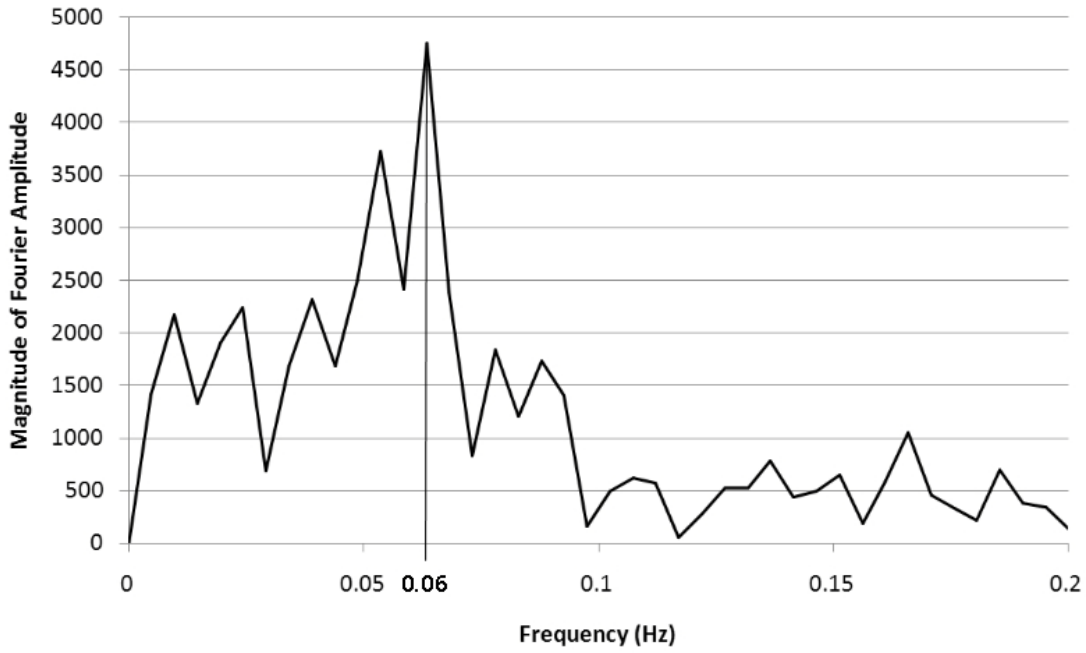

Figure 4-48: Fast Fourier transform performed on oscillating temperature data of AA3003.

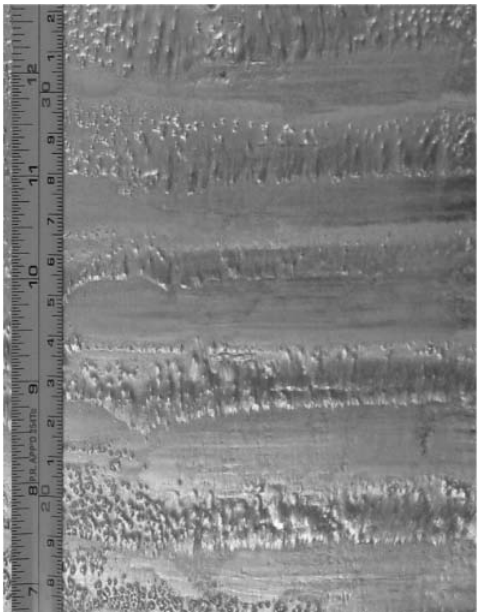

Figure 4-49: Remelting band spacing of Cast 1 casting AA3003 at 1.69 mm/s.

The mould thermocouple data from Cast 8 of the second series of experiments is plotted in Figure 4-50. AA4045 was used in this experiment and was cast at 2.12 mm/s. As in the previous case, a fast Fourier transform was used to determine the frequency, shown in Figure 4-51, and compared with the ingot surface of Cast 8, shown in Figure 4-52. A frequency of 0.059 Hz was obtained from the fast Fourier transform, and with a casting speed of 2.12 mm/s, the predicted cycle spacing was 36 mm. The measurements of the remelted bands on the ingot surface shown in Figure 4-52 confirmed that the cycle spacing was 36 mm.

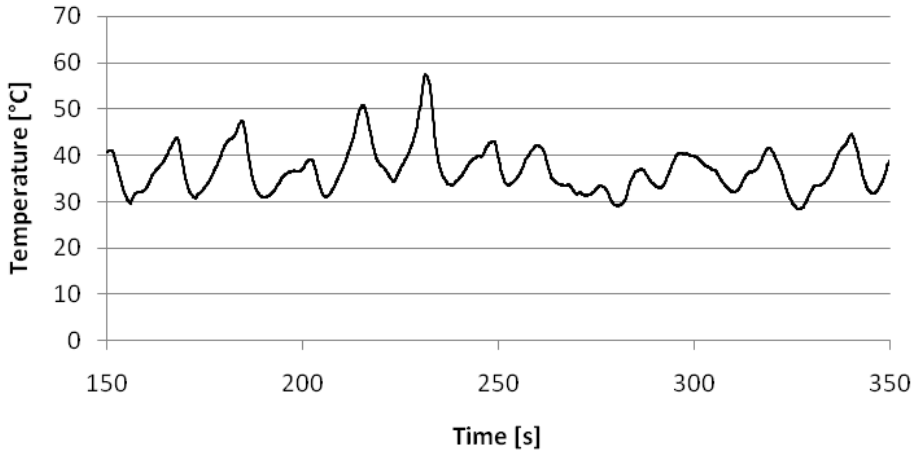

Figure 4-50: Mould temperature oscillations of Cast 8 casting AA4045 at 2.12 mm/s.

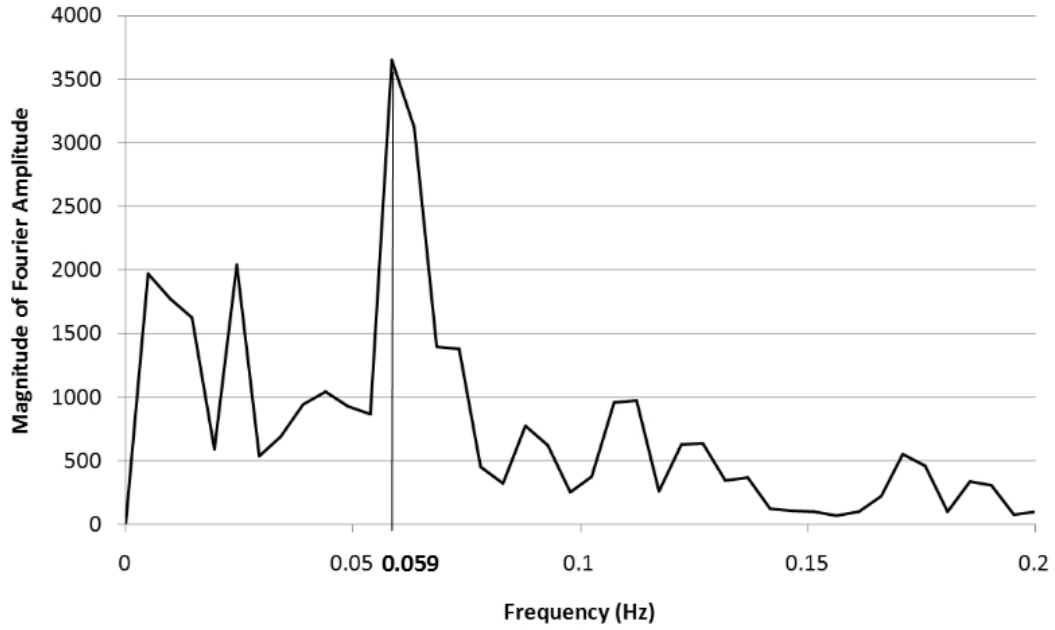

Figure 4-51: Fast Fourier transform performed on oscillating temperature data of AA4045.

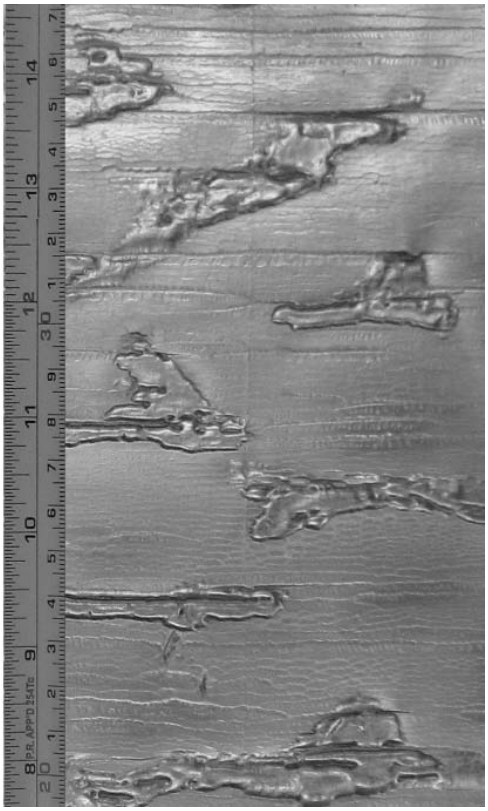

Figure 4-52: Remelting band spacing of Cast 8 casting AA4045 at 2.12 mm/s.

Similar analyses were performed on Cast 2, casting AA3003 at 2.33 mm/s, and Cast 7, casting AA4045 at 1.69 mm/s, from the second series of experiments as well as Cast 3, casting AA3003 at 2.54 mm/s, from the first series of experiments. A summary of the results is shown in Table 4-5. The frequency was observed to increase with casting speed in both alloys, and AA3003 had a higher frequency than AA4045.

Table 4-5: Summary of mould thermocouple data results.

	Series 2 Cast 1	Series 2 Cast 2	Series 1 Cast 3	Series 2 Cast 7	Series 2 Cast 8
Alloy	AA3003	AA3003	AA3003	AA4045	AA4045
Frequency of Oscillations [Hz]	0.06	0.063	0.078	0.049	0.059
Period for Oscillations [s]	16.67	15.87	12.82	20.4	16.95
Cast Speed [mm/s]	1.69	2.33	2.54	1.69	2.12
Distance Between Remelting Bands [mm]	28	37	33	34	36

Unlike AA3003 and AA4045, AA6111 ingots did not show signs of remelting and therefore, the mould thermocouples did not oscillate periodically (see Figure 4-53). An interesting behaviour in AA6111 was that the centre mould thermocouple, 23, had the highest temperature reading, followed by the top thermocouple, 24, and finally the bottom thermocouple, 22. This was counterintuitive, as one would expect the top thermocouple 24, to have the highest temperature similar to what was seen when AA3003 and AA4045 were cast. However, a higher temperature in the centre was consistent with what was seen in the etched sumps since higher mould temperature readings indicated higher rates of heat transfer leading to thicker shells as observed in the AA6111 etched sumps.

The results of the mould thermocouples are summarized in Figure 4-54. The averages of thermocouples 22, 23, and 24, for the bottom, middle, and top positions respectively were plotted for the three alloys. The plots for AA3003 and AA4045 showed an approximately linear trend with the temperatures cooling by approximately 10°C from the top, thermocouple 24, to the bottom, thermocouple 22. AA6111 behaved differently with the centre thermocouple having the peak temperature rather than the top thermocouple. The figure also showed that the mould thermocouples in AA6111 had a higher average temperature indicating that the heat transfer from primary cooling was more effective than for AA3003 and AA4045. This may be due to a smaller air gap formation between the ingot and the mould wall for AA6111, while AA3003 and AA4045 had a larger air gap, which acted as insulation reducing the rate of heat transfer.

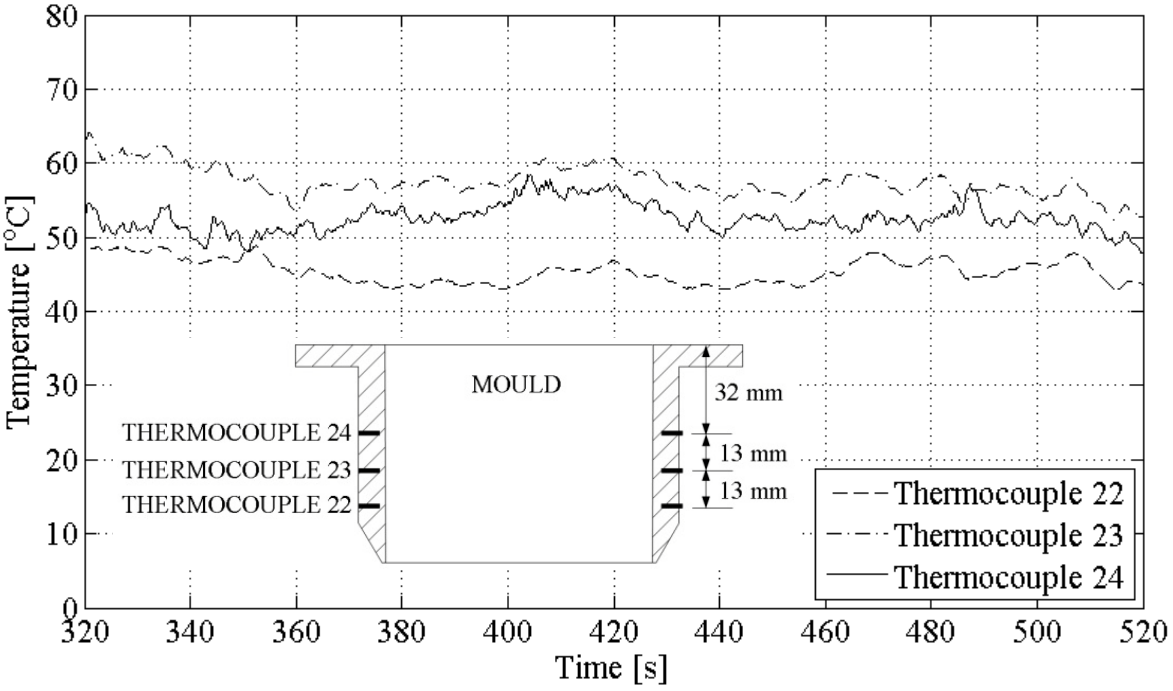

Figure 4-53: Mould temperature of Cast 6 casting AA6111 at 2.12 mm/s.

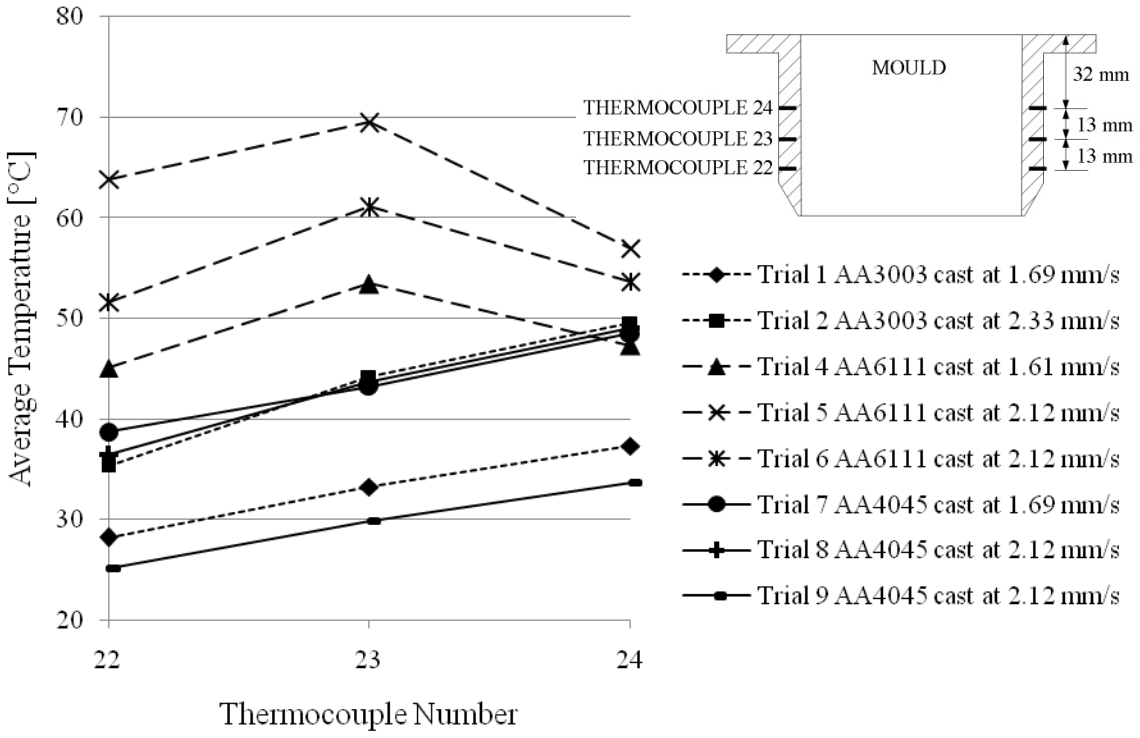

Figure 4-54: Average mould temperatures compared.

Based on the results of the etched sumps, the ingot thermocouple readings, and the mould thermocouple data, it was apparent that the three alloys all behaved differently. AA3003 and AA4045 both had very similar sump shapes where a thin shell was formed in the mould due to primary cooling before a sudden change in slope due high rates of heat transfer from secondary cooling. AA6111 appeared to have higher rates of heat transfer resulting in a thicker shell due to primary cooling and a much more gradual transition in the sump shape when the effects of secondary cooling were felt. Measured mould temperatures were higher when casting AA6111 which is indicative of higher heat transfer rates than when casting the other two alloys studied.

4.9 Summary

The second series of experiments had significant improvements of the measurement technique over the first series of experiments. It was essential to secure the thermocouples in the desired position to ensure the positional reliability of the data. The Al-Zn melt poisoning technique and embedded thermocouples should be used in conjunction. The zinc melt poisoning delineated the entire shape of the sump, especially the primary shell. While the thermocouples provided the sump position at a limited number of discrete positions only, they were important in providing a thermal history of the ingot as it was cast including the temperature of the sump interface. Both techniques had excellent agreement.

It was found that water flow rates beyond 1.79 L/s did not have a significant impact on the sump depth. Increasing the superheat by 40°C did not significantly increase the sump depth. DC casting was found to be very sensitive to the casting speed and the sump depth increase with higher casting speed. A linear regression model could be used to predict the sump depth if the Péclet number is known since the sump depth increased with increasing Péclet number in a directly proportional manner. Periodic remelting was observed in AA3003 and AA4045, but not in AA6111. Thermocouples in the mould indicated that AA6111 had a higher rate of heat transfer with its higher average temperature than AA3003 and AA4045. This was evidence that the insulating air gap between the ingot and the mould was thinner in AA6111 than in AA3003 and AA4045. The results of these series of experiments and the improved experiment technique gained will aid in the development of Fusion™ Casting Technology, as well as provide validation data for the CFD model.

Chapter 5
Summary, Conclusions, and Recommendations

Conventional DC casting experiments were performed using three alloys, AA3003, AA6111 and AA4045 casting in a 95 mm x 227 mm rectangular mould using various casting speeds, molten metal superheats, and cooling water flow rates. The results allowed analysis to be made on how changing casting parameters affect the solidification of the DC cast ingot and are useful in validating CFD models as well as helping to develop co-casting of composite ingots and to design an experiment to validate the co-casting model. CFD models of co-casting allowed different casting parameters and alloys to be tested using simulations rather than expensive and time consuming experimentation.

To ensure the results of the experiments with DC casting of three difference aluminum alloys were reliable for CFD model validation, the accuracy and precision of the measuring instruments were tested to ensure the equipment was operating within allowable uncertainties. Two independent methods, melt poisoning with a molten Al-50% Zn alloy and thermocouple implants, were used to determine the sump depth and to demonstrate the consistency of the results. Two series of experiments were run to show that the results were repeatable. In the second series of experiments, ingots were cast with and without thermocouples in the mould so that the etched sumps could be compared to ensure the sump depth and shape was the same. This demonstrated that the experimental equipment did not disturb the environment in the mould significantly.

Several improvements made to the experiment design of the second series of experiments helped improve the quality of the measurements. It was important to support the thermocouples using a rigid vertical framework so they were not pushed out of position by the jet of molten aluminum entering the mould. The number of thermocouples in the mould should be kept at a minimal so that the flow of molten aluminum in the mould is not disturbed significantly. It was better to run thermocouple wires up in a single location than to create an array of thermocouples that disturbed the natural convection in the mould. Thermocouples must not be blocked by any supporting device since any obstructions would create a bias in the reading.

Using a rod-shaped spacer to position the thermocouples was a more streamlined method than using flat steel spacers. Another advantage of using steel rod spacers was that they were more structurally rigid, while steel flat spacers tended to warp at high temperatures and moved the thermocouples out of position.

Grounded thicker thermocouples of 1.5 mm Ø survived at high temperatures much better than the 1 mm Ø thermocouples with the exposed beads. Smaller thermocouples were more prone to failure and exposed bead tended to dissolve and malfunction under the high heat in the molten aluminum.

During the study of the effect of casting parameters, it was found using water flow rates beyond 1.79 L/s did not significantly affect the rate of cooling of the ingot. In addition, it was demonstrated that cast sump profiles were not very sensitive to the use of higher superheats of the aluminum alloy, but were very sensitive to the casting speed. The casting speed is the most important process parameter in determining the cast sump profile. Higher casting speeds resulted in deeper sumps in all experiments.

The sump depth increased with increasing Péclet number. The least squares regression line produced by plotting the sump depth versus Péclet number showed that the data had an excellent fit with the linear regression model. The sump depth increased directly proportionally with increasing Péclet number, so given the Péclet number, the sump depth could be predicted using the linear regression model.

In all three alloys, AA3003, AA6111, and AA4045, the liquidus sump profile matched very closely with the etched sumps indicating reliable results. The technique of using the distance between the metal level and the liquidus temperature based on the thermocouple readings to determine the sump depth gave excellent correlation with the etched sump. Micrographs of the zinc-aluminum interface in all three alloys showed that this technique was effective in delineating the liquidus isotherm and sump profile at the moment the molten Al-Zn alloy was introduced into the sump.

Melt poisoning and thermocouples were complementary techniques that should be used together. Thermocouples provided actual continuous measurements of temperatures along discrete vertical lines in a cast ingot; however, it was very difficult to get them close enough to the ingot surface and enough of them to get accurate measurements of the thin primary shell profile adjacent to the mould. On the other hand, melt poisoning provided a continuous and complete indication of the liquidus isotherm and shape of the sump including the thin shell adjacent to the mould that can be used for CFD model validation in the region of primary cooling within the mould. This melt poisoned sump profile was obscured towards the centre of AA4045 ingots due to dendrite fragments acting as nuclei for equiaxed dendritic grains which were carried down by fluid flow in the sump to accumulate at the bottom and centre of the sump. This accumulation of equiaxed dendritic grains obscured the trace location of the liquidus in the melt poisoned and sump profile in the centre of the AA4045 ingots.

More rapid changes in shell thickness occurred at slower casting speeds and resulted in thicker primary shells since faster casting rates allowed less time for the centre to cool. The mushy zone of the alloys was approximately 9 mm thick and constant spacing between the liquidus and solidus isotherms indicated that the cooling rate in this temperature range remained uniform.

Remelting and liquid metal exudation occurred in AA3003 and AA4045 ingots, but did not occur in the AA6111 ingots. The AA6111 shell that formed in the mould due to the primary cooling was significantly thicker than what was seen in AA3003 and AA4045. The shell caused by primary cooling and secondary cooling in AA6111 was difficult to distinguish and demonstrated that the heat flux in the primary cooling region was nearly as high as in the secondary cooling region. The primary and secondary sump shells of AA4045 were thicker than the sump shell of AA3003, which indicated that the rate of heat transfer was higher in AA4045. A fast Fourier transform performed on the mould thermocouples illustrated that the temperatures in the mould oscillated at regular intervals to create consistent remelting band spacing. The frequency of the remelting band was observed to increase with casting speed in both alloys, with AA3003 having a higher frequency than AA4045.

Although the results of the mould thermocouples used in the casts for AA6111 appeared counterintuitive, where the centre mould thermocouple had the highest temperature reading, followed by the top thermocouple and finally the bottom thermocouple, it is consistent with the etched sump results. The higher mould temperature readings was evidence of higher rates of heat transfer and explained the thick shells due to primary cooling in AA6111. The material AA6111 had a higher average mould temperature than AA3003 or AA4045, indicating that the heat transfer from primary cooling was more effective. AA6111 experienced smaller thermal contractions resulting in a smaller air gap between the shell and the mould than for the other alloys so improved cooling rates were observed. Higher rates of heat transfer found in AA6111 appeared to yield better ingot surface finish by avoiding remelting bands.

The behaviour of the three alloys studied and the effect the casting parameters have on them will be beneficial in the development of the co-caster and the experiment design for co-casting CFD model validation.

References

[1] D. G. Eskin, *Physical Metallurgy of Direct Chill Casting of Aluminum Alloys*, Taylor & Francis Group, Ed.: CRC Press, New York, 2008.

[2] Y. Zuo, H. Nagaumi, and J. Cui, "Study on the sump and temperature field during low frequency electromagnetic casting a superhigh strength Al-Zn-Mg-Cu alloy," *Journal of Materials Processing Technology*, 2007, Vol. 197, pp. 109-115.

[3] J.F. Grandfield, "DC Casting of Aluminum: A Short Review of Process Development," in *Aluminum Cast House Technology*, Gold Coast, Australia, 1997, pp. 231-243.

[4] D. C. Weckman and P. Niessen, "A Numerical Simulation of the D.C. Continuous Casting Process Including Nucleate Boiling Heat Transfer," *Metallurgical Transactions B*, December 1982, Vol. 13B, pp. 593-602.

[5] H. Hao, D. M. Maijer, M. A. Wells, S. L. Cockcroft, and D. Sediako, "Development and Validation of a Thermal Model of the Direct Chill Casting of AZ31 Magnesium Billets," *Metallurgical and Materials Transactions*, December 2004, Vol. 35A, pp. 3843-3854.

[6] A. Larouche and C. Brochu, "Solidification Conditions in Aluminum DC Sheet Ingot: Understanding and Control," in *31th Annual Conference of Metallurgists on Light Metals (CIM)*, Montreal, Quebec, 1996, pp. 597-604.

[7] D. C. Weckman, R. J. Pick, and Paul N., "A Numerical Heat Transfer Model of the DC Continuous Casting Process," *Zeitschrift Fur Metallkunde*, 1979, Vol. 70, pp. 750-757.

[8] D. C. Weckman and P. Niessen, "Mathematical Models of the DC; Continuous Casting Process," *Canadian Metallurgical Quarterly*, 1984, Vol. 23, No. 2, pp. 209-216.

[9] J. F. Grandfield, "DC Casting: Threats and Challenges," in *3rd Australian/Asian/Pacific Course and Conference on Aluminium Cast House Technology*, Warrendale, PA, 1993, pp. 351-357.

[10] M. D. Anderson, K. T. Kubo, W. J. Fenton, E. W. Reeves, and B. Spendlove, Method for Casting Composite Ingot, 2005, Patent Application Publication No: US 2005/0011630 A1.

[11] R. B. Wagstaff, D. J. Lloyd, and T. F. Bischoff, "Direct Chill Casting of CLAD Ingot," *Materials Science Forum*, 2006, Vol. 519-521, pp. 1809-1814.

[12] A. Gupta, S. T. Lee, R. B. Wagstaff, M. Gallerneault, and J. W. Fenton, "The Distribution of Magnesium and Silicon across the As-Cast Interface of Aluminum Laminates Produced via the Novelis Fusion Process," *JOM*, August 2007, pp. 62-65.

[13] P. R. Riosa and A. F. Padilhab, "Microstructural Path of Recrystallization in a Commercial Al-Mn-Fe-Si (AA3003) Alloy," *Materials Research*, 2003, Vol. 6, No. 4, pp. 605-613.

[14] G. K. Quainoo and S. Yannacopoulos, "The Effect of Cold Work on the Precipitation Kinetics of AA6111 Aluminum," *Journal of Materials Science*, 2004, Vol. 39, pp. 6495-6502.

[15] R. Nakamura, T. Yamabayashi, T. Haga, S. Kumai, and H. Watari, "Roll Caster for the Three-Layer Clad-Strip," *Materials Science and Engineering*, February 2010, Vol. 41, No. 2, pp. 112-120.

[16] J. B. Wiskel and S. L. Cockcroft, "Heat-Flow-Based Analysis of Surface Crack Formation During the Start-Up of the Direct Chill Casting Process Part II. Experimental Study of an AA5182 Rolling Ingot," *Metallurgical and Materials Transactions B*, February 1996, Vol. 27B, pp. 129-137.

[17] J. B. Wiskel, "Thermal Analysis of the Startup Phase for D.C. Casting of an AA5182 Aluminum Ingot," PhD Thesis. 1995. University of British Columbia. Vancouver, Canada.

[18] M. A. Wells and S. L. Cockcroft, "Influence of Surface Morphology, Water Flow Rate, and Sample Thermal History on the Boiling-Water Heat Transfer during Direct-Chill Casting of Commercial Aluminum Alloys," *Metallurgical and Materials Transactions*, October 2001, Vol. 32B, pp. 929-939.

[19] J. F. Grandfield, A. Hoadley, and S. Instone, "Water Cooling in Direct Chill Casting: Part 1: Boiling Theory and Control," in *Technical Session on Light Metals, at the 126th TMS Annual Meeting*, Orlando, FL, 1997, p. 691.

[20] L. C. Burmeister, *Convective Heat Transfer*, 2nd ed. Danvers, MA: John Wiley & Sons Inc., 1993.

[21] J. F. Grandfield, K. Goodall, P. Misic, and X. Zhang, "Water Cooling in Direct Chill Casting: Part 2, Effect on Billet Heat Flow and Solidification," in *Technical Session on Light Metals at the 126th TMS Annual Meeting*, Orlando, Fl, 1997, The Minerals Metals and Materials Society. Warrendale, Pennsylvania, pp. 1081-1089.

[22] D. C. Weckman, Personal Communications, University of Waterloo, Waterloo, Ontario, 2010.

[23] J.F. Grandfield and P.T. McGlade, Materials Forum, 1996.

[24] J. Langlais, T. Bourgeois, Y. Caron, G. Beland, and D. Bernard, "Measuring the Heat Extraction Capacity of DC Casting Cooling Water," *Light Metals*, The Metallurgical Society of the AIME, Warrendale, PA, 1995, pp. 979-986.

[25] V. A. Livanow, R. M. Gabidullin, and V. S. Shepilov, "Continuous Casting of Aluminum Alloys," *Moscow: Metallurgiya*, 1977.

[26] D. C. Prasso, J. W. Evans, and I. J. Wilson, *Metall. Mater. Trans.*, 1995, Vol. 26B, No. B, pp. 1243-1251.

[27] J. M. Reese, "Characterization of the Flow in the Molten Metal Sump during Direct Chill Aluminum Casting," *Metallurgical and Materials Transactions*, June 1997, Vol. 28B, pp. 491-499.

[28] J. M. Drezet, M. Rappaz, B. Carrupt, and M. Plata, "Experimental Investigation of Thermomechanical Effects during Direct Chill and Electromagnetic Casting of Aluminum Alloys," *Metallurgical and Materials Transactions*, August 1995, Vol. 26B, pp. 821-829.

[29] Amir Baserinia, Personal Communications, University of Waterloo, Waterloo, Ontario, 2010.

[30] ASM International, *ASM Specialty Handbook Aluminum and Aluminum Alloys*. Materials Park, OH, USA, 1993.

[31] Simon Barker, Personal Communications, Novelis Global Technologies Centre, Kingston, Ontario, 2010.

[32] National Instruments, SCXI Chassis, 2005.

[33] National Instruments. (2010) Taking Thermocouple Temperature Measurements. [Online]. http://zone.ni.com/devzone/cda/tut/p/id/4237

[34] National Instruments, SCXI Thermocouple Input Modules, 2010.

[35] National Instruments, LabVIEW, 2007.

[36] Omega Engineering, Metal Sheathed Thermocouple Probe, 2010.

[37] J. P. Holman, *Experimental Methods for Engineers*, 7th ed. New York, USA: The McGraw Hill Company, 2001.

[38] J. T. Nakos, "Uncertainty Analysis of Thermocouple Measurements Used in Normal and Abnormal Thermal Environment Eperiments at Sandia's Radiant Heat Facility and Lurance Canyon Burn Site," Sandia National Laboratories, Albuquerque, NM, 2004.

[39] G. F. Vander Voort, *Metallography Principles and Practice*. ASM International. Materials Park, OH, 1999.

[40] Struers. (2010) Epoxy Specifications Sheet. [Online]. http://www.struers.com/resources/elements/12/121260/Epoxy_sheet.pdf

[41] Struers. (2010) Metallographic Preparation of Aluminum and Aluminum Alloys. [Online]. http://www.struers.com/resources/elements/12/104900/Application%20Notes%20Aluminium%20English.pdf

[42] M. A. Wells, Personal Communications, University of Waterloo, Waterloo, Ontario, 2010.

[43] M. C. Flemings, *Solidification Processing*. New York: McGraw-Hill, 1974.

[44] Thermo-Calc Software AB, Stockholm, Sweden, 2010.

[45] FactSage, ThermalFact Inc. and GTT-Technologies, 2010.

[46] Rosa Pelayo, Personal Communications, University of Waterloo, Waterloo, Ontario, 2010.

[47] D. C. Weckman, *A Thermal and Thermoelastic Stress Analysis of Concast Zinc Ingots by Finite Element Methods*. Waterloo, Canada: University of Waterloo, MASc Thesis, 1978.

[48] J. Sengupta, B. G. Thomas, and M. A. Wells, "The Use of Water Cooling during the Continuous Casting of Steel and Aluminum Alloys," *Metallurgical and Materials Transactions A*, January 2005, Vol. 36A, pp. 187-204.

[49] A. J. Wheeler and A. R. Ganji, *Introduction to Engineering Experimentation*, 3rd ed. United States: Prentice Hall Inc., 1996.

[50] R. J. Moffat, "Using Uncertainty Analysis in the Planning of an Experiment," *Journal of Fluids Engineering*, June 1985, Vol. 107, pp. 173-178.

[51] S. J. Kline and F. A. McClintock, "Describing Uncertainties in Single Sample Experiments," *Mech. Eng.*, January 1953, p. 3.

Appendix A
Uncertainty in Thermocouple Measurements

Uncertainty analysis is an important part of proper experiment design and is used to demonstrate the validity of the data [49][50]. The sources are uncertainties in the experiments are discussed in this section.

The stainless steel sheathed type K thermocouple wire used in the experiment had an accuracy of 0.75% or 2.2°C whichever was greater with 99% confidence. For example, for the liquidus temperature of pure aluminum, which occurs at 660°C or 933 K, the uncertainty is 933 K × 0.0075 = ±7°C [36]. The type K extension cables used in the experiment had an uncertainty of ±2.2°C at room temperature with 99% confidence [36]. The thermocouple connectors was estimated to have a maximum temperature difference of up to 0.5°C across the connectors which resulted in an uncertainty of ±0.5°C with 99% confidence [38]. The reference junction had a sensor accuracy of ±1°C with 99% confidence [34]. The SCXI-1102 32 Channel Voltage Input Module had a measurement accuracy of ±0.7°C for temperatures between 0°C and 500°C and a measurement accuracy of ±1°C between 500°C and 1000°C with 99% confidence [34]. The voltage to temperature conversion had a maximum uncertainty of ±0.8°C with 99% confidence [38]. Table A-1 below summarizes the uncertainties of each source.

Table A-1: Uncertainty of temperature measurements caused by various sources.

Independent Variable	Nomenclature	Uncertainty	Confidence
Type K Stainless Steel Sheathed Thermocouple Wire Accuracy	W_{TC}	±2.2°C or 0.75% whichever is greater	99%
Type K Extension Cable at 25°C	W_{EC}	±2.2°C	99%
Type K Thermocouple Connector	W_{C}	±0.5°C	99%
Reference Junction	W_{RJ}	±1°C	99%
SCXI-1102 Voltage Input Module	W_{M}	±0.7°C (0°C-500°C) ±1°C (500°C-1000°C)	99%
Voltage to Temperature Conversion	W_{VT}	±0.8°C	99%

To calculate the uncertainty in the thermocouple measurements, let temperature, T, be a function of independent variables $x_1, x_2, \ldots, x_n$.

$T = T(x_1, x_2, \ldots, x_n)$ [37][51].

The uncertainty in the temperature, W_T, is found using the root sum square (RSS) method and calculated using the following equation [37] [38] [49] [50] [51]:

$$w_T = \left[\left(\frac{\partial T}{\partial x_1} w_1\right)^2 + \left(\frac{\partial T}{\partial x_2} w_2\right)^2 + \ldots + \left(\frac{\partial T}{\partial x_n} w_n\right)^2\right]^{1/2} \quad \text{(A.1)}$$

where:

T is the temperature [°C]

x_1, x_2, …, x_n are the independent variables

W_1, W_2, …, W_n are the uncertainties in the independent variables

When measuring the liquidus temperature of pure aluminum, a value of 656°C was obtained. The uncertainty of the measurement with 99% confidence is calculated below.

The nominal temperature, T, is:

$T = T_{TC} + T_{EC} + T_C + T_{RJ} + T_A + T_{VT} = 656°C$

Using Equation A.1, the uncertainty, W_T, is calculated below.

$$w_T = \left[\left(\frac{\partial T}{\partial T_{TC}} w_{TC}\right)^2 + \left(\frac{\partial T}{\partial T_{EC}} w_{EC}\right)^2 + \left(\frac{\partial T}{\partial T_C} w_C\right)^2 + \left(\frac{\partial T}{\partial T_{RJ}} w_{RJ}\right)^2 + \left(\frac{\partial T}{\partial T_M} w_M\right)^2 + \left(\frac{\partial T}{\partial T_{VT}} w_{VT}\right)^2\right]^{1/2}$$

The values of the terms are:

$$\frac{\partial T}{\partial T_{TC}} = \frac{\partial T}{\partial T_{EC}} = \frac{\partial T}{\partial T_C} = \frac{\partial T}{\partial T_{RJ}} = \frac{\partial T}{\partial T_M} = \frac{\partial T}{\partial T_{VT}} = 1$$

$W_{TC} = (933\ K) \times (0.75\%) = 7°C$

$W_{EC} = 2.2°C$

$W_C = 0.5°C$

$W_{RJ} = 1°C$

$W_M = 1°C$

$W_{VT} = 0.5°C$

The uncertainty in the temperature is:

$$W_T = [(1)^2(7)^2 + (1)^2(2.2)^2 + (1)^2(0.5)^2 + (1)^2(1)^2 + (1)^2(1)^2 + (1)^2(0.5)^2]^{1/2} = 7.5°C$$

The measured liquidus temperature of aluminum is 656°C ± 7.5°C with 99% confidence.

The same method was used for temperature measurements of ice water and boiling water. The temperatures of ice water and boiling water were measured to be -0.2°C and 98.6°C, respectively. The uncertainty values of the sources used in the calculation are listed below.

W_{TC} = 2.2°C

W_{EC} = 2.2°C

W_{C} = 0.5°C

W_{RJ} = 1°C

W_{M} = 0.7°C

W_{VT} = 0.5°C

The uncertainty in the temperature is:

$$W_T = [(1)^2(2.2)^2 + (1)^2(2.2)^2 + (1)^2(0.5)^2 + (1)^2(1)^2 + (1)^2(0.7)^2 + (1)^2(0.5)^2]^{1/2} = 3.5°C$$

The measured temperature of ice water is -0.2°C ± 3.5°C with 99% confidence.

The measured temperature of boiling water is 98.6°C ± 3.5°C with 99% confidence.

Appendix B

Melt Poisoned Ingot Sump Measurements

The ingot was sectioned at various distances along the length and width of the ingot to provide more information for model validation. Table B-1, Table B-2, and Table B-3 compare the sump depth obtained from the experiment's thermocouples with the measured zinc melt poisoned sectioned ingots for AA3003, AA6111, and AA4045 respectively. The close correlation between the two different methods indicated that the experiment techniques used gave consistent results.

Table B-1: Comparing experimental and measured results for AA3003.

AA3003 Casts	Casting Speed [mm/s]	Distant From Wide Face [mm]	Distant From Narrow Face [mm]	Sump Depth (Melt Poisoned Measurements) [mm]	Sump Depth (Thermocouple Estimates) [mm]
Cast 1	1.69	47		45	
Cast 1	1.69		96	55	55
Cast 1	1.69		111	56	
Cast 2	2.33	47		45	
Cast 2	2.33		96	72	74
Cast 2	2.33		111	73	
Cast 3	2.33	15		25	
Cast 3	2.33	25		36	
Cast 3	2.33	35		44	
Cast 3	2.33	47		45	
Cast 3	2.33		20	50	
Cast 3	2.33		40	57	
Cast 3	2.33		60	61	
Cast 3	2.33		80	67	
Cast 3	2.33		100	72	
Cast 3	2.33		111	73	

Table B-2: Comparing experimental and measured results for AA6111.

AA6111 Casts	Casting Speed [mm/s]	Distant From Wide Face [mm]	Distant From Narrow Face [mm]	Sump Depth (Melt Poisoned Measurements) [mm]	Sump Depth (Thermocouple Estimates) [mm]
Cast 4	1.61	47		35	
Cast 4	1.61		96	41	40
Cast 4	1.61		111	45	
Cast 5	2.12	47		49	
Cast 5	2.12		96	62	64
Cast 5	2.12		111	63	
Cast 6	2.12	15		27	
Cast 6	2.12	25		38	
Cast 6	2.12	35		52	
Cast 6	2.12	47		55	
Cast 6	2.12		20	43	
Cast 6	2.12		40	52	
Cast 6	2.12		60	57	
Cast 6	2.12		80	60	
Cast 6	2.12		100	62	
Cast 6	2.12		111	64	

Table B-3: Comparing experimental and measured results for AA4045.

AA4045 Casts	Casting Speed [mm/s]	Distant From Wide Face [mm]	Distant From Narrow Face [mm]	Sump Depth (Melt Poisoned Measurements) [mm]	Sump Depth (Thermocouple Estimates) [mm]
Cast 7	1.69	47		51	
Cast 7	1.69		96	60	62
Cast 7	1.69		111	62	
Cast 8	2.12	47		65	
Cast 8	2.12		96	70	73
Cast 8	2.12		111	74	
Cast 9	2.12	15		43	
Cast 9	2.12	25		55	
Cast 9	2.12	35		60	
Cast 9	2.12	47		77	
Cast 9	2.12		20	51	
Cast 9	2.12		40	86	
Cast 9	2.12		60	90	
Cast 9	2.12		80	85	
Cast 9	2.12		100	85	
Cast 9	2.12		111	74	